Five talks will provide an overview of direct-drive OMEGA cryogenic implosion results

1. **Overview of stagnation properties from direct-drive cryogenic OMEGA implosions (speaker: Valeri Goncharov via WebCon) - ~40 min**

   - Key physics issues relating to stagnation (1D and multi-D)

   - What are the important quantities that characterize stagnation and what are 1D/multiD effects on these quantities?

   - Wish list of simulations and diagnostics

2. **Hot-spot size (speaker: Sean Regan) - ~20 min**

   - Comparison of observables to simulated observables

   - How do we measure hot-spot size in OMEGA implosions?

   - 1D versus multi-D effects?

   - What facility/target improvements are planned to improve observed stagnation properties

UNIVERSITY of ROCHESTER

Five talks will provide an overview of direct-drive cryogenic results

3. Confinement Time (speaker: Sean Regan) - ~20 min

- How do we measure neutron rate and extract a burn width?
- What improvements are needed in measurements and analysis?

4. Ion temperature (speaker: Jim Knauer) – ~20 min

- How do we measure ion temperature? (# measurements etc.)
- What improvements are needed in measurements and analysis?
- How do we extract a value?
- Do we see dependence on viewing direction?

5. Areal density (speakers: Jim Knauer and Maria Gatu-Johnson) – ~25 min

- How do we measure areal density? (# measurements etc.)
- How do we extract a value?
- Do we see dependence on viewing direction?

Stagnation physics of ICF implosions

3-D simulation of temperature and density near peak burn of OMGEA cryogenic implosion

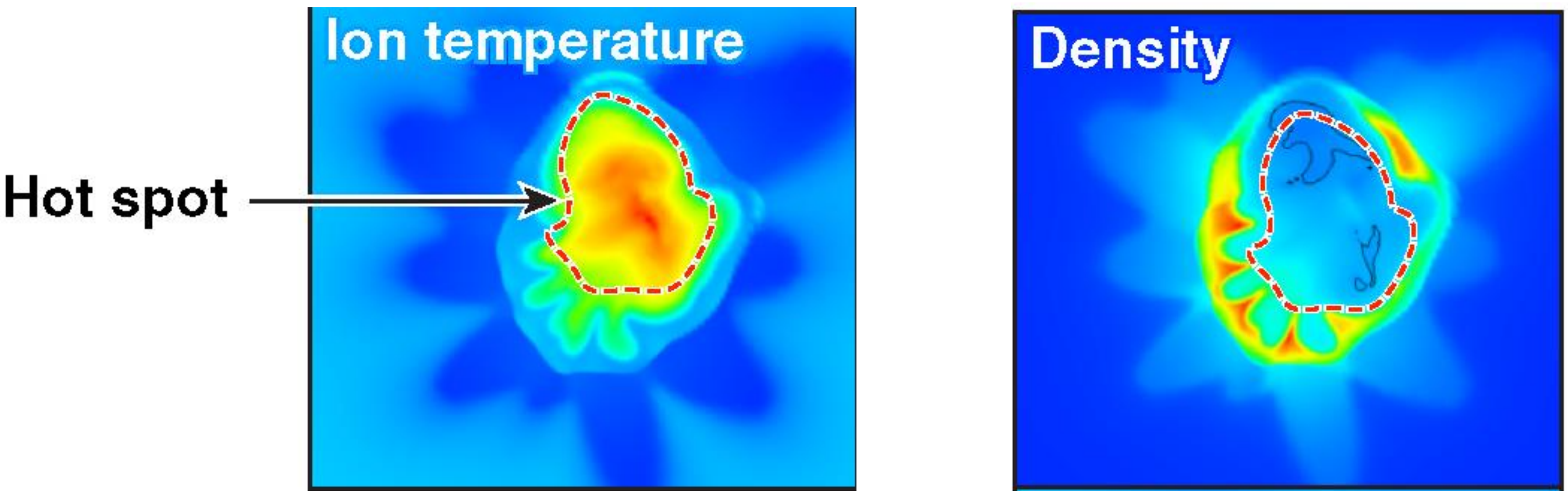

V.N. Goncharov

National Implosions Stagnation Physics Working Group Meeting at LLNL, October 27-28, 2015

One of key questions is how much energy couples into the hot spot

$P_{hs}^{ign} \sim E_{hs}^{-1/2}$

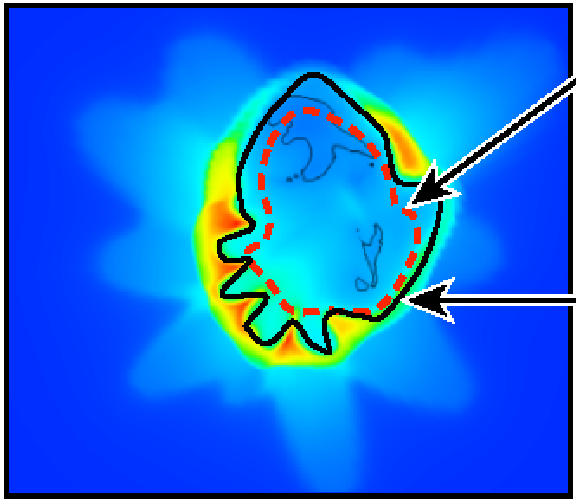

Hot spot, $V_{hs,\,3\text{-}D} < V_{hs,\,1\text{-}D}$

Neutron rate $\sim P_{hs}^2 \frac{\langle \sigma v \rangle}{T^2} V_{hs}$

Central region,
$V_{c,\,3\text{-}D} > V_{c,\,1\text{-}D}$

Hot-spot pressure evolves as $P_{hs} \sim V_c^{-5/3}$

As shell implodes, V_c shrinks, P_{hs} increases

$1-D$: $V_c \sim V_{hs}$

$3-D$: $V_c > V_{hs}$, $V_c - V_{hs}$ - volume of “dark” region

Hot spot gains its energy from pdV work and shell kinetic energy

Beginning of shell deceleration, $E_{hs} << E_{kin,\ shell}$

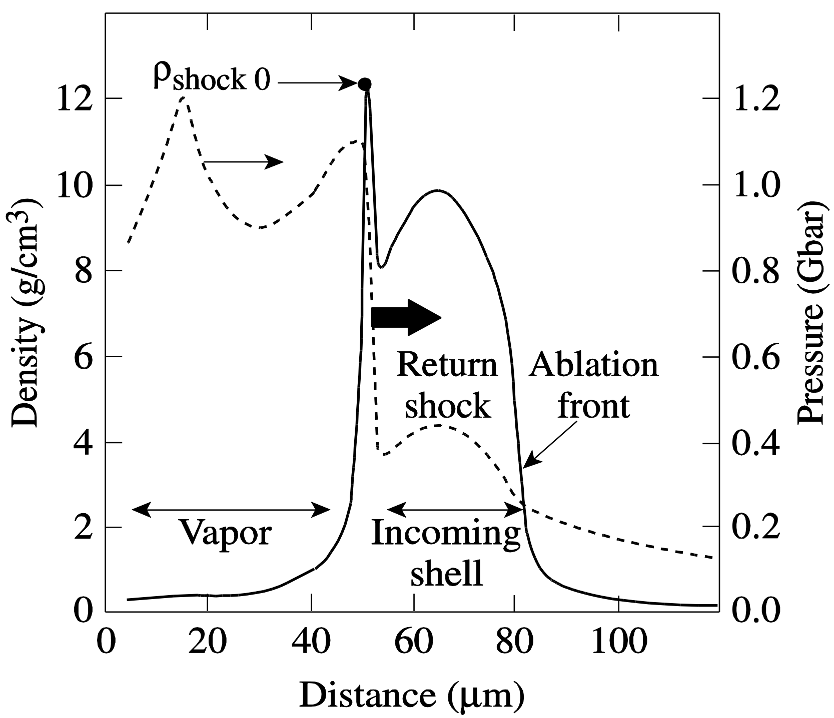

Shell deceleration, $E_{hs} < E_{kin,\ shell}$

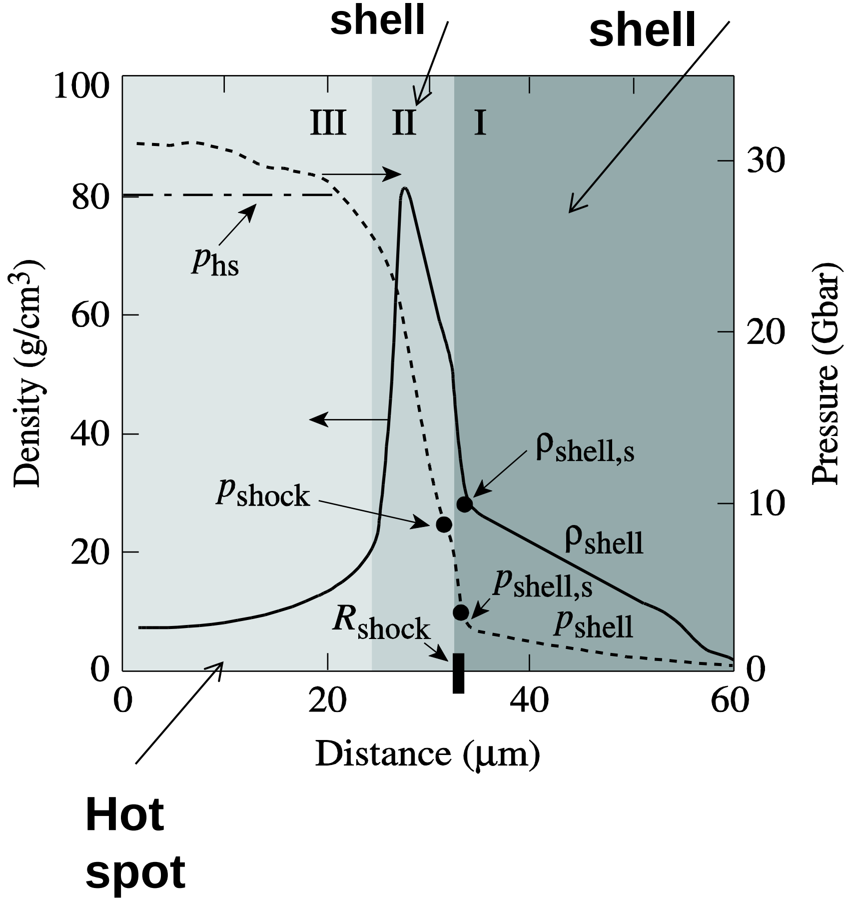

Hot-spot failure mechanisms

- Too much mass in the hot-spot (vapor) prior to deceleration
- short-scale mix/jets mix cold DT and ablator into hot-spot
- Excessive shell relaxation (rarefaction) at the inner fuel boundary (EOS, secondary shocks …)

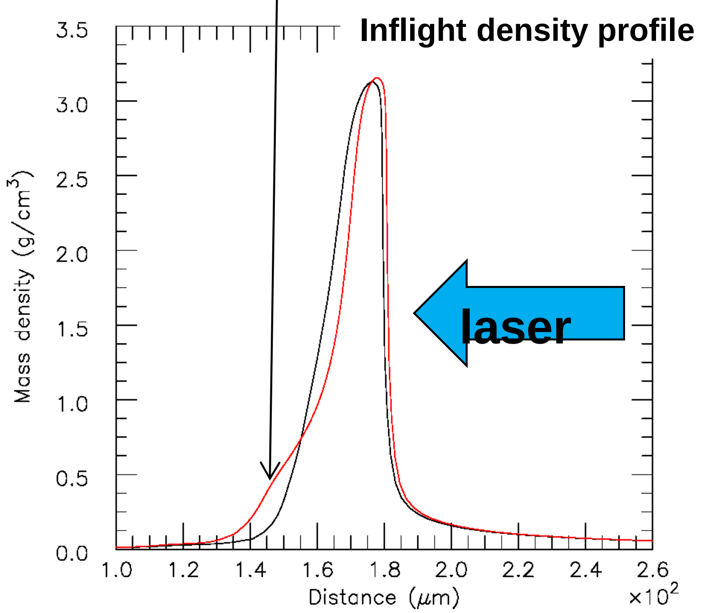

Hot-spot failure mechanisms

- **Too much mass in the hot-spot (vapor) prior to deceleration**

- **short-scale mix/jets mix cold DT and ablator into hot-spot**
- **Excessive shell relaxation (rarefaction) at the inner fuel boundary (EOS, secondary shocks …)**
- **This leads to an increase in hot-spot internal energy at peak burn, but reduces pressure, rR, and yield**

Hot-spot failure mechanisms

- **Too much mass in the hot-spot (vapor) prior to deceleration**
- **short-scale mix/jets mix cold DT and ablator into hot-spot**
- **Excessive shell relaxation (rarefaction) at the inner fuel boundary (EOS, secondary shocks …)**
- **This leads to an increase in hot-spot internal energy at peak burn, but reduces pressure, rR, and yield**

- **Incoming shell density is too low (ineffective piston)**
- **short-scale mix at abl front, preheat increase effective shell adiabat (both fuel and ablator)**

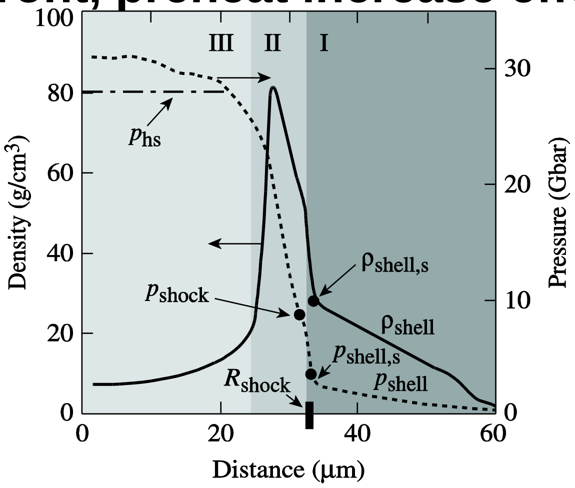

$\rho_{shell,s}$, P_{shock} low -> strong deceleration

Hot-spot failure mechanisms

- Too much mass in the hot-spot (vapor) prior to deceleration
- short-scale mix/jets mix cold DT and ablator into hot-spot
- Excessive shell relaxation (rarefaction) at the inner fuel boundary (EOS, secondary shocks …)
- This leads to an increase in hot-spot internal energy at peak burn, but reduces pressure, rR, and yield
- Incoming shell density is too low (ineffective piston)
- short-scale mix at abl front, preheat increase effective shell adiabat (both fuel and ablator)
- Excessive long-wavelength shell modulation growth during deceleration

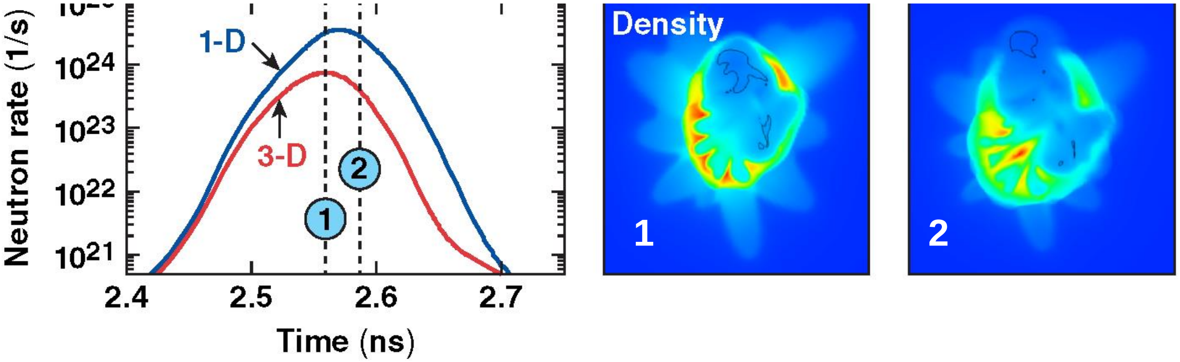

Hot-spot failure mechanisms

- Too much mass in the hot-spot (vapor) prior to deceleration
- short-scale mix/jets mix cold DT and ablator into hot-spot
- Excessive shell relaxation (rarefaction) at the inner fuel boundary (EOS, secondary shocks,…)
- This leads to an increase in hot-spot internal energy at peak burn, but reduces pressure, rR, and yield
- Incoming shell density is too low (ineffective piston)
- short-scale mix at abl front, preheat increase effective shell adiabat (both fuel and ablator)
- Excessive long-wavelength shell modulations during deceleration
- Hot-spot confinement by shell is compromised, V_c increases while majority of the shell still moves in, leads to RKE

There is residual kinetic energy at peak neutron production even in 1-D

Peak neutron production, E_{hs} <~ $E_{kin,\ shell}$

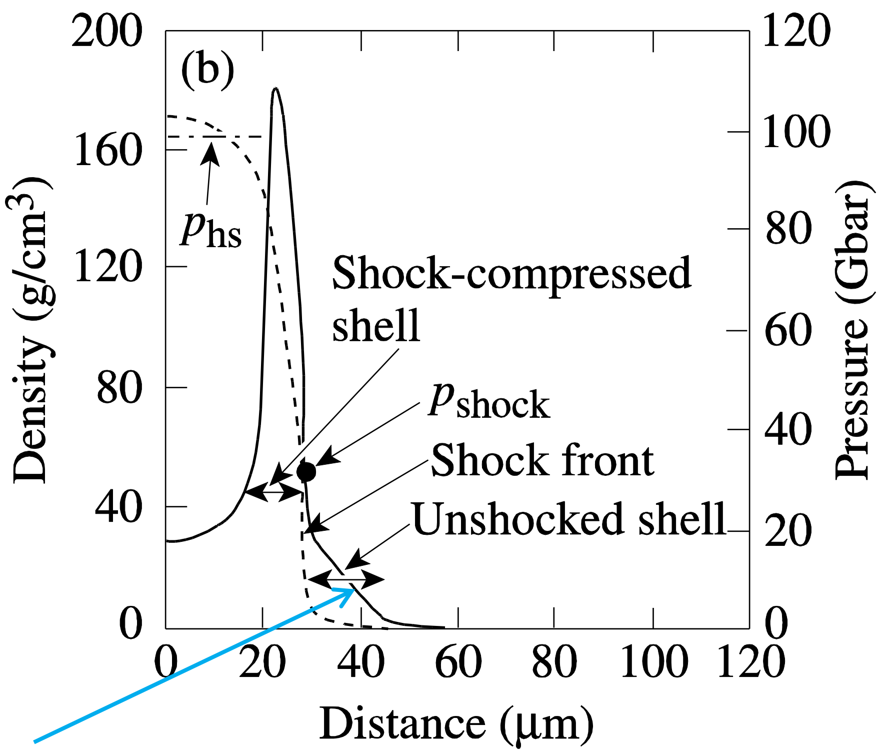

Unconverted shell energy

15%-20% of shell kinetic energy is not converted at peak burn in 1-D

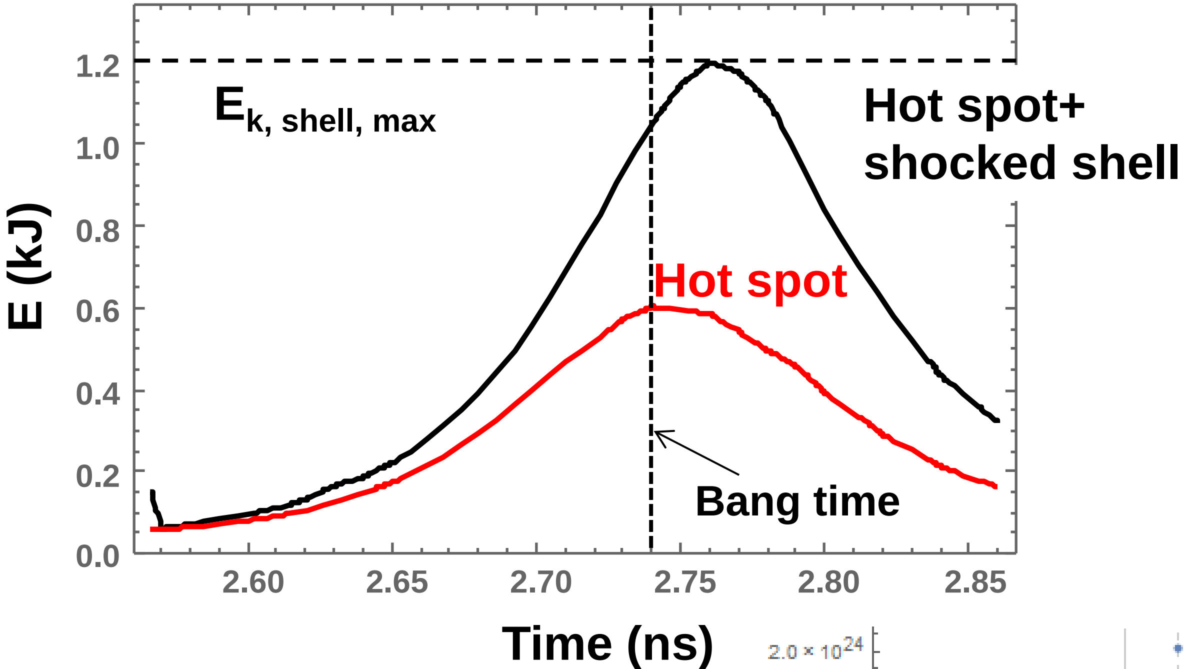

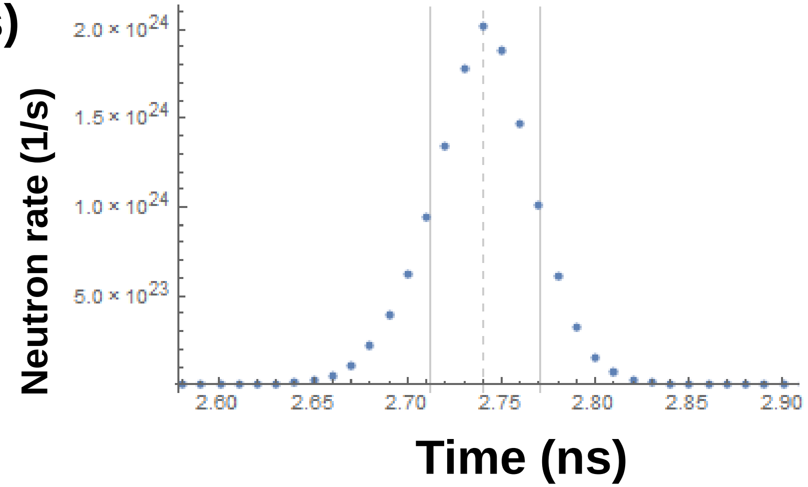

Hot-spot energy during deceleration increases as Cr^2

$$PV_{hs}^{\frac{5}{3}} = const, \qquad E_{hs} \sim PV_{hs} \sim V_{hs}^{-\frac{2}{3}} \sim R_{hs}^{-2} \sim Cr^2$$

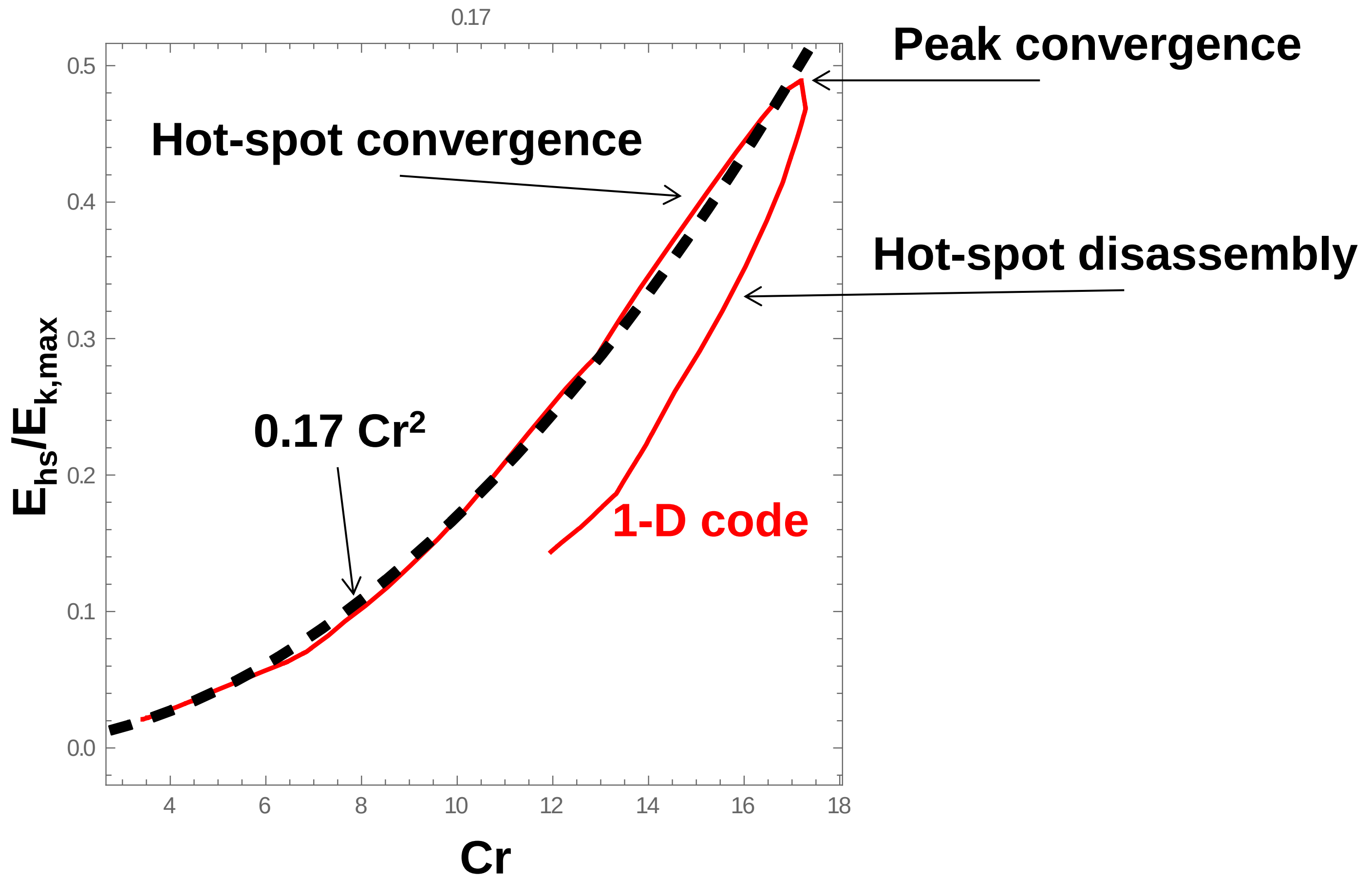

Hot-spot acceleration reaches maximum at Cr~14

Final stage. Shell nonuniformity growth can prevent E_{hs} gain

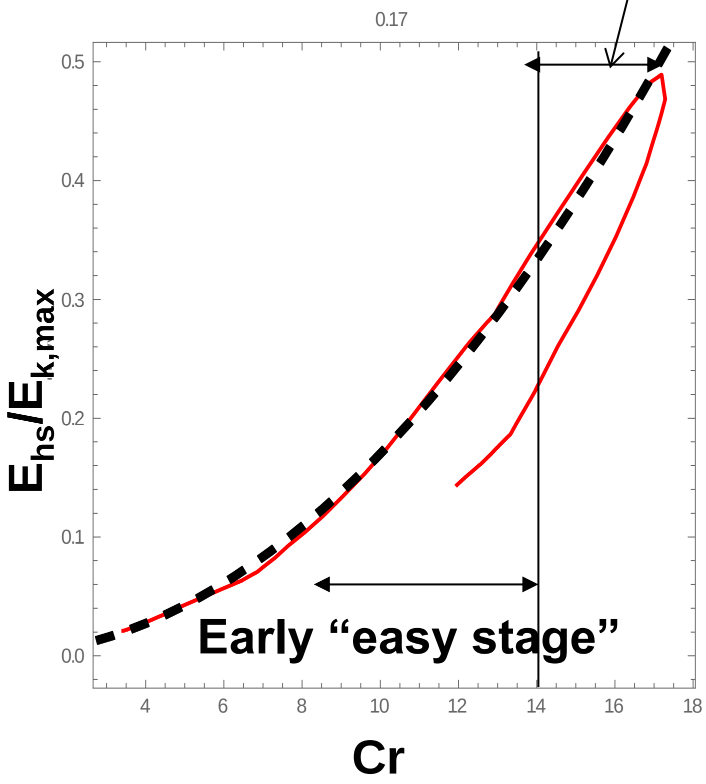

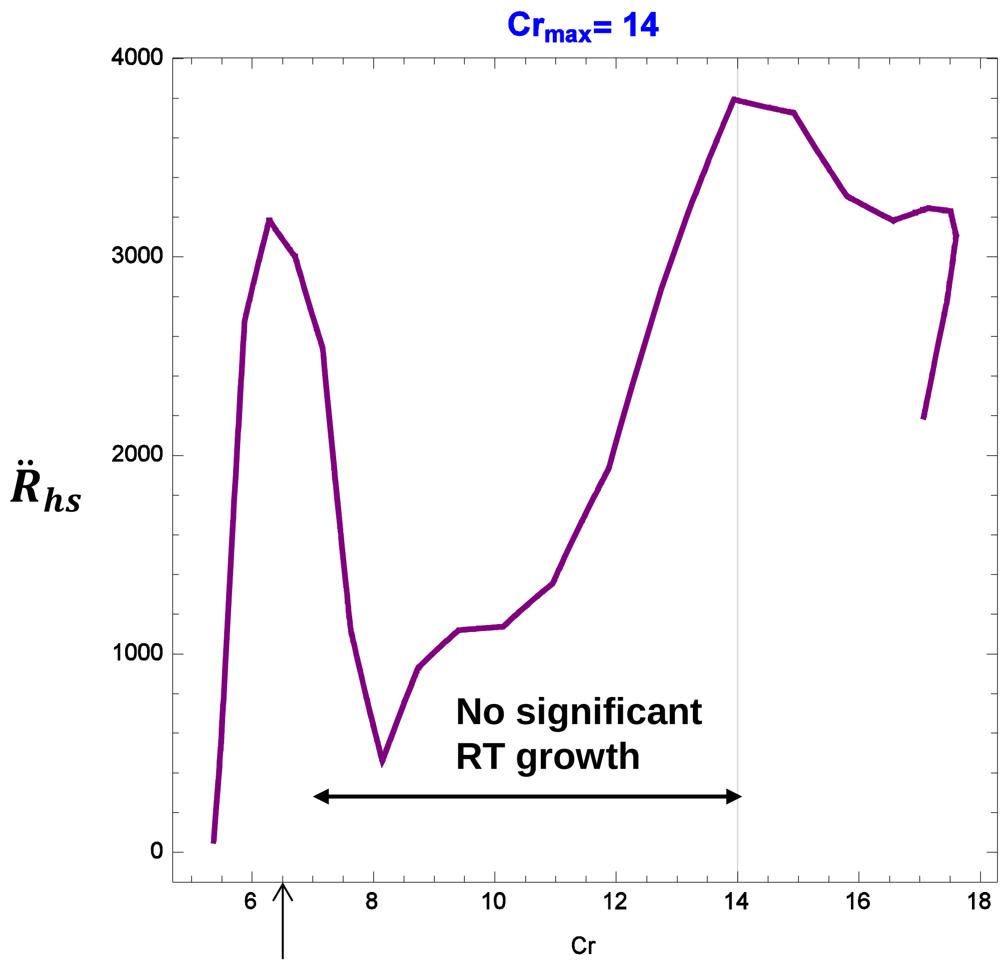

Deceleration onset

Code simulations and experimental data suggest a strong performance degradation in the final stage of hot-spot formation

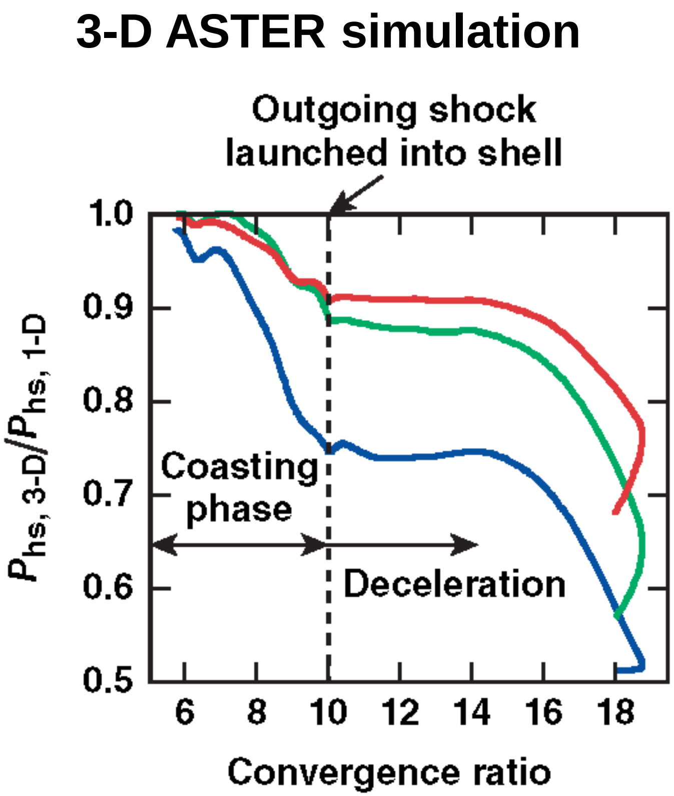

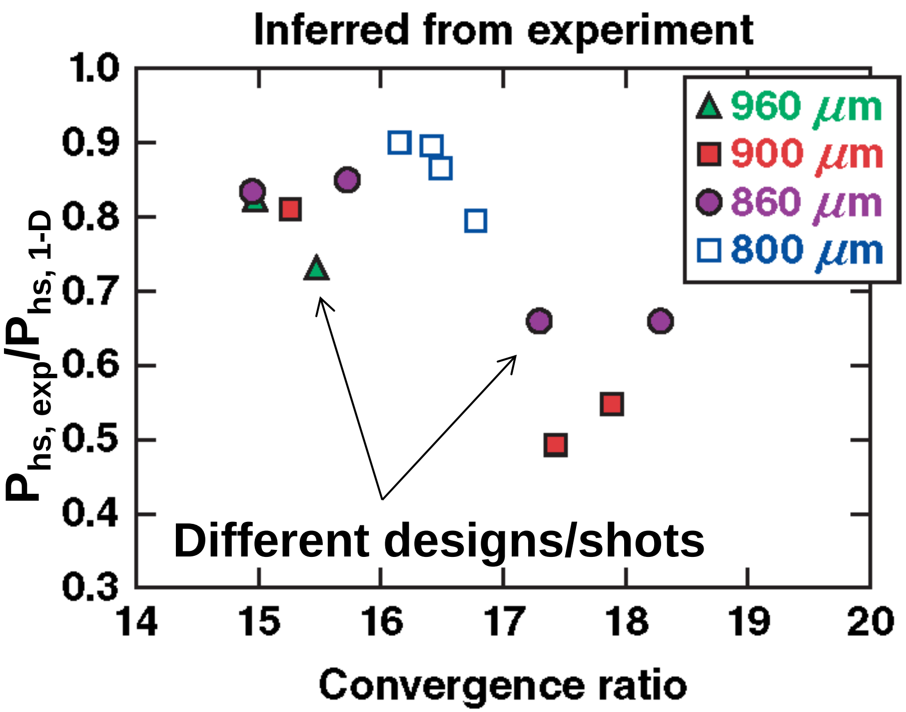

Higher hot-spot mass at the onset of deceleration leads to larger hot-spot energy at peak burn

Larger vapor mass leads to stronger shell deceleration

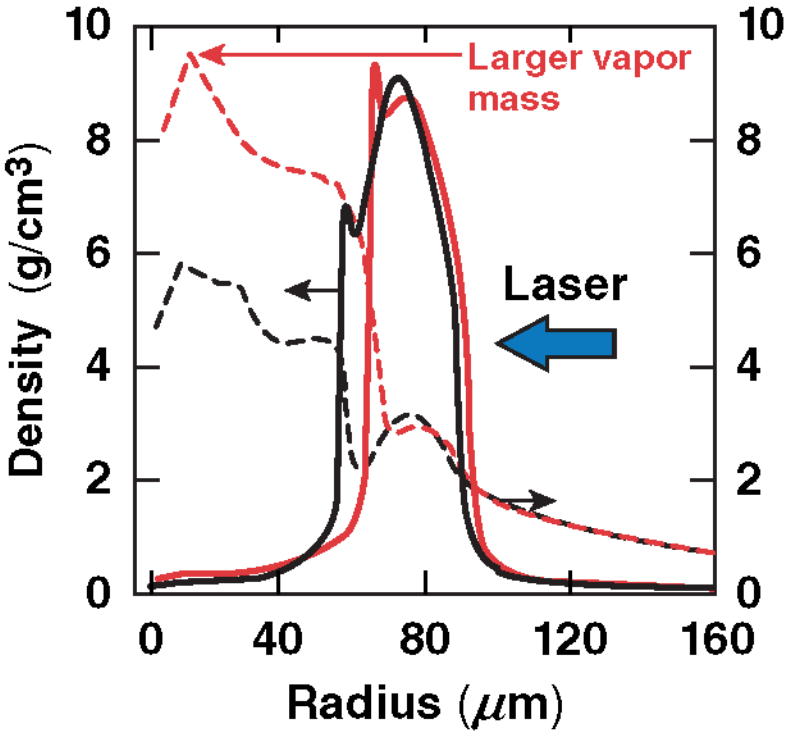

A shell with more vapor mass stagnates at a larger radius

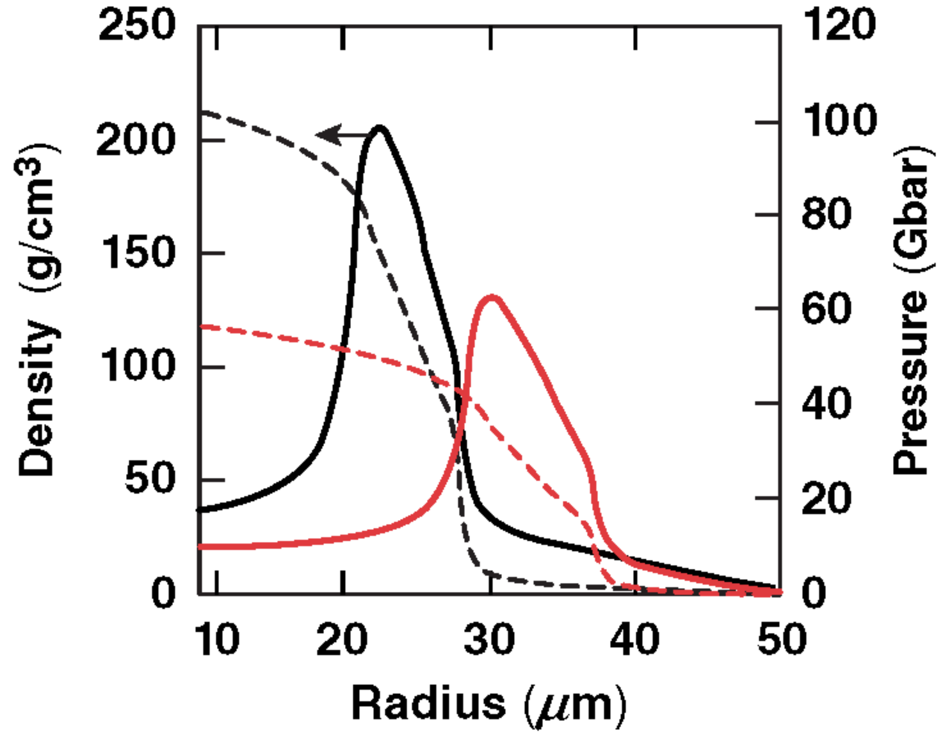

Internal energy partition between shocked shell and hot spot depends on shell aspect ratio at peak burn

$$E_{hs} \simeq \frac{3}{2}\frac{4\pi}{3}P_{hs}R_{hs}^3$$

$$E_{shocked\ shell} \sim \frac{3}{2}\frac{4\pi P_{hs}R_{hs}^2\Delta R}{2}$$

$$\frac{E_{hs}}{E_{sh.s}} \simeq \frac{2}{3}(R_{hs}/\Delta R)$$

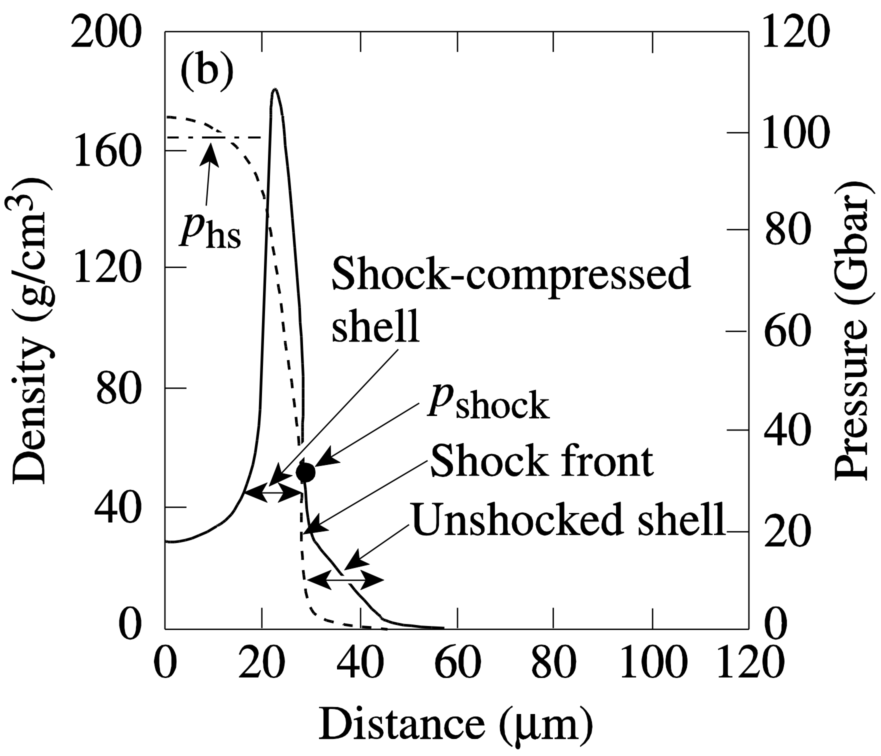

In this example: $R_{hs}/\Delta R$~2, $E_{hs}/E_{sh.s}$~4/3

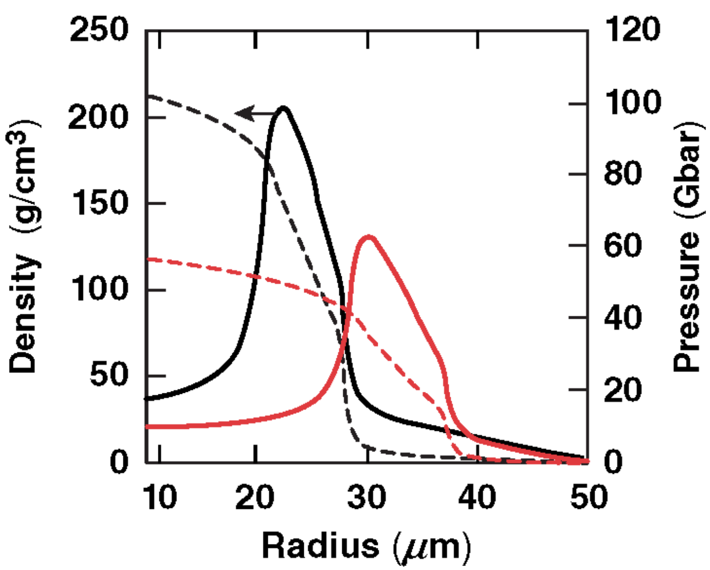

ΔR is similar, $E_{hs}/E_{sh.s}$~ R_{hs}

Higher hot-spot mass at the onset of deceleration leads to larger hot-spot energy at peak burn

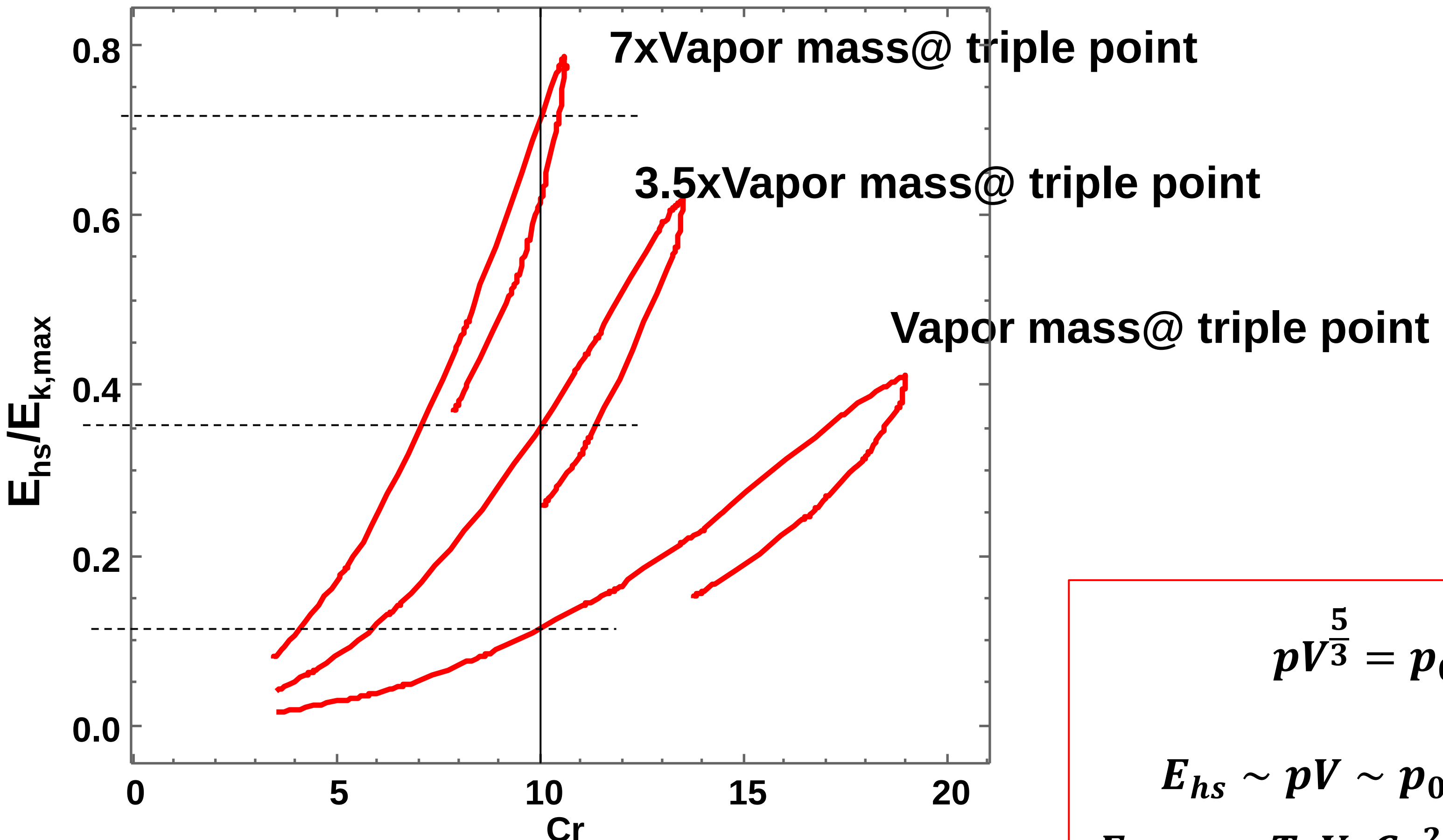

$$pV^{\frac{5}{3}} = p_0 V_0^{\frac{5}{3}}$$

$$E_{hs} \sim pV \sim p_0 V_0 \left(\frac{V_0}{V}\right)^{\frac{2}{3}}$$

$$E_{hs} \sim \rho_0 T_0 V_0 Cr^2 \sim M_0 T_0 Cr^2$$

Hot-spot energy~ (initial hot-spot mass) x Cr^2

Higher hot-spot mass at the onset of deceleration leads to larger hot-spot energy at peak burn,… but reduced target performance

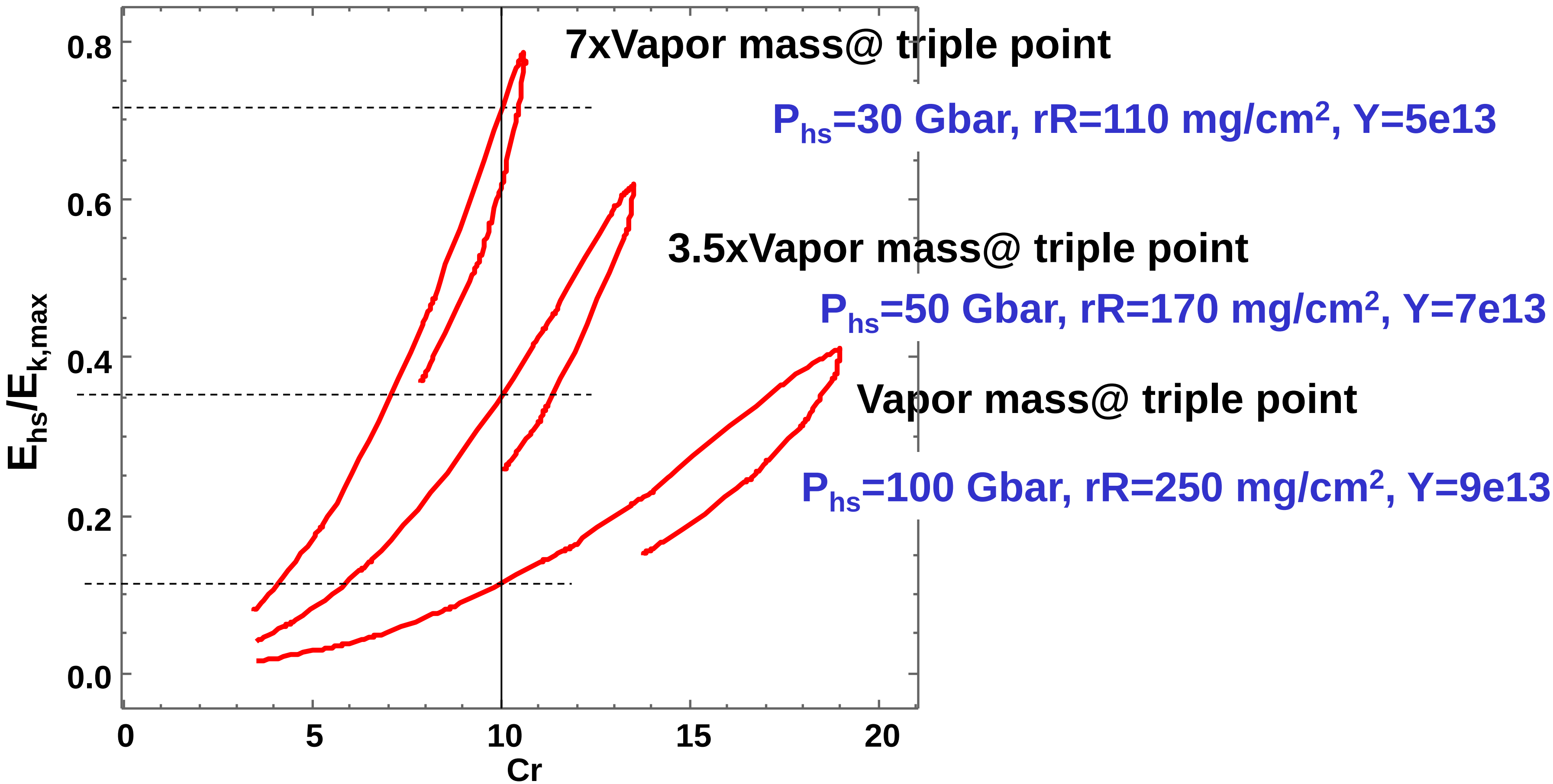

Measurements relevant to hot-spot formation physics

- **Inflight shell density profile (especially gradients on the back)**
- **Affects initial hot-spot mass**
- **Piston effectiveness (low shell density leads to early hs stagnation)**

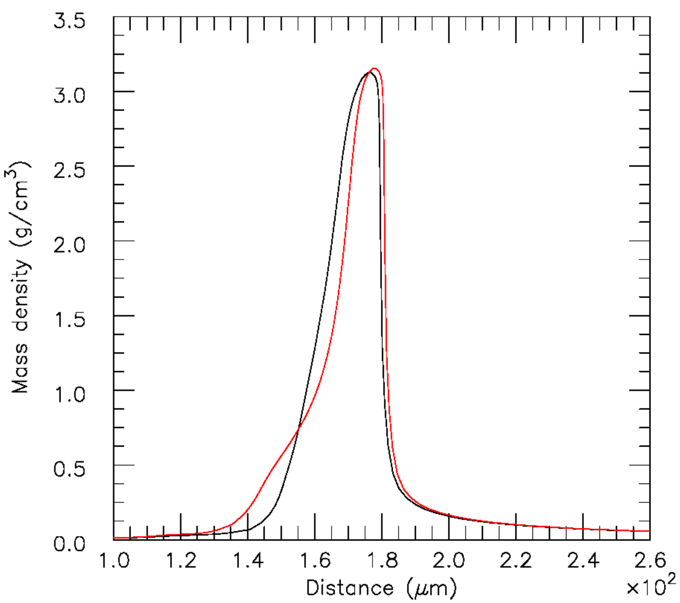

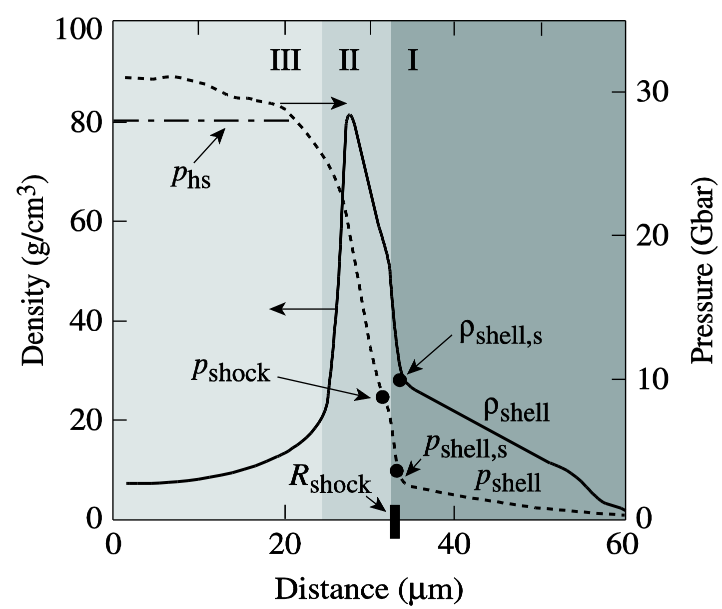

Measurements relevant to hot-spot formation physics

- Inflight shell density profile (especially gradients on the back)
  - Affects initial hot-spot mass
  - Piston effectiveness (low shell density leads to early hs stagnation)
- Cold shell position and geometry
  - Helps resolving hot-spot energy partition by inferring volume of "dark" central region

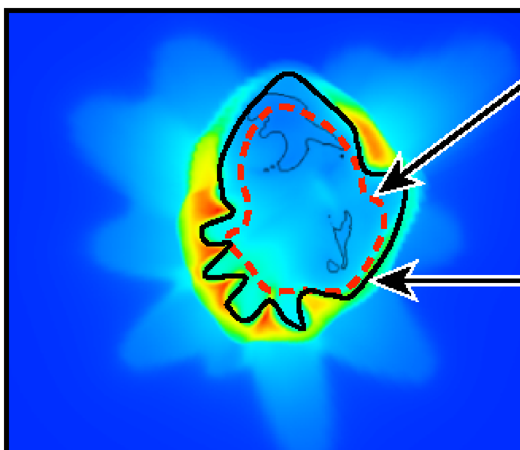

Hot spot, $V_{hs,\,3\text{-}D} < V_{hs,\,1\text{-}D}$

Neutron rate $\sim P_{hs}^2 \frac{\langle \sigma v \rangle}{T^2} V_{hs}$

Central region, $V_{c,\,3\text{-}D} > V_{c,\,1\text{-}D}$

Hot-spot pressure evolves as $P_{hs} \sim V_c^{-5/3}$

Measurements relevant to hot-spot formation physics

- Inflight shell density profile (especially inner surface gradients)
- Affects initial hot-spot mass
- Piston effectiveness (low shell density leads to early hs stagnation)
- Cold shell position and geometry
- Helps resolving hot-spot energy partition by inferring volume of "dark" central region
- "True" (hydrodynamic) ion temperature excluding effect of bulk flow
- Helps resolving pot-spot energetics

OMEGA Direct-Drive DT layered cryogenic implosions: hot-spot size, neutron rate, ion temperature

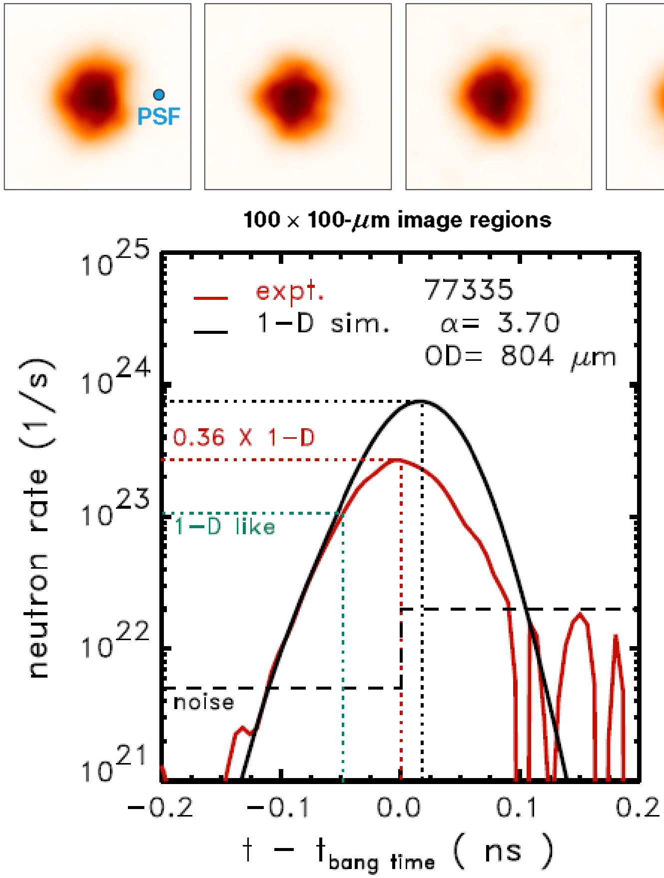

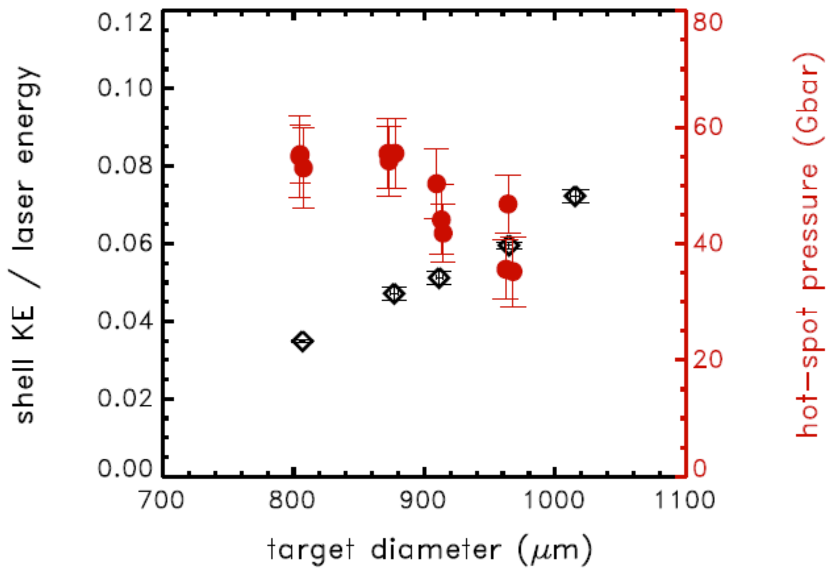

S. P. Regan
Laboratory for Laser Energetics
University of Rochester

National Implosion
Stagnation Physics Group
LLNL
27-28 October 2015

University of Rochester

OMEGA Direct-Drive DT layered cryogenic implosions: hot-spot size, neutron rate, ion temperature

OMEGA Direct-Drive DT layered cryogenic implosions

Diagnostic development for 50 Gbar campaign

- **16 channel, gated Kirkpatrick-Baez microscope (KBFRAMED)**
- **Neutron temporal diagnostic (P11NTD)**

Path to 100 Gbar

- **Laser, target, diagnostic upgrades**

Collaborators

V. N. Goncharov, T. C. Sangster, R. Epstein, P. B. Radha, R. Betti,
T. R. Boehly, R. Earley, C. J. Forrest, D. H. Froula, V. Yu Glebov, D. R. Harding,
E. M. Hill, S. X. Hu, I. V. Igumenshchev, R. T. Janezic, J. H. Kelly, T. J. Kessler,
J. P. Knauer, T. Z. Kosc, J. Kwiatkowski, J. A. Marozas, F. J. Marshall,
R. L. McCrory, P. W. McKenty, D. T. Michel, J. F. Myatt,
J. Puth, N. Redden, J. Reid, W. Seka, W. T. Shmayda, A. Shvydky,
C. Stoeckl, and M. D. Wittman, W. Theobald, E. M. Campbell

University of Rochester
Laboratory for Laser Energetics

J. A. Frenje, M. Gatu Johnson, and R. D. Petrasso

Massachusetts Institute of Technology

D. D. Meyerhofer

Los Alamos National Laboratory

S. P. Obenschein, M. Karasik, J. Weaver, and A. Schmitt

Naval Research Laboratory

OMEGA cryogenic implosions are hydrodynamically scaled from symmetrically-symmetric, direct-drive ignition designs

1.5-MJ, spherically symmetric direct-drive design

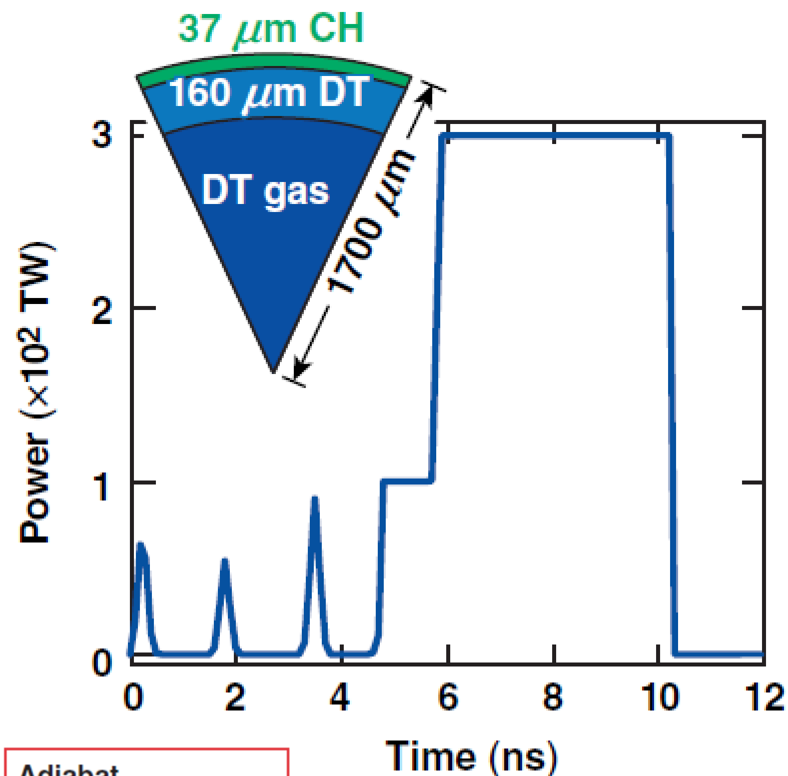

26-29 kJ OMEGA DT cryogenic target design

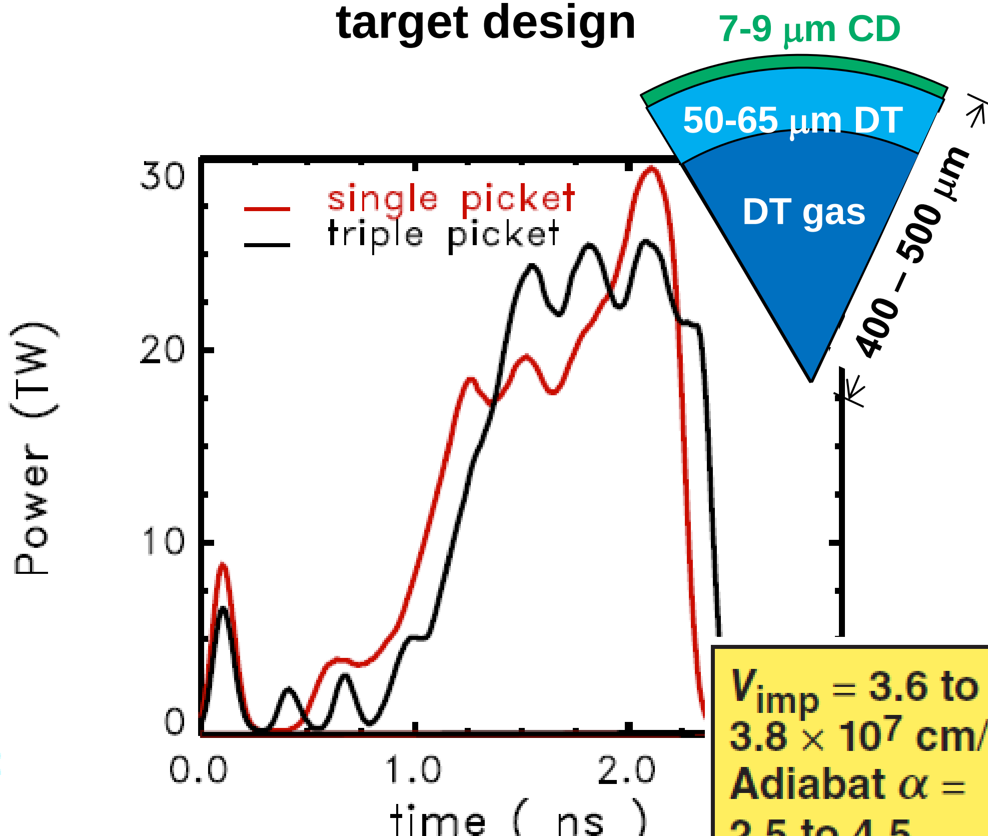

V_{imp} = 3.6 to 3.8 × 10⁷ cm/s
Adiabat α = 2.5 to 4.5
CR = 20 to 23
IFAR = 15 to 25

Adiabat
$\alpha = P/P_{Fermi}$

IFAR = shell radius/ shell thickness

E~R³, P~R², t~R

A technique to reduce CBET by increasing the initial target diameter while keeping fixed the single beam laser spot size (ϕ=820 μm) was examined

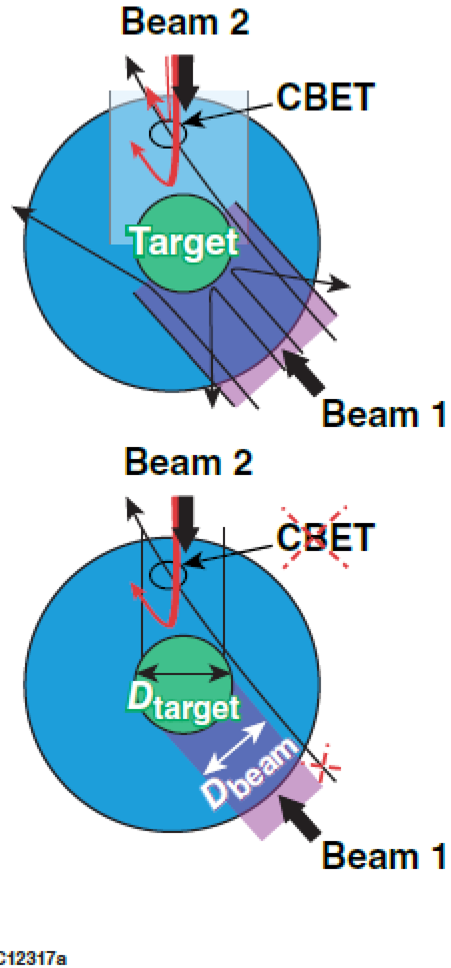

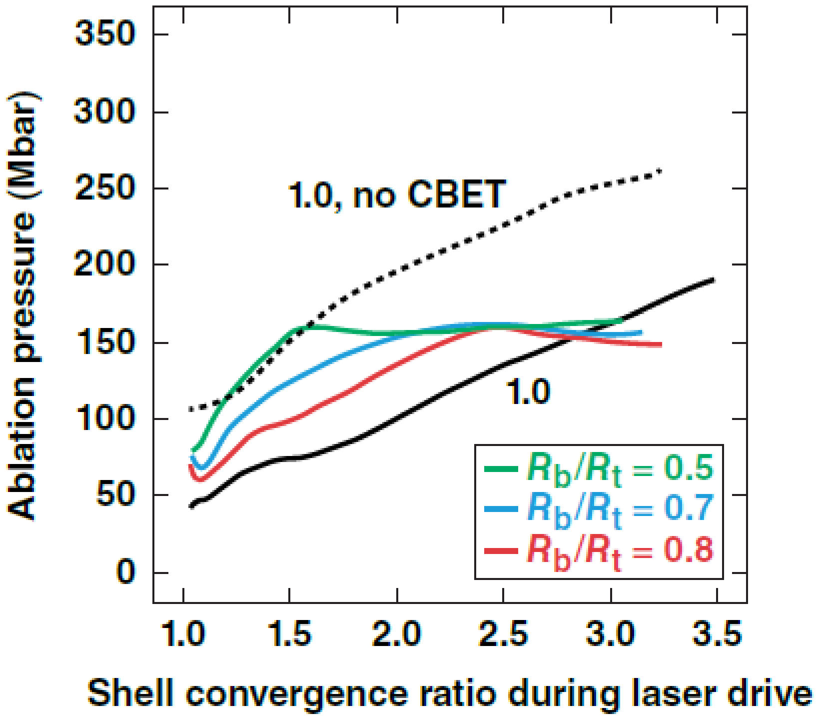

CBET reduces the drive pressure by 40% on OMEGA and 60% at the National Ignition Facility (NIF).

* V. N. Goncharov et al., Phys. Plasmas 21, 056315 (2014).
**I. V. Igumenshchev et al., Phys. Plasmas 17, 122708 (2010).

A primary DT neutron yield of ~5 x 10^{13} with a ρR of ~200 mg/cm^2 has been recorded in this campaign

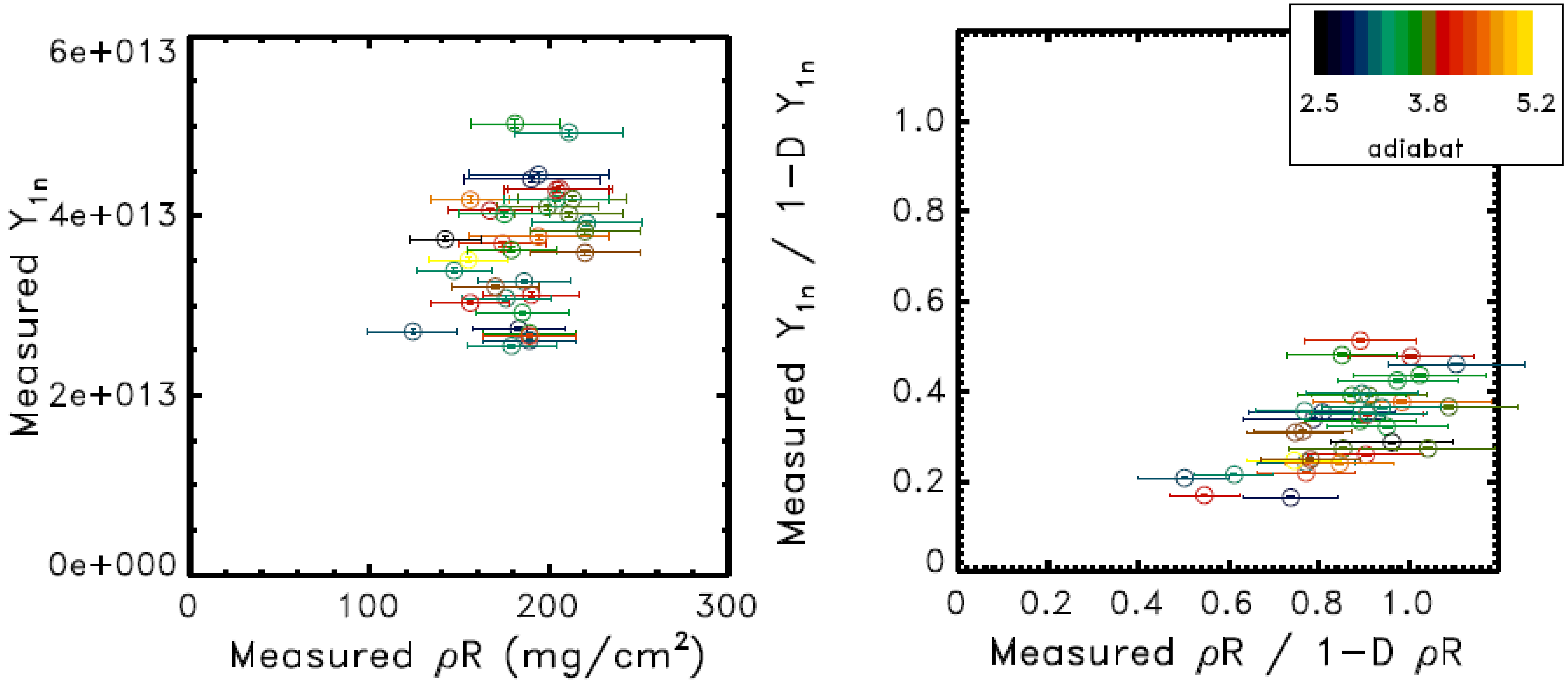

YOC ≡ measured Y_{1n} / 1-D Y_{1n} = 0.2 to 0.6;
ρROC ≡ measured ρR / 1-D rR = 0.5 to 1

ρR is diagnosed with a neutron time-of-flight (nTOF) detector and the magnetic recoil spectrometer (MRS)

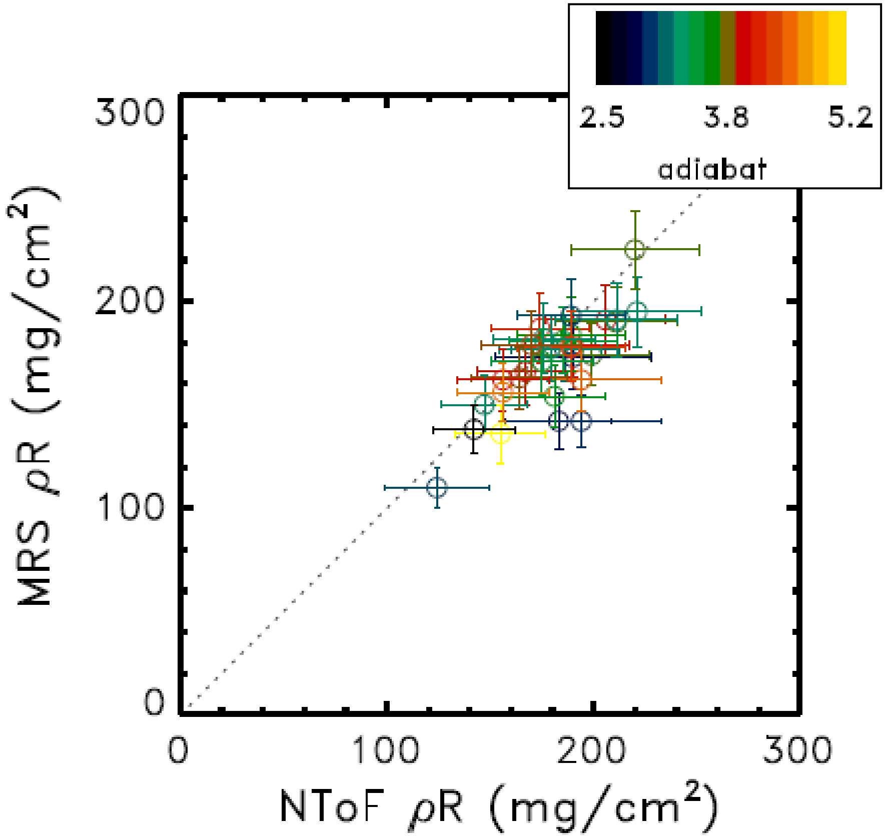

Difference in the areal density along the two lines of sight is attributed to a spatial variation in the areal density due to non-uniform laser drive

Hot-spot pressure is inferred from the measured hot-spot size, burnwidth, $\langle T_i \rangle$, and neutron yield

UR LLE

$$\text{Yield} = \int_{\Delta t_{burn}} dt \int_{V_{hs}} n_D\, n_T \langle \sigma v \rangle\, dV$$

$$\text{Yield} \sim \underbrace{n_D\, n_T}_{} \ldots$$

$$\underbrace{\text{Yield}}_{\text{Measured yield}} \sim \underbrace{n_D\, n_T T^2}_{P_{hs}^2} \underbrace{\left(\int_{V_{hs}} \frac{\langle \sigma v \rangle}{T^2} dV \right)}_{\text{Depends on measured } T_i \text{ and } V_{hs}} \underbrace{\Delta t_{burn}}_{\text{Measured burnwidth}}$$

Parameter	Measured	Limitations
T_i	Neutron time-of-flight (nTOF) detector	Bulk flow broadening; 3 lines-of-sight (LOS); ±0.3 keV
Yield	nTOF, Cu activation	5% error
Δt	NTD, neutrons	10% width error
	Sydor framing camera (SFC), x rays	Frame timing
V_{hs}	Time-resolved Kirkpatrick–Baez (KB), SFC3	±0.2 to 1.0 μm

$P_{hot\ spot}$>120-150 Gbar for direct-drive hot-spot ignition

TC12319a

KBFRAMED and P11NTD were critical diagnostics to infer the hot-spot pressure

KBFRAMED: 30 ps resolution, 6 um spatial resolution

P11NTD: 40 ps impulse response time

Framed X-Ray Imaging of Cryogenic Target Implosion Cores on OMEGA

F. J. MARSHALL, V. N. GONCHAROV, V. YU. GLEBOV, S. P. REGAN,
T. C SANGSTER, and C. STOECKL
University of Rochester, Laboratory for Laser Energetics

KBFRAMED is a 16-channel Kirkpatrick–Baez (KB) x-ray microscope that provides time-resolved images of the core around stagnation

Gate width: ~30 ps
Image to image: 15 to 60 ps
Spatial resolution: ~6 μm
Energy range: 2 to 8 keV

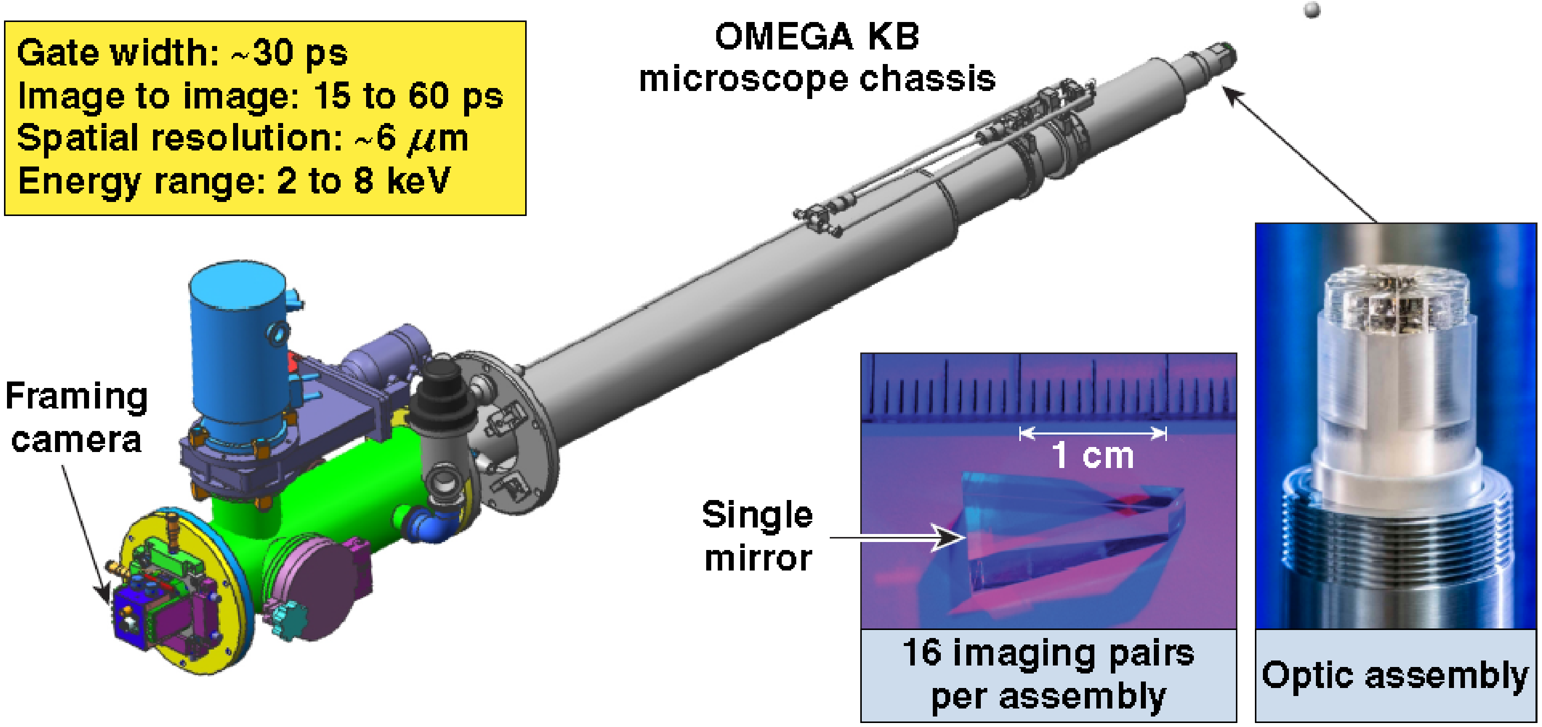

E22996b

F. J. Marshall, J. A. Oertel, and P. J. Walsh, Rev. Sci. Instrum. 75, 4045 (2004).

The KBFRAMED fixed port installation allows the framing-camera electronics and film back to be operated in air

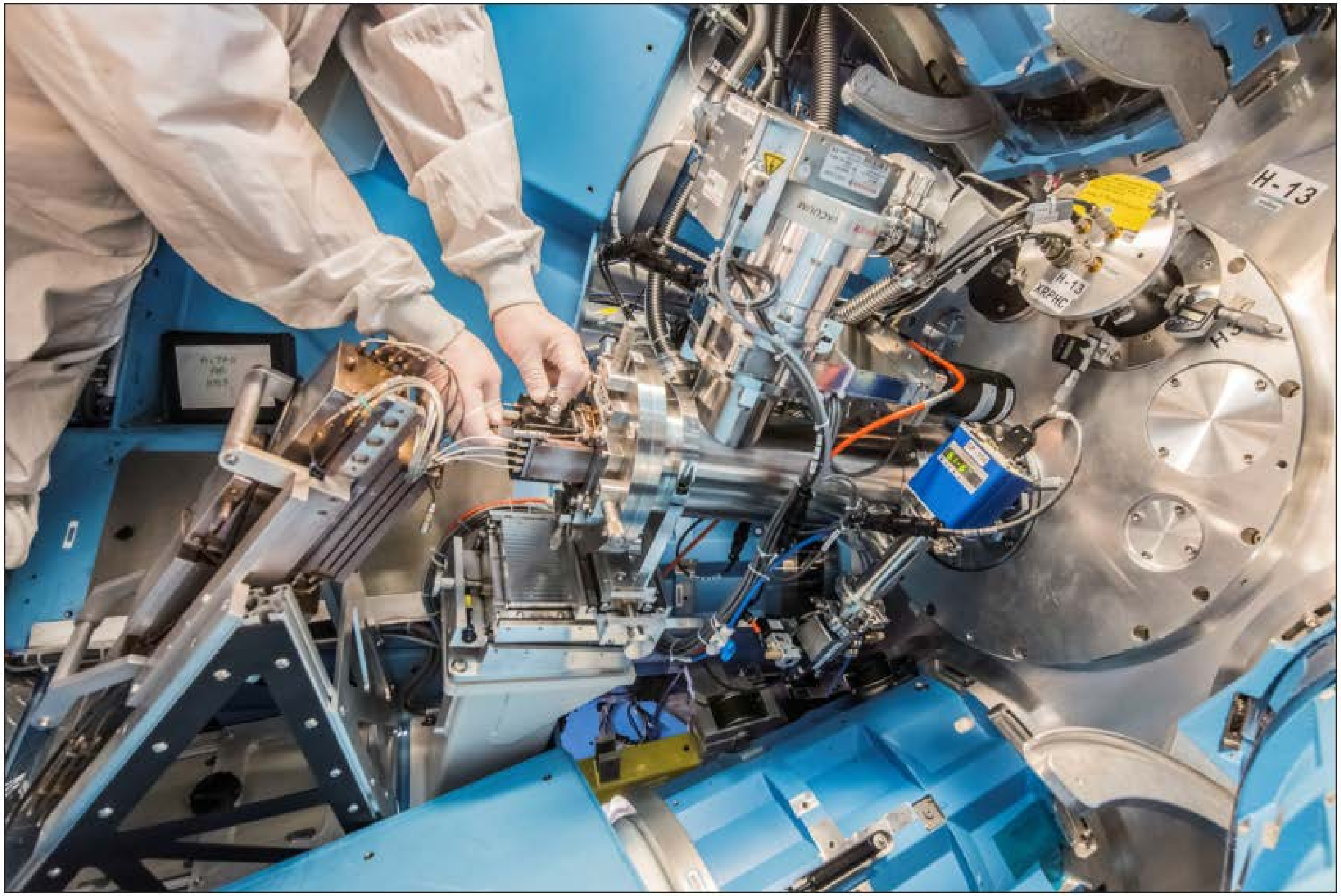

E24508

KBFRAMED optic magnification and framed resolution have been measured using an x-ray backlit grid on OMEGA

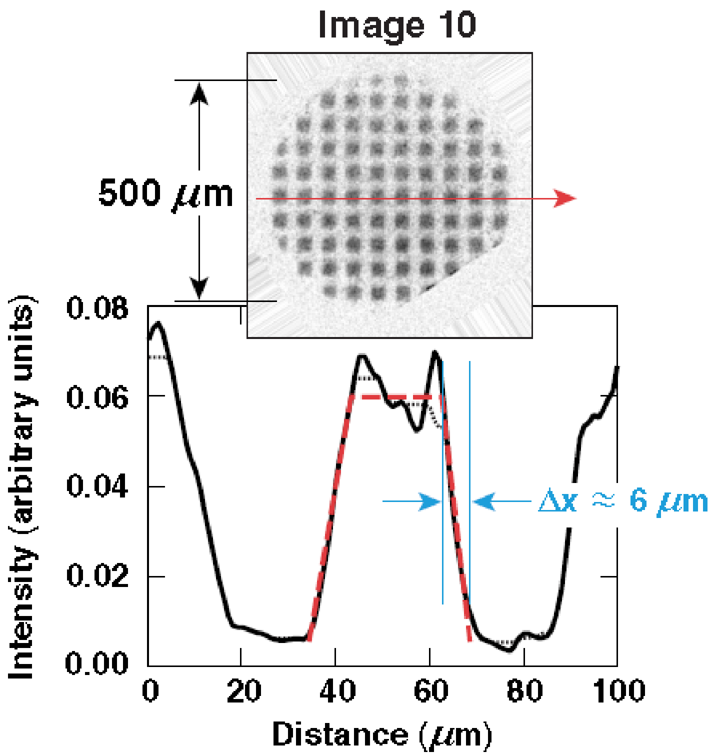

M = 12 with 6-μm resolution

KBFRAMED OMEGA shot 76806

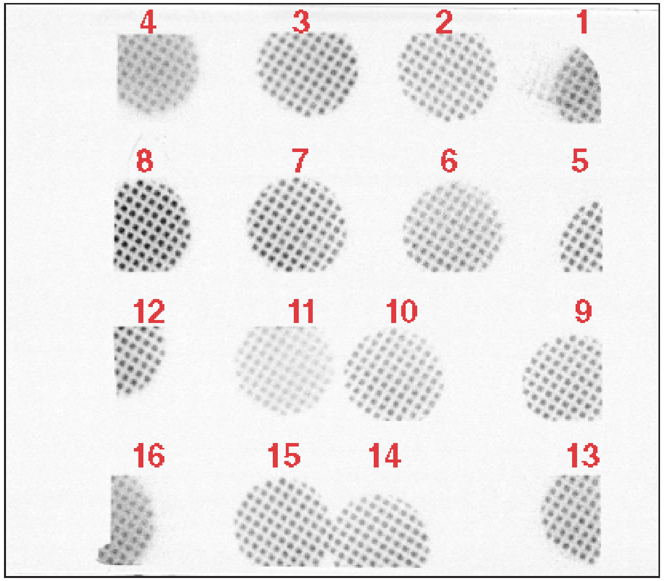

M = 12.0 within 1%
Resolution (FWHM* of the PSF**) ≈ 6 μm
varies from image to image

*FWHM: full width at half maximum
**PSF: point spread function

E23991

KBFRAMED records an image (Δt = 30 ps) of the stagnating core every ~15 ps in the 4- to 8-keV photon-energy range

OMEGA shot 76828

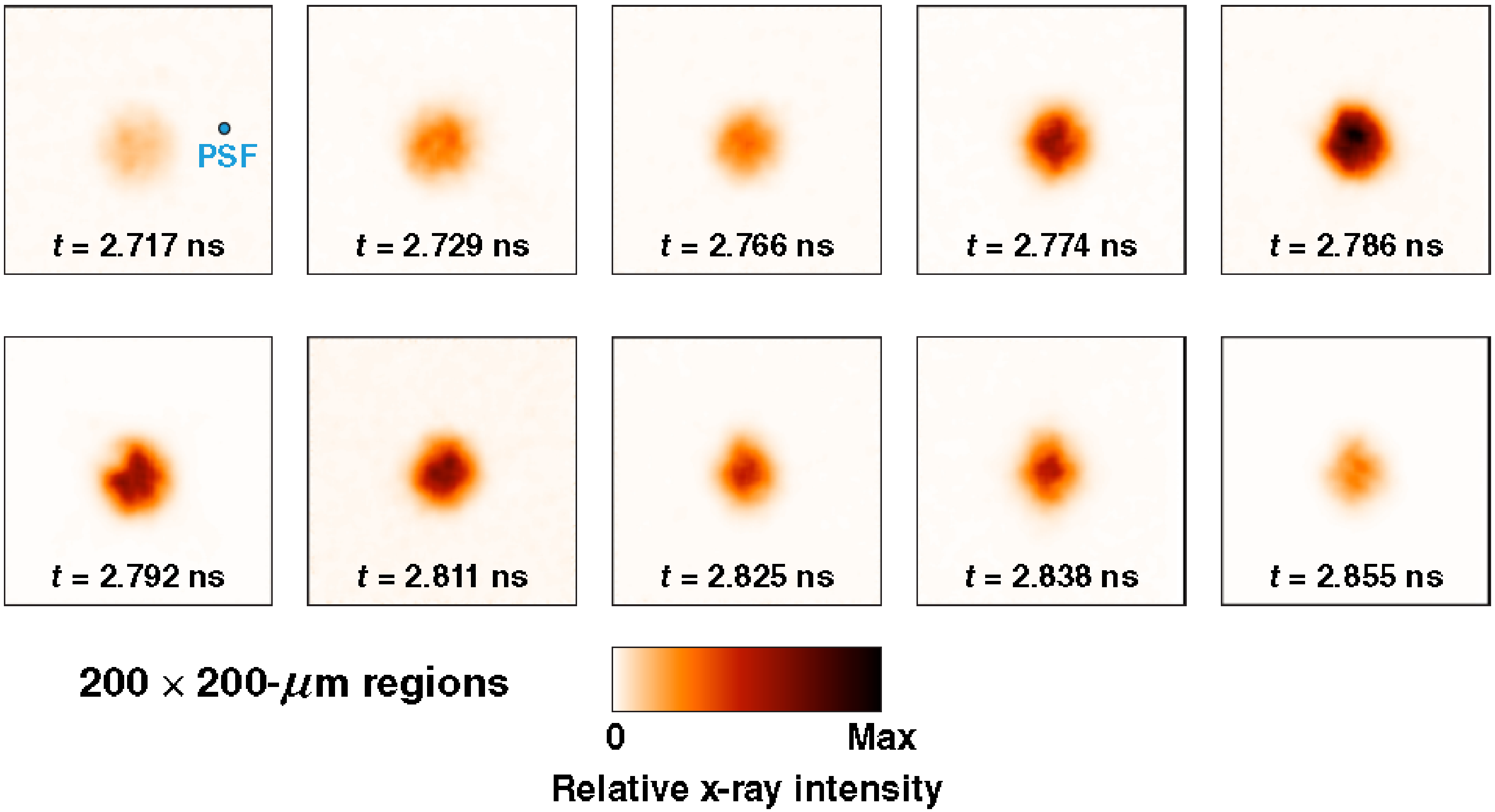

E24014a

The cryogenic-target implosion, hot-spot size is determined from an elliptical super-Gaussian fit

UR LLE

OMEGA shot 77064 KBFRAMED core image near peak compression

$$I = I_0 \times \exp\left[-\frac{(x - x_c)^2}{a^2} - \frac{(y - y_c)^2}{b^2}\right]^{n/2}$$

$$I^* = I \otimes PSF\,(x, y)$$

$$R_{1/e} = \sqrt{ab}$$

$$R_{17} = (1.77)^{1/n} \times R_{1/e}$$

Image | Super-Gaussian fit | Difference

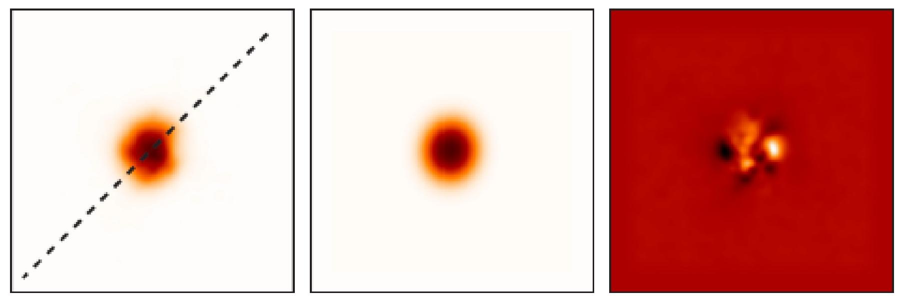

Lineout indicated by dotted line

200 × 200 μm regions

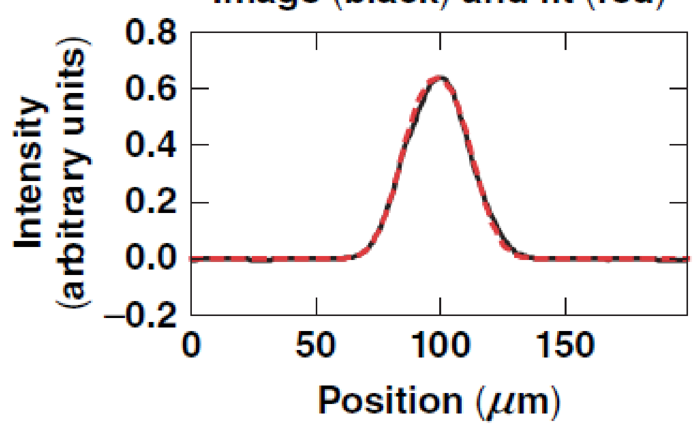

- Fit is to super-Gaussian Convolved with PSF (I^*)
- For KBFRAMED: PSF ≈ 6 μm FWHM Gaussian

E24509

Comparison of 17% of peak intensity contour (R17) for measurement and simulation

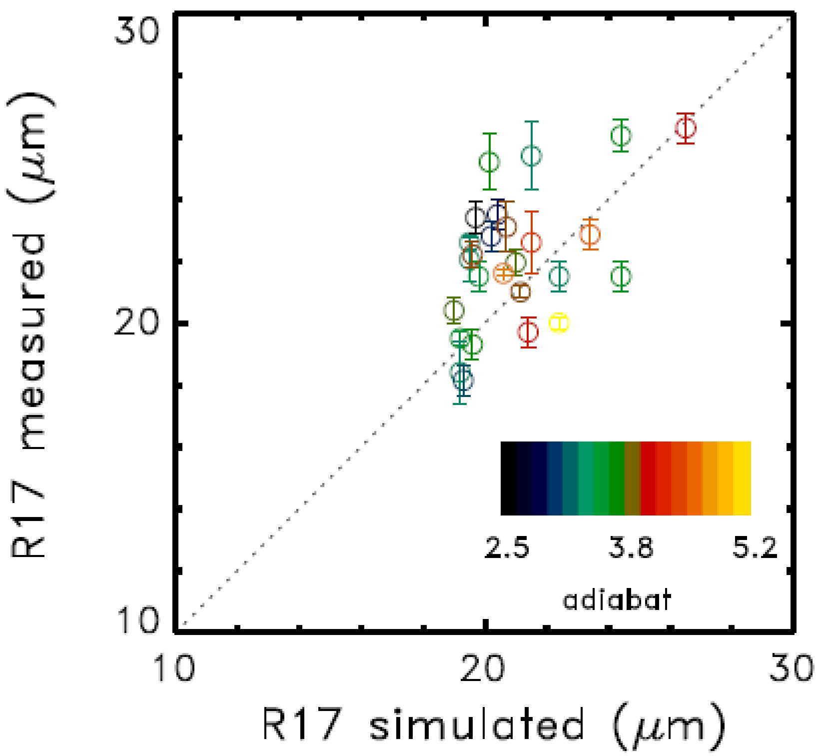

Comparison of rho-R with 1/R^2 scaling using R17

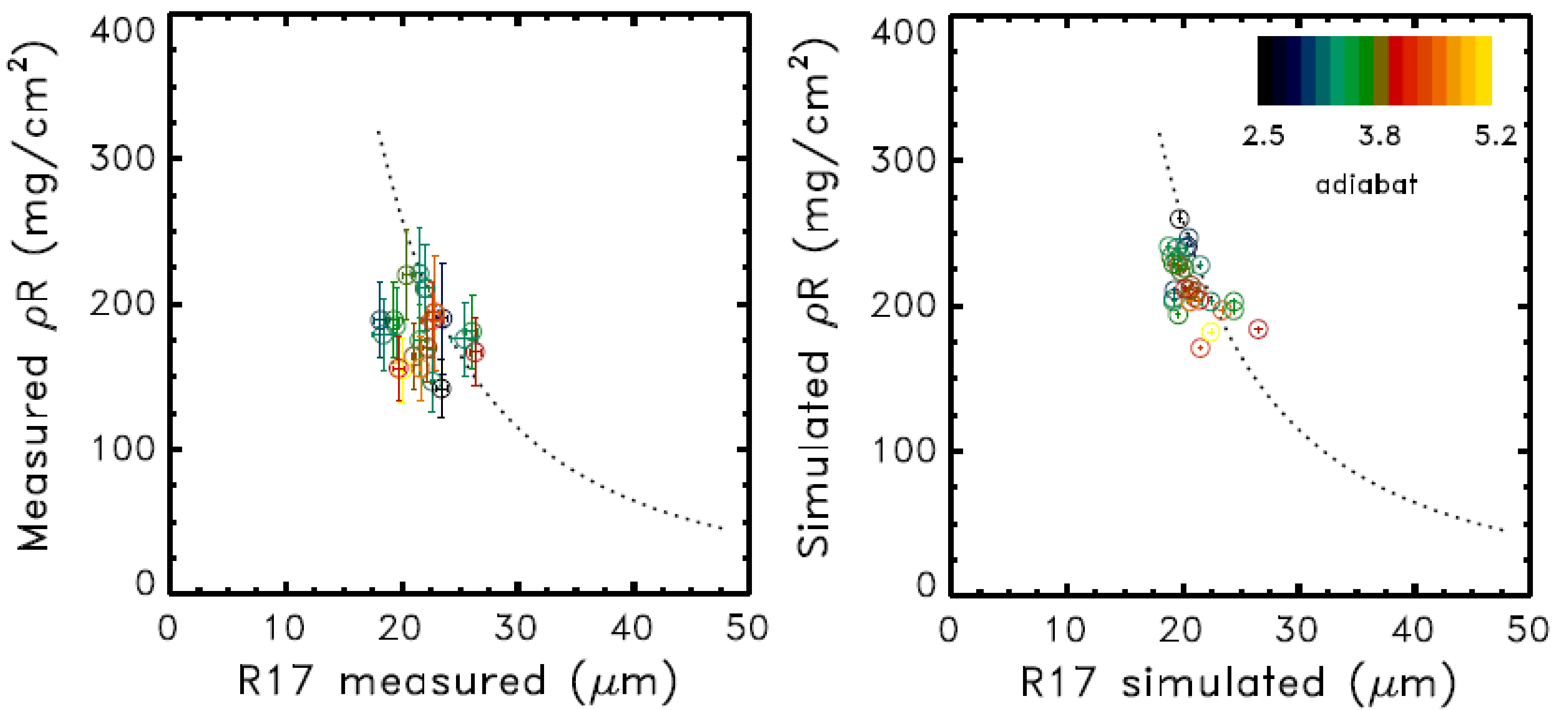

A Neutron Temporal Diagnostic for High-Yield DT Cryogenic Implosions on OMEGA

C. STOECKL, R. BONI, M. E. COUCH, F. EHRNE, C. J. FORREST, V. YU GLEBOV, J. KATZ, D. J. LONOBILE,
J. MAGOON, S. P. REGAN, M. J. SHOUP III, A. SORCE, C. SORCE, and T. C. SANGSTER
University of Rochester • Laboratory for Laser Energetics

The NTD measures the neutron production rate and bang time

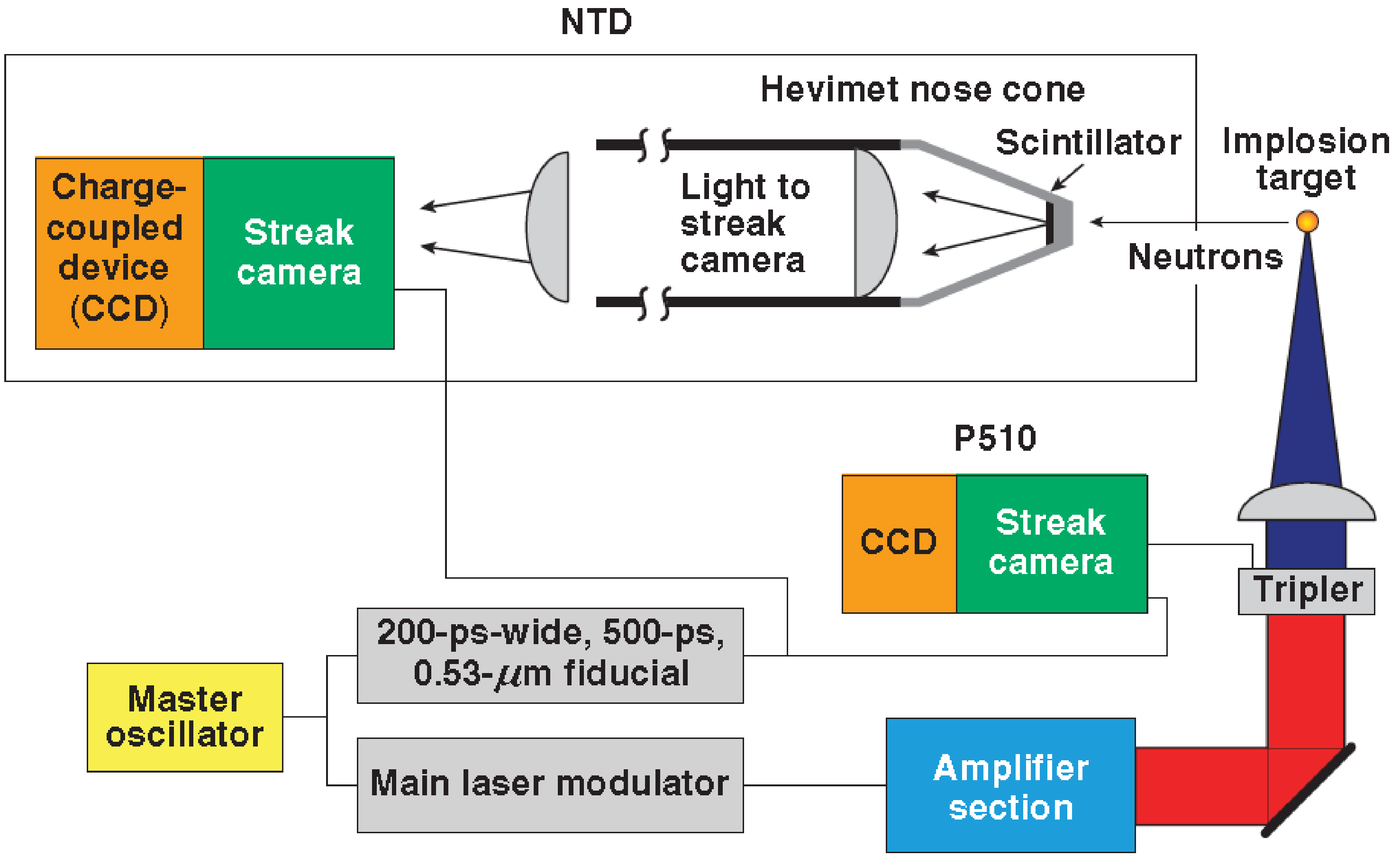

E23900a

The P11-NTD delivers the instrument performance required to support the current and future LLE cryogenic campaign

UR LLE

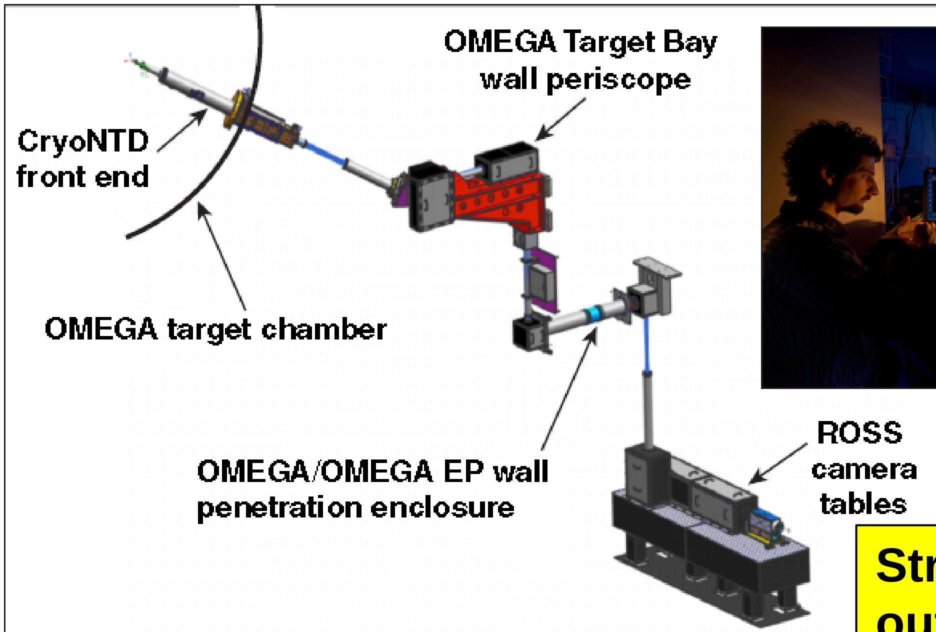

Streak camera is positioned outside of shield wall

Performance metric	Performance status
Minimum burnwidth	50 ps
Bang-time measurement accuracy	$\pm$50 ps
Detectable DD neutron-yield range	5×10^{9} to 1×10^{13}
Detectable DT neutron-yield range	5×10^{10} to 1×10^{15}

E23902a

The neutron production rate is inferred from the unfolded scintillator signal

CCD image

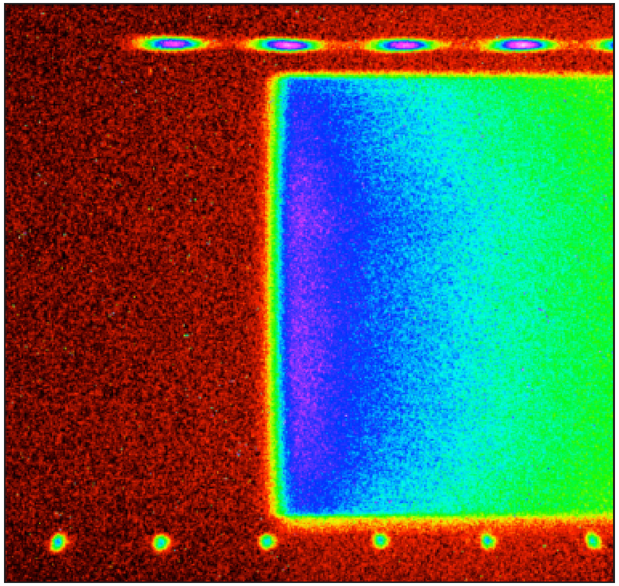

Data reduction

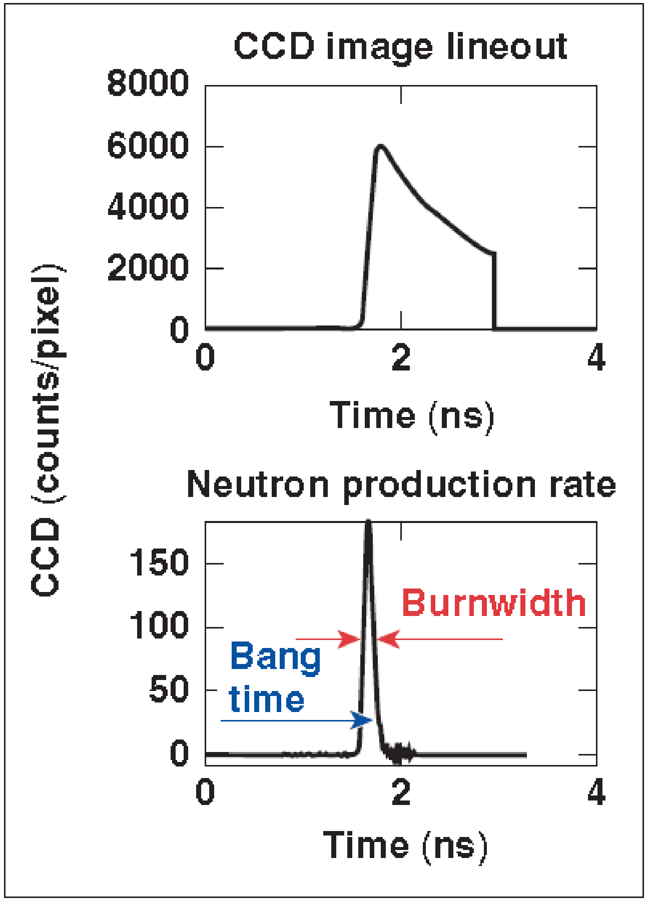

UNIVERSITY of ROCHESTER

With the standard 3-ns sweep window, P11-NTD has a measured impulse response of 40±10 ps

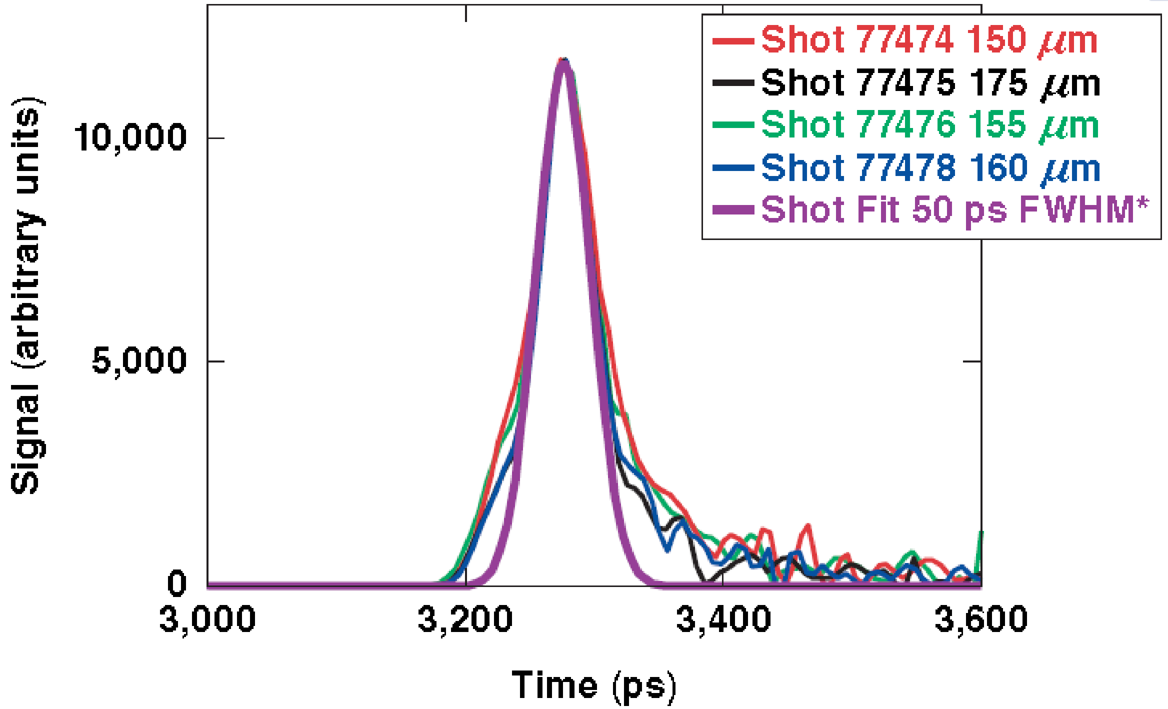

- Using an intrinsic width of the x-ray signal, 25±10 ps, the measured width of ~50 ps deconvolves to an impulse response of 40±10 ps
- The absolute timing of P11-NTD is calibrated against NTD with an accuracy of ~50 ps

*FWHM: full width at half maximum

E24385

Comparison of measured and simulated neutron burnwidth

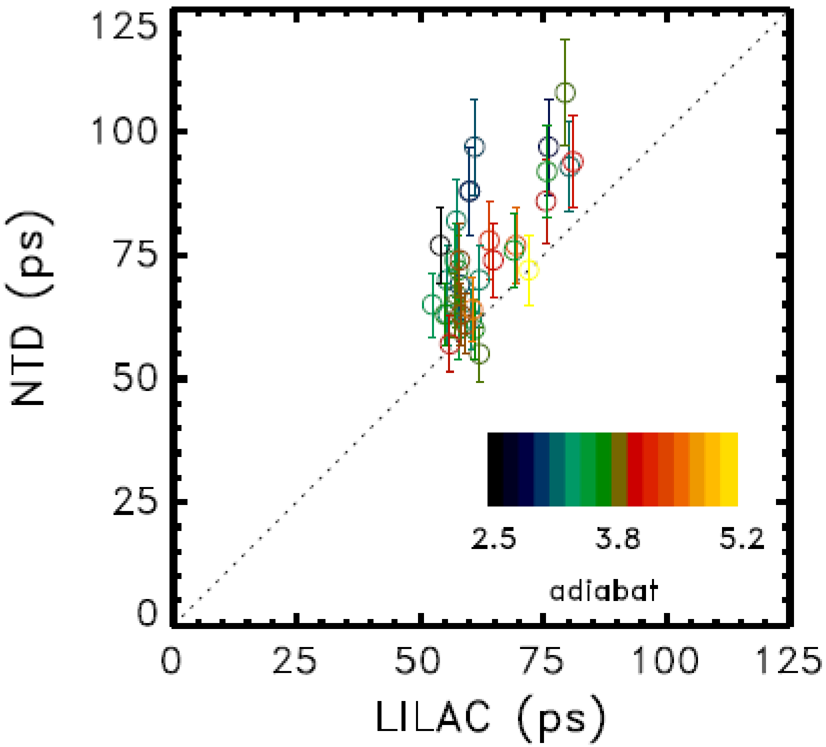

The neutron rate gives more insight than the neutron burn width

The onset of neutron burn truncation occurs earlier for implosions of larger diameter targets

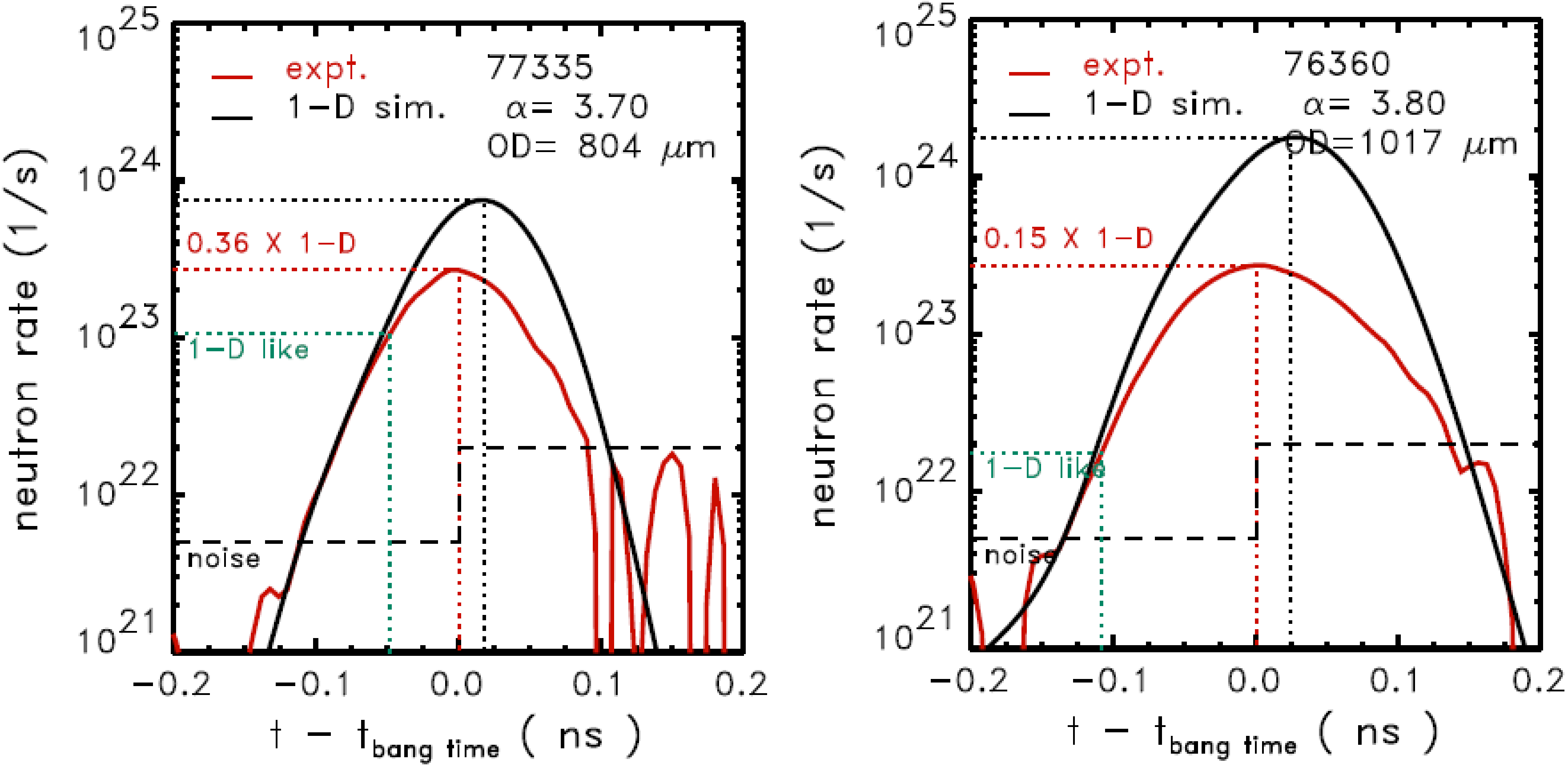

The rising edge is more 1-D like for smaller targets and the ratio of the measured peak neutron rate to 1-D is twice as high

Tion for DT cryo campaign inferred from nTOF detectors compared with 1-D prediction

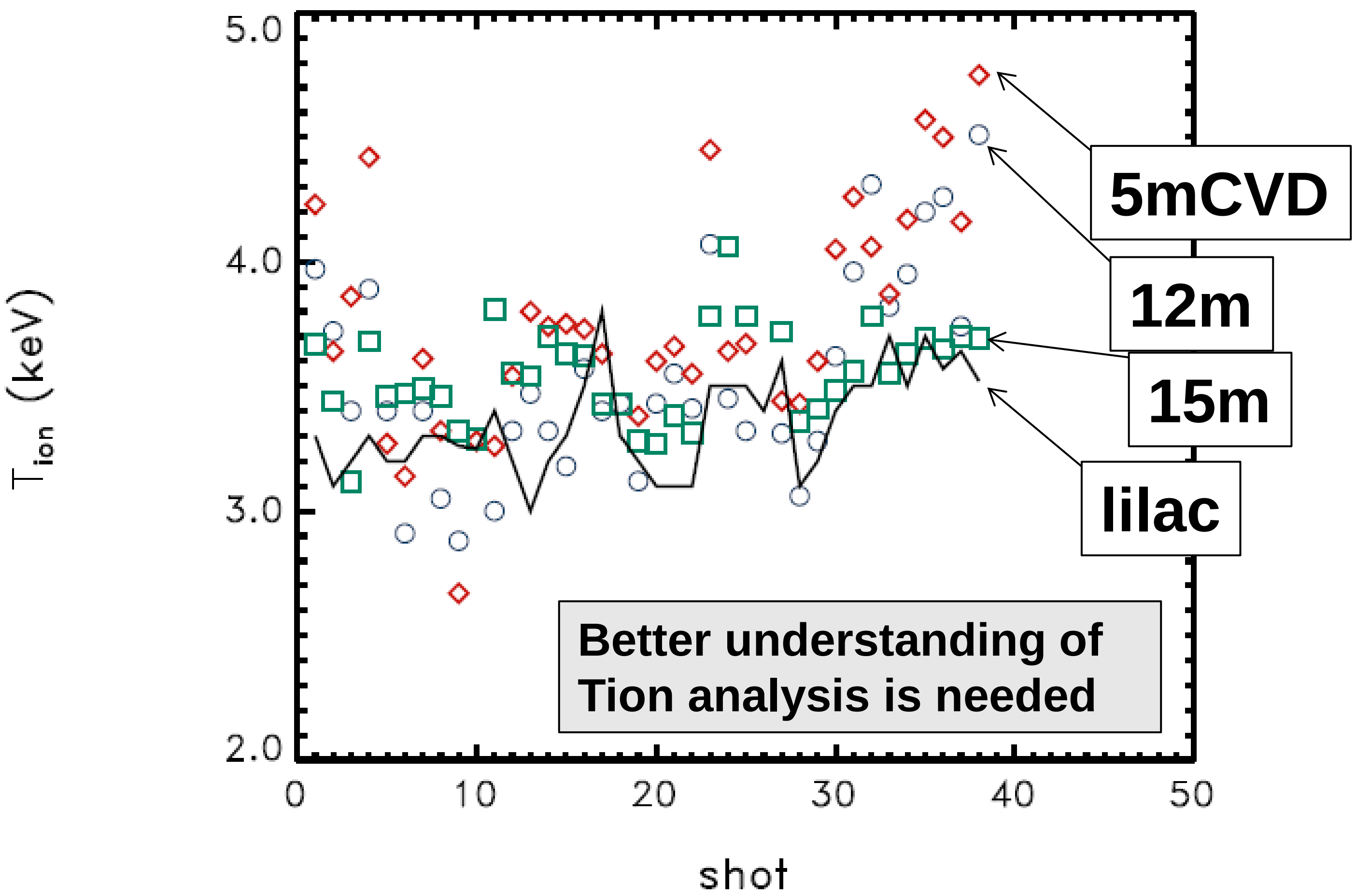

Minimum Tion is used to infer hot-spot pressure

Three-dimensional simulations predict an early burn truncation because of long-wavelength, hot-spot distortion growth

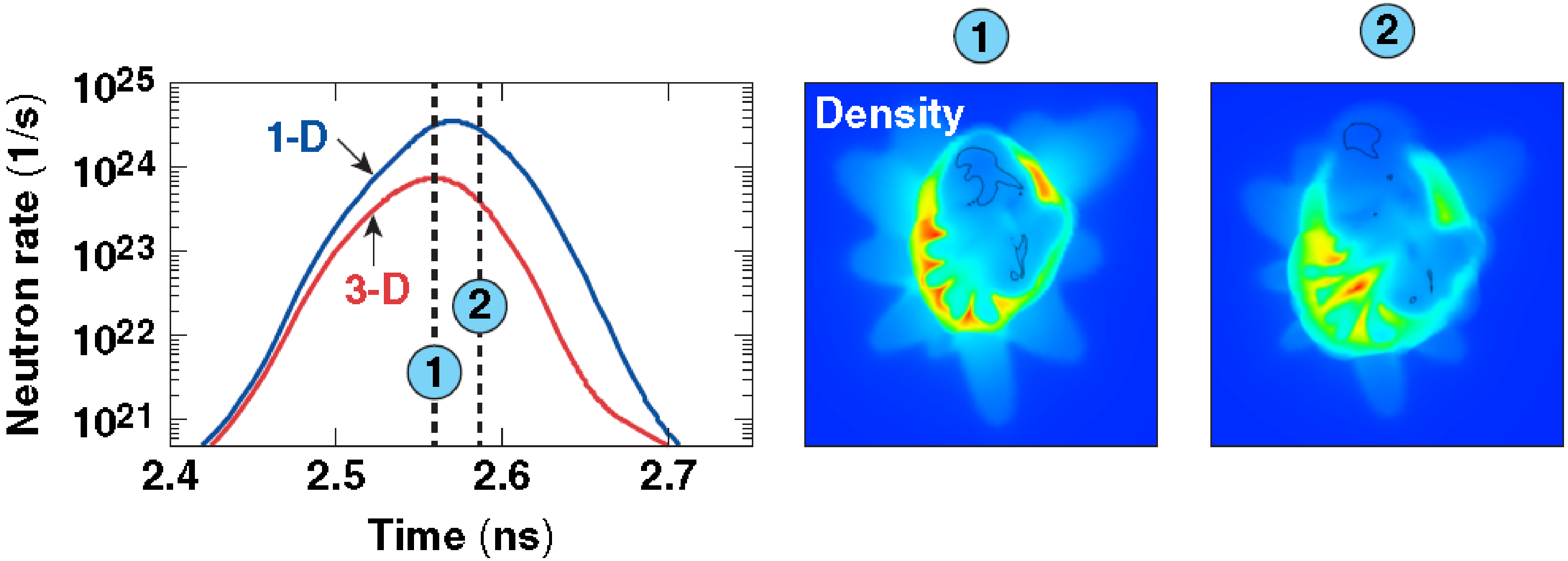

Larger targets have less beam overlap, more drive nonuniformity, and higher level of long-wavelength, hot-spot distribution compared to smaller targets ⟶ lower P_{hs} for larger targets.

TC12376a

The observed increase in energy coupling with target diameter does not result in a higher hot-spot pressure

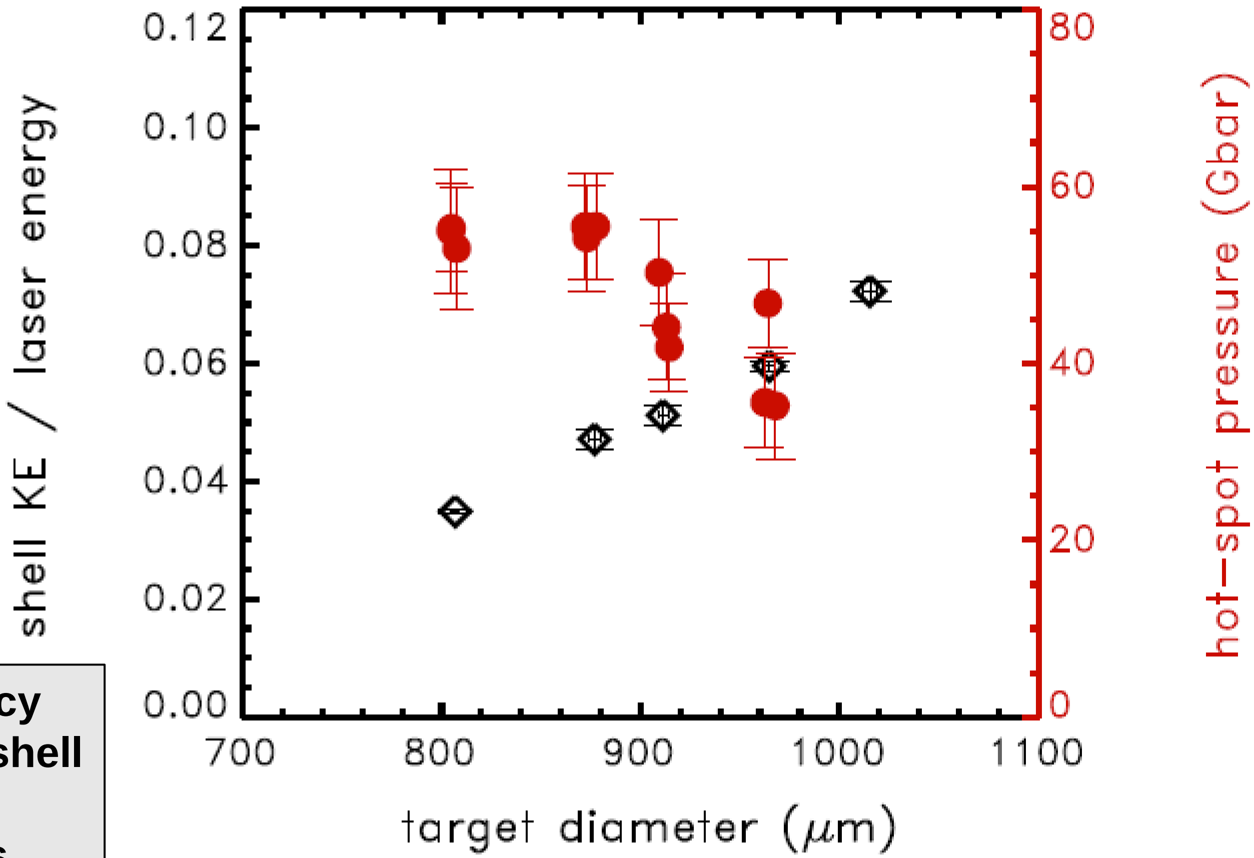

Hydro-efficiency inferred from shell trajectory measurements

A peak hot-spot pressure of 56±7 Gbar was inferred for the smaller targets

Peak hot-spot pressure of 56±7 Gbar was inferred in current DT cryo campaign

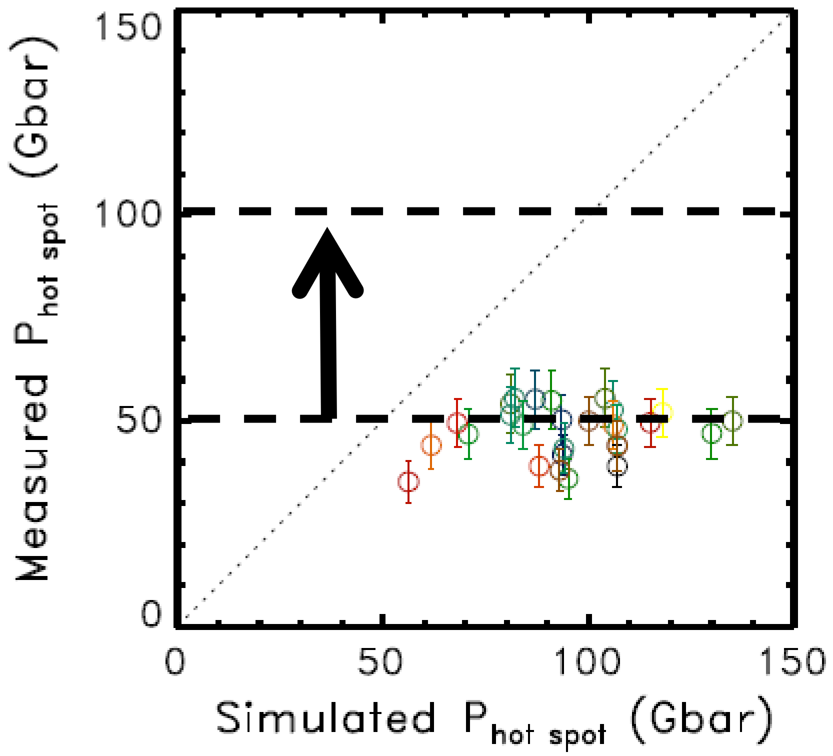

<u>Path to 100 Gbar</u>

- **Precision laser power balance**
- **Laser beam zooming (CBET mitigation)**
- **Target metrology for μm-scale surface debris**
- **X-ray imaging along multiple lines of sight**
- **Better understanding of Tion analysis**
- **3-D nTOF**
- **X-ray backlighting/Compton radiography of compressed shell**
- **Time-resolved x-ray continuum measurement to infer Te(t) of hot spot**

OMEGA T_{ion}(Brysk, Ballabio) and rho-r

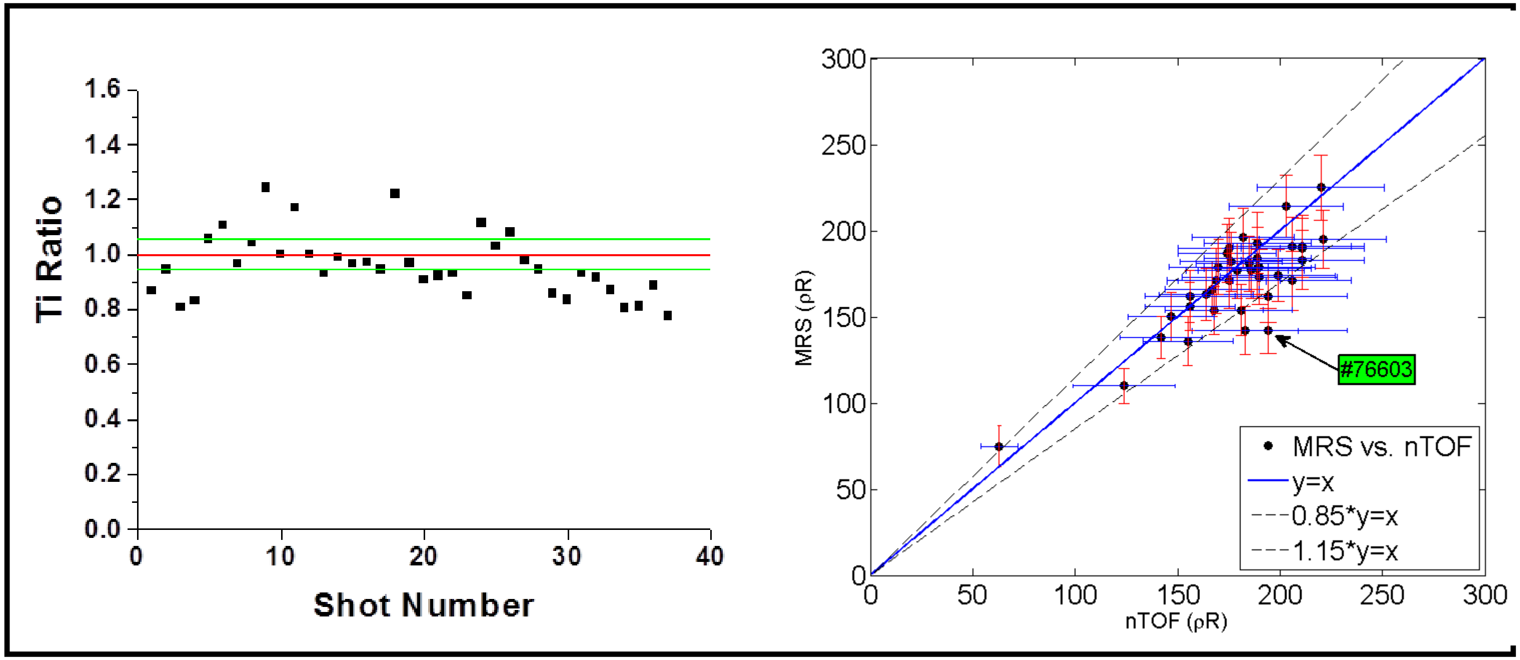

J. P. Knauer
University of Rochester
Laboratory for Laser Energetics

DOE Stagnation Workshop
LLNL
Livermore, Ca
27-28 October 2015

Work presented from OMEGA nTOF team

V. Yu. Glebov, C. Forrest, C. Stoeckl

Laboratory for Laser Energetics
University of Rochester

OMEGA nTOF detectors measure T_{ion} (Brysk/Ballabio) and the cold fuel areal density

- Measurement of the ion temperature with nTOF detectors is evolving
  - Data are now fit with an exponential convolved with a Gaussian
  - A forward fit analysis using a measure IRF is in development (Used for 13.4 m data)
- Ion temperature for non-cryogenic targets have an error of 3%
- Ion temperatures of cryogenic implosions show an angular variation
- The areal density is directly proportional to the down-scattered neutron yield from the neutron-tritium (n-T) elastic scattering
- A background measurement and a transport code to model the individual neutron contributions is required to fit the nTOF data
- OMEGA NTOF systems will focus on measurement of 1^{st} and 2^{nd} moments of DT and DD neutron spectra peaks

OMEGA T_{ion}(Brysk, Ballabio) and rho-r

- **Tion measurements**
- **Rho-r measurements**

OMEGA has 6 nTOF detectors that can measure the DT peak along different lines of sight

OMEGA nTOF detectors used for cryogenic experiments

- **15.8 m nTOF**
- **12 m nTOF**
- **5.2 m nTOF**
- **5.4 m PD040**
- **5.0 m CVD**
- **8 X 4 nTOF**

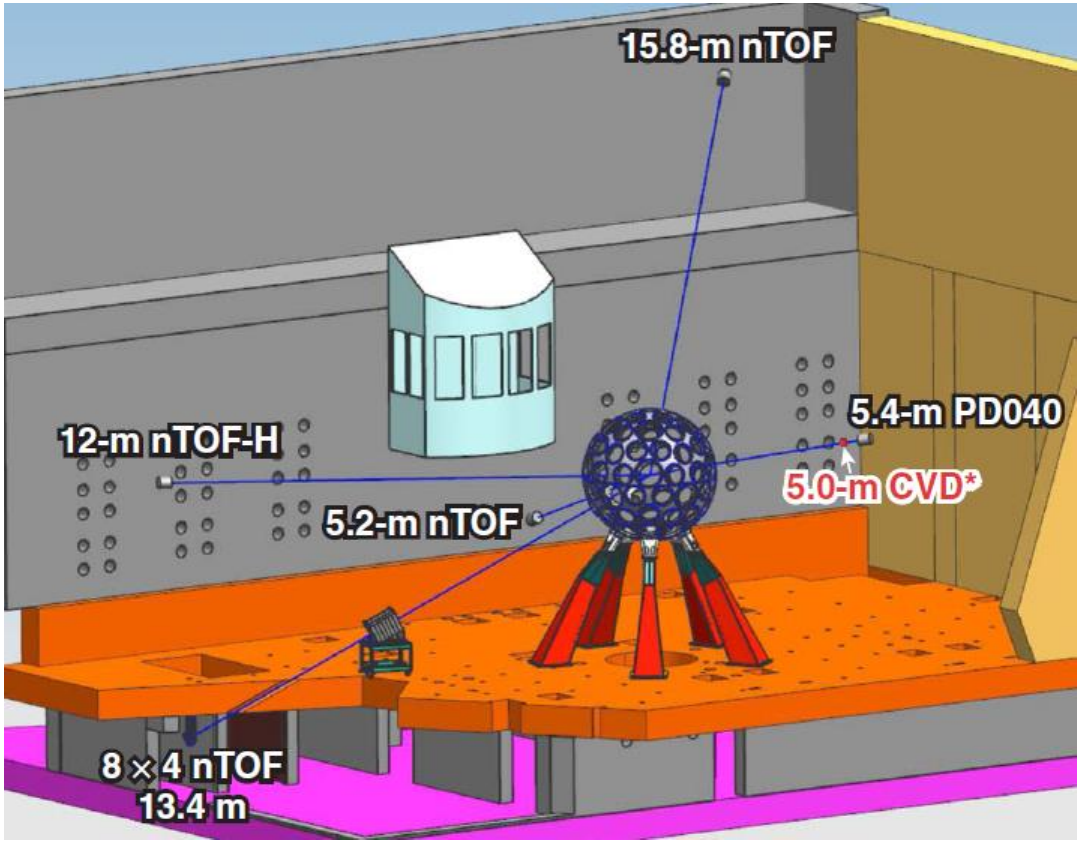

OMEGA T_{ion}(Brysk, Ballabio) and rho-r

- **Tion measurements**
- Rho-r measurements

Several methods can be used to evaluate the ion temperature from an ICF implosion

- **A simple approach to infer the ion temperature is to fit the neutron peak with exponentially modified Gaussian.***

  -- Performed on all nTOF detectors except the 13.4 meter nTOF.

- **A more sophisticated function with additional decay terms convolved with a relativistic thermal broadening can be used to infer the ion temperature.**

  -- Integrated into the analysis on the NIF. (R. Hatarik , J. Knauer)

- **A more complete method to infer the ion temperature requires the detector IRF and simulations of the neutron transport through the detector.**

  -- Presently used to measure the Ti of the DD on the 13.4 meter nTOF.

*** T.J. Murphy et al., "Rev. Sci. Instrument." 86, (610) (1997)**

The absolute DT *Ti* was inferred from directly measured neutron IRF of 5.0mCVD in low T_i, low yield DT shots at 40 cm from TCC

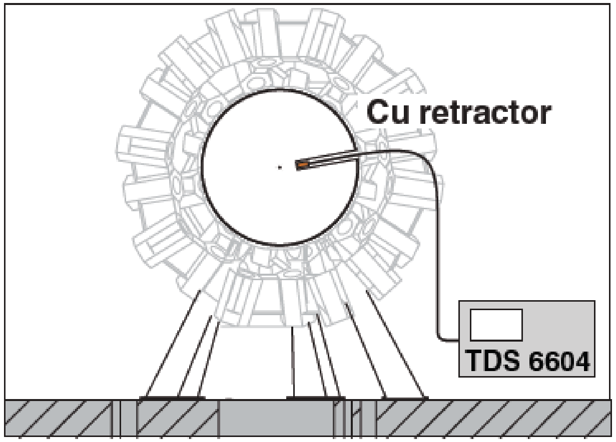

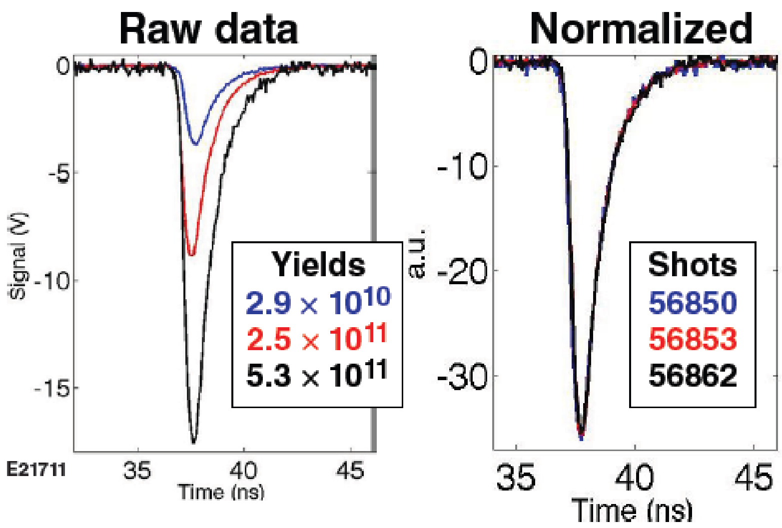

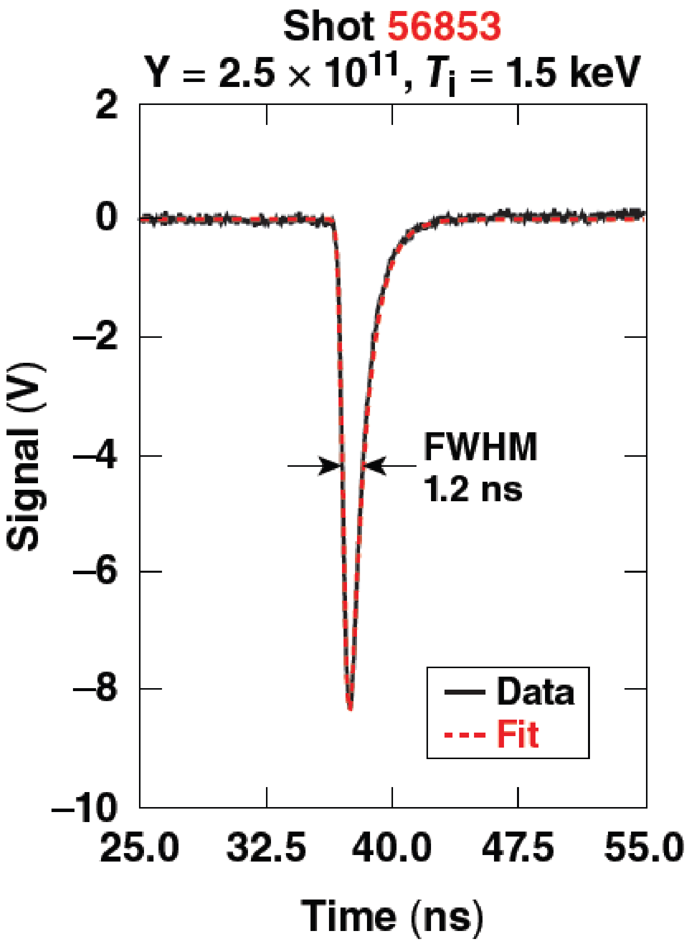

The nTOF yield and *Ti* errors depend on measurement statistics

1. nTOF signal is proportional to neutron energy deposition
2. Divide by average energy per neutron for detected neutrons
3. Statistics for error must be modified for pulse-height distribution in detector [1]

$$\sigma_N = \sqrt{1 + \left(\frac{\Delta E}{\langle E \rangle}\right)^2}\sqrt{N}$$

4. For scintillator based nTOF detectors this is about [1]

$$\sigma_N = 2\sqrt{N}$$

Thus, 10% error requires 400 detected events
5% error requires 1600 detected events
3% error requires 4.4 E3 detected events

1. R.A. Lerche *et al*., RSI, 61, 3131 (1990)

There are enough neutron statistics in all nTOF detectors at DT cryogenic yield ~ 4×10^{13}

UR LLE

Plastic scintillator
40 mm ∅ x 20 mm thick

	5 m	12.4 m	15.8 m
$\Delta\Omega$	4×10^{-6}	6.5×10^{-7}	4.0×10^{-7}
$Nh\|_{10^{12}}$	2.9×10^{5}	4.8×10^{4}	2.9×10^{4}
$Nh\|_{4 \times 10^{13}}$	1.2×10^{7}	1.9×10^{6}	1.2×10^{6}

CVD diamond detector
10 mm ∅ x 1 mm thick

	5 m	7.5 m	15.8 m
$\Delta\Omega$	2.5×10^{-7}	1.1×10^{-7}	2.5×10^{-8}
$Nh\|_{10^{12}}$	4.2×10^{3}	1.85×10^{3}	4.2×10^{2}
$Nh\|_{4 \times 10^{13}}$	1.68×10^{5}	7.4×10^{4}	1.68×10^{4}

In the tables : $\Delta\Omega$ - detector solid angle, $Nh|10^{12}$ – number of “hits” in the detector produced by 10^{12} neutrons

We need at least 4.4×10^{3} detected events to satisfy 3% shot to shot precision requirements.

The *Ti* ratio in different LOS is close to one for DT room-temperature targets with high-adiabat implosions

2012 to 2014 data

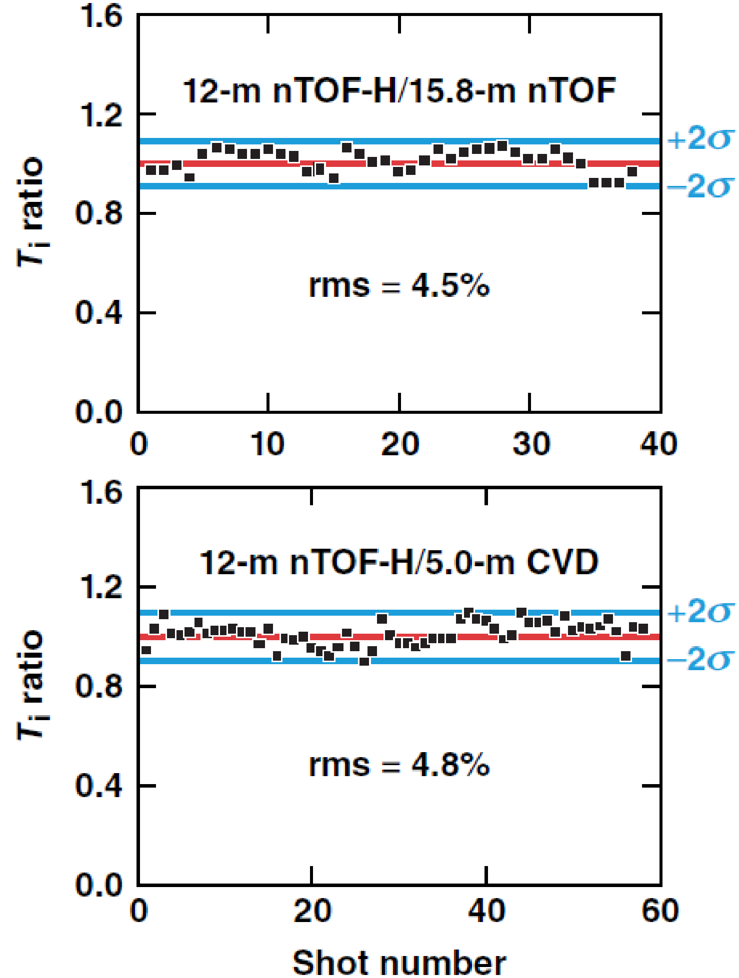

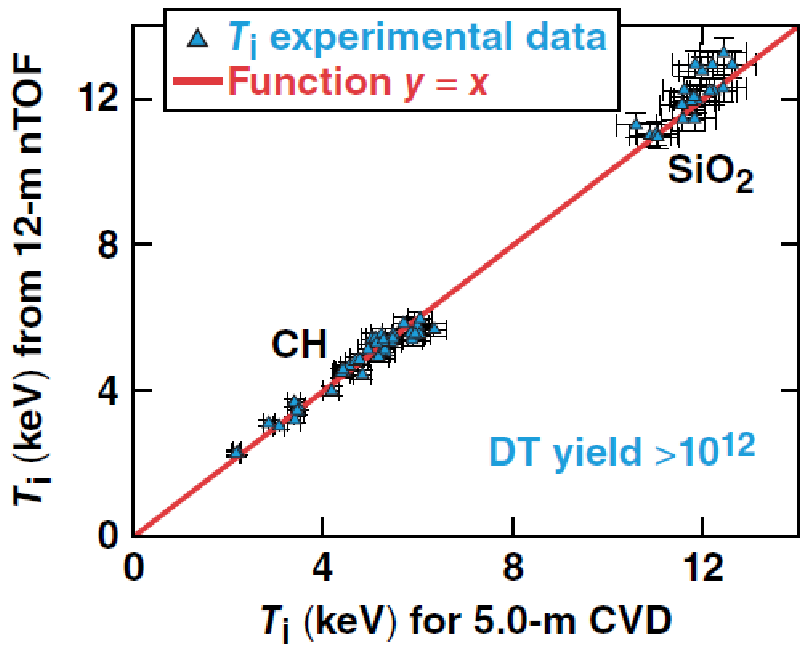

All shots are taken with 1-ns square laser pulses with $6 \leq \alpha \leq 20$ and a convergence ratio (CR) from 4 to 11. Target offset is less than 10 μm.

The *Ti* ratio in different LOS can very by a factor of 2 in low-adiabat DT cryogenic implosions

DT yield > 10^{12} 2012 to 2014 data

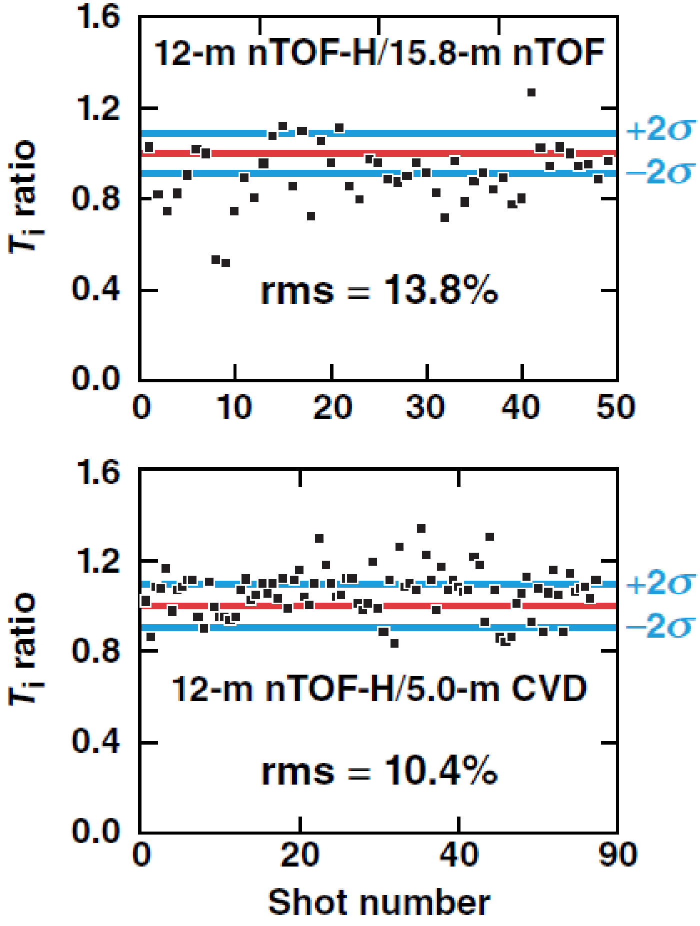

CR from 14.5 to 22

Typical pulse shapes

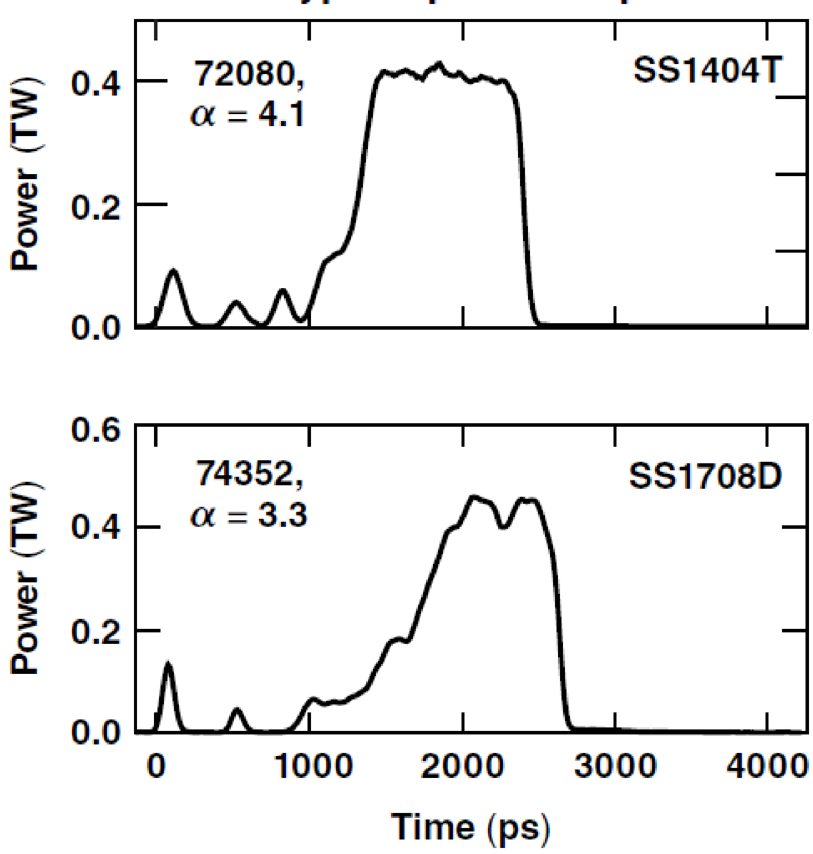

E23656

The 15.8mnTOF and 12mnTOFN detectors measure ion temperature with precision of better than 3%

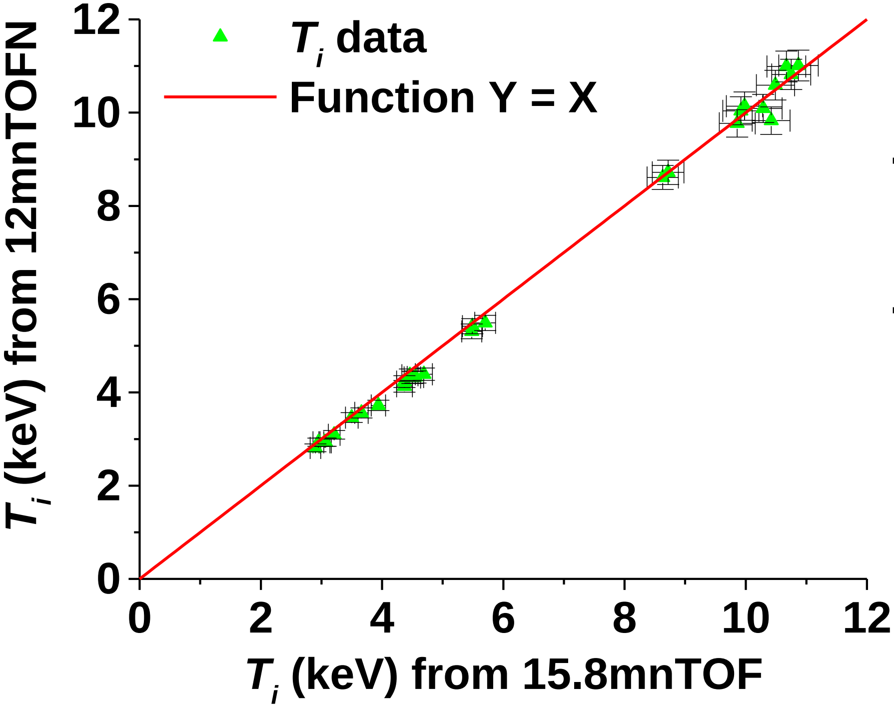

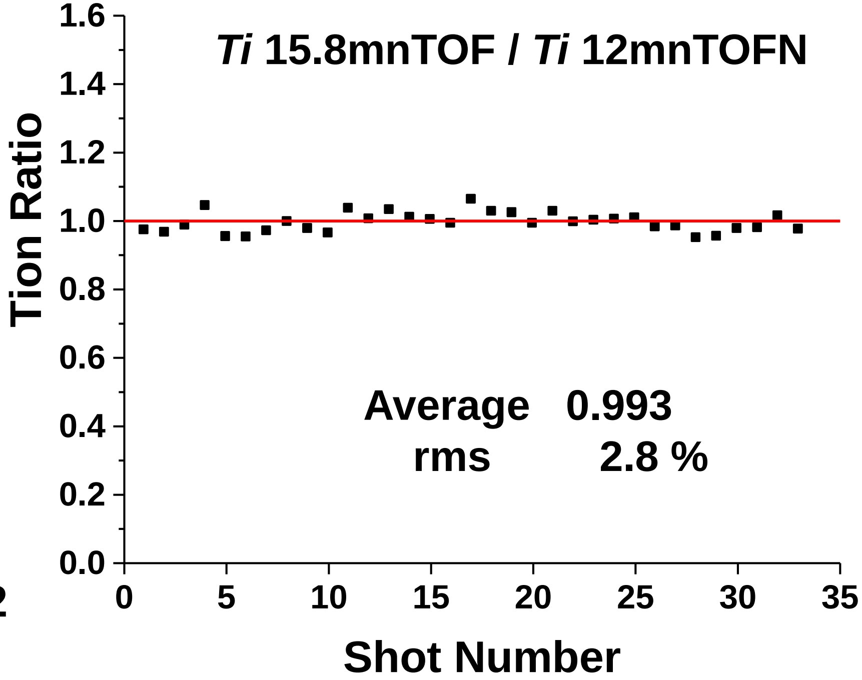

All data on this slide were recorded during room-temperature target implosions

The *Ti* ratio in different LOS varies more in cryogenic implosions then in with room-temperature targets

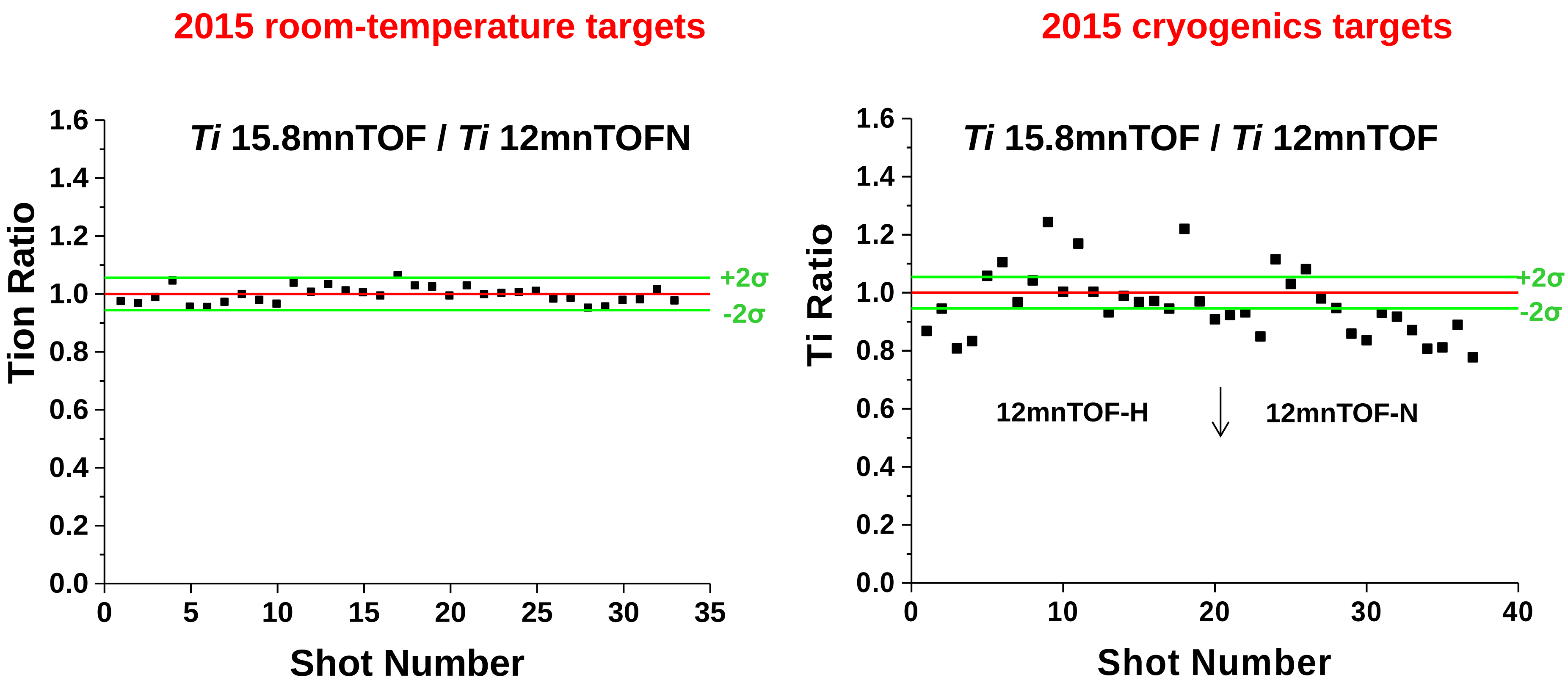

Large differences in the *Ti* in different LOS in cryogenics implosions suggests bulk fuel flows because of perturbation growth or nonuniform drive

Four approved projects for FY2016 will improve ion temperature measurements on OMEGA

- **Two additional LOS for DT ion temperature (Ti_LOS)**
  Move PD040 from 5.2 m to 10 m to 15.8 m from TCC
  Move 5.2nTOF from 5.2 m to 10 m to 15.8 m from TCC

- **Petal nTOFs for DT ion temperature (Petal_nTOF)**
  Petal nTOF in front of 8x4nTOF and in second LOS
  Will measure DD and DT *Ti* in the same LOS

- **Second LOS for nTOF *ρR* measurement (2nTOFrhoR)**
  Will measure *ρR*
  Will measure DT yield and *Ti*
  Will measure DD yield and *Ti*

- **3dNTOF**
  6 CVD diamond detectors along 3 nearly orthogonal axes
  Shared lines-of-sight with 15.8 m NTOF and 12 m NTOF

UNIVERSITY of ROCHESTER

A different method to infer *Ti* is using forward fitting

- MCNP is used to simulate the neutron spectrum.
- To model the response of the detector system from neutron signals, X ray IRF is convolved with the neutron transport function and Energy function(folded from energy domain to time domain).

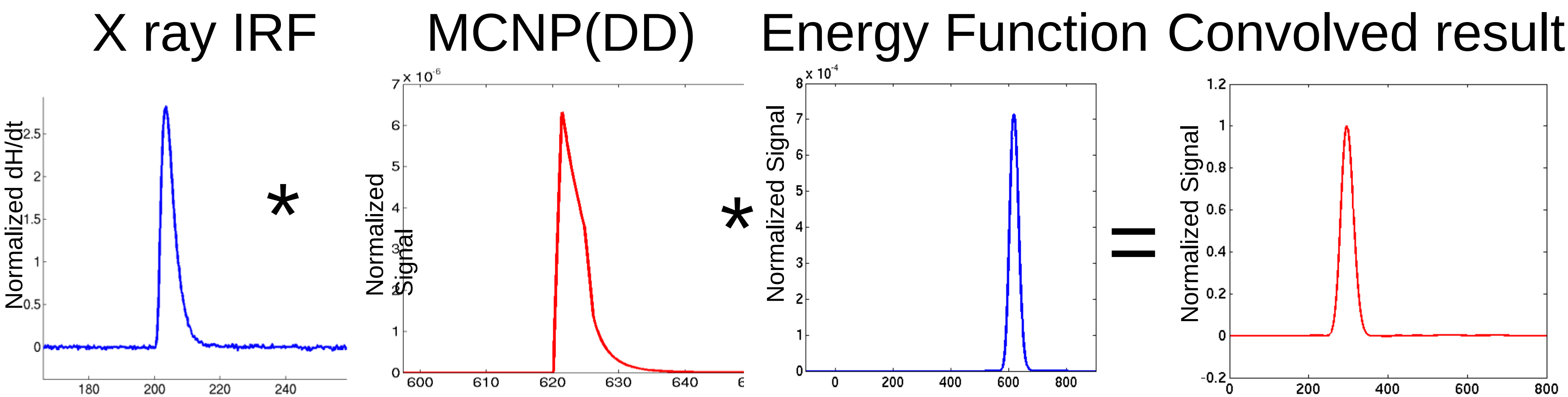

C. Forrest is using forward fitting to infer DD ion temperature from 8x4nTOF (13.4 m) detector

Comparison of DD ion temperature measured in two different detectors with different methods

T_{ion} DD

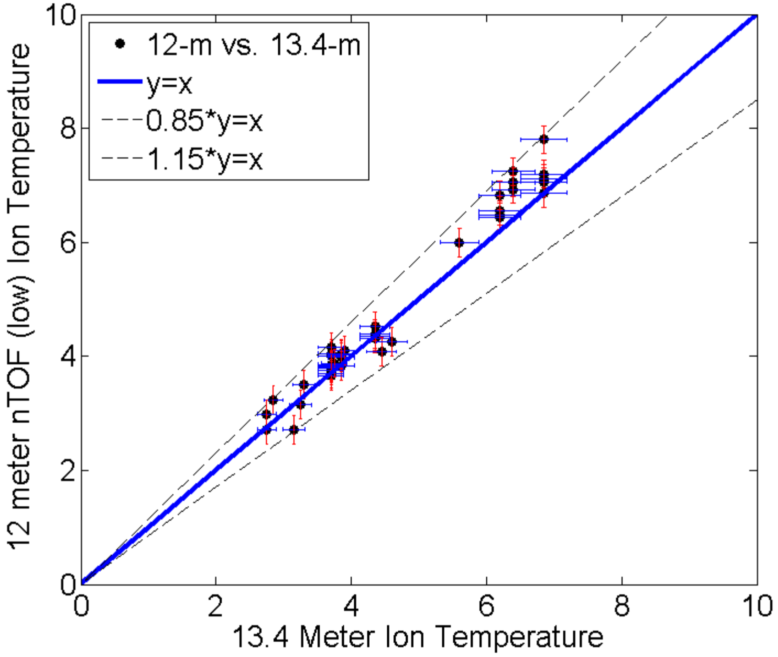

T_{ion} DT

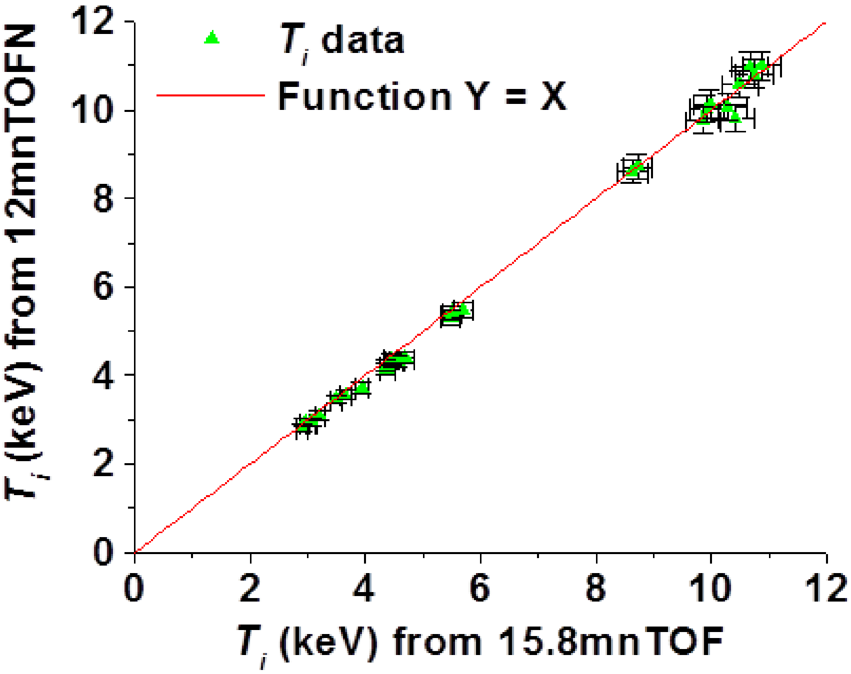

The 3dNTOF project has evolved from the OMEGA NTOF system and will provide complimentary data

Three nearly orthogonal axes used

- P2 – P11 (15.8 m nTOF)
- H8 – H13 (12 m nTOF)
- H4 – H17

Data will compliment existing OMEGA nTOF data

- Measure velocity of bulk fusion plasma motion
- Provide additional measures of the DT Brysk ion temperature
- Provide a platform for measures of the DD Brysk ion temperature

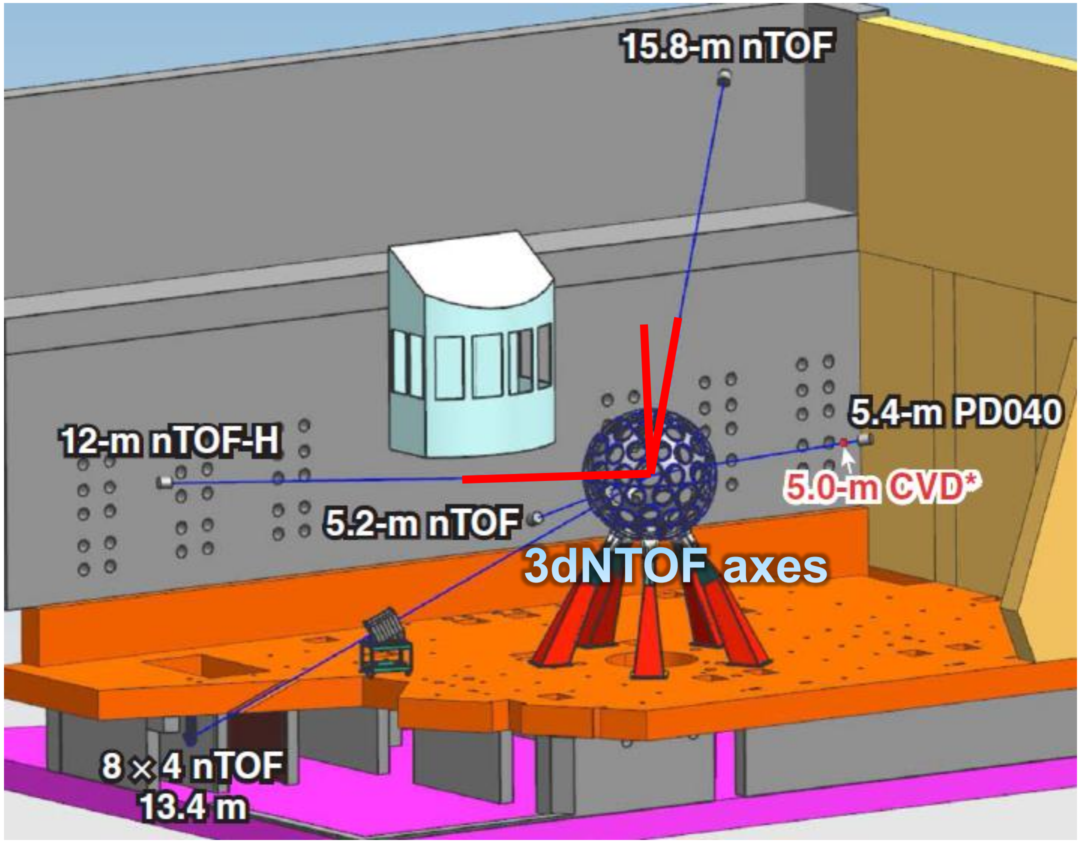

CVD diamond is the technology used for the 3dNTOF project

OMEGA T_{ion}(Brysk, Ballabio) and rho-r

- Tion measurements
- **Rho-r measurements**

The areal density is directly proportional to the number of elastically scattered neutrons

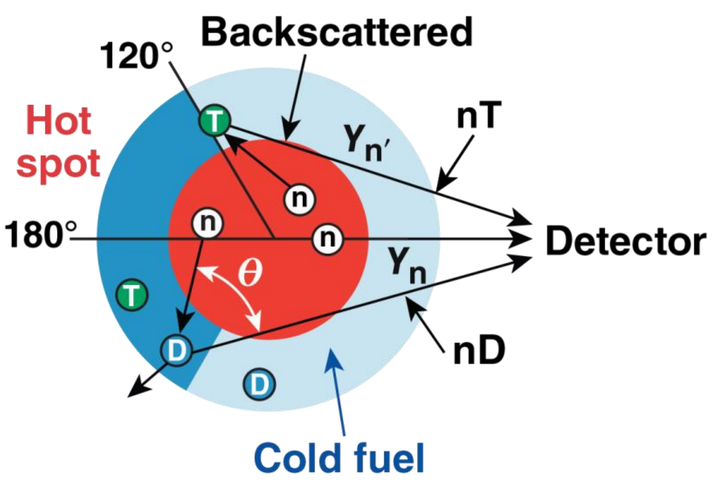

200 mg/cm²

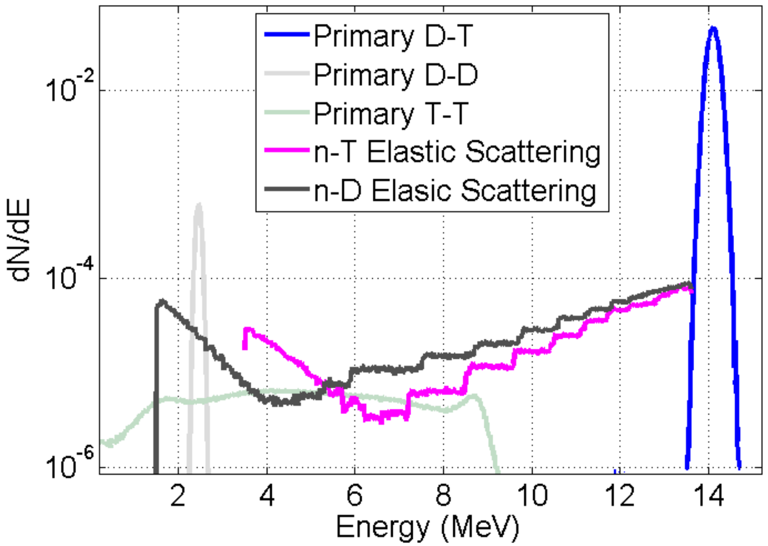

$$\frac{E_S}{E_n} = \frac{4A}{(1+A)^2}(\cos\theta^2)$$

$$\frac{Y_{ES}}{Y_{DT}} = \frac{N_A}{M_A}\rho R \int_{E_i}^{E_f} \frac{d\sigma}{dE} dE*$$

The scattering angle determines the energy of the scattered neutron

* S. Skupsky, "J. Appl. Phys." 54, (4) (1981)

The 13.4 meter nTOF detector records neutrons in the energy region from 1-6 MeV

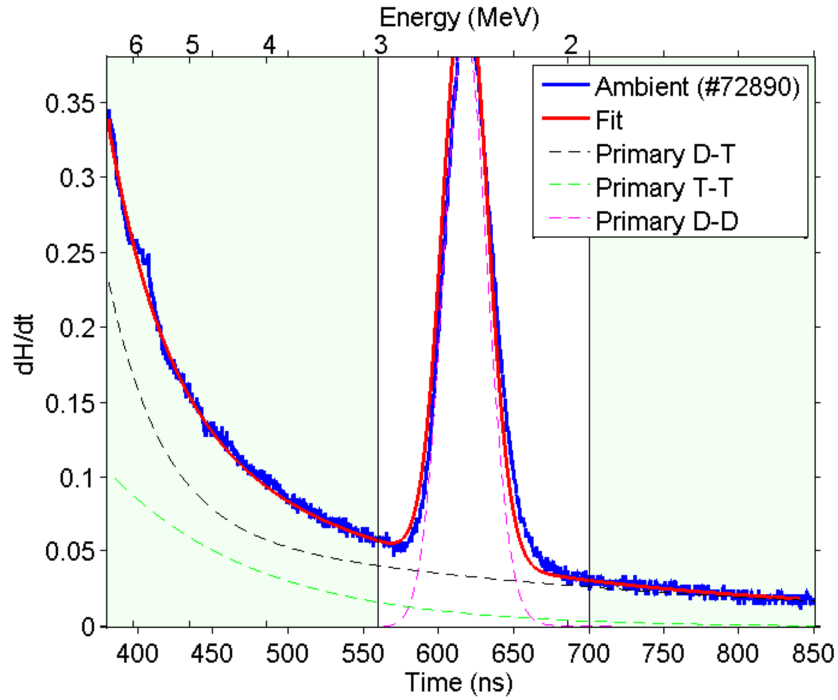

A background for the nTOF signal is constructed from near-zero areal density implosions with fixed components:

Primary D-T
Primary D-D
Primary T-T

The light decay from the scintillation and inherent neutron background from the surrounding structure is convolved with the fixed components

Scattering components are included to fit the time-of-flight spectrum from cryogenic implosions

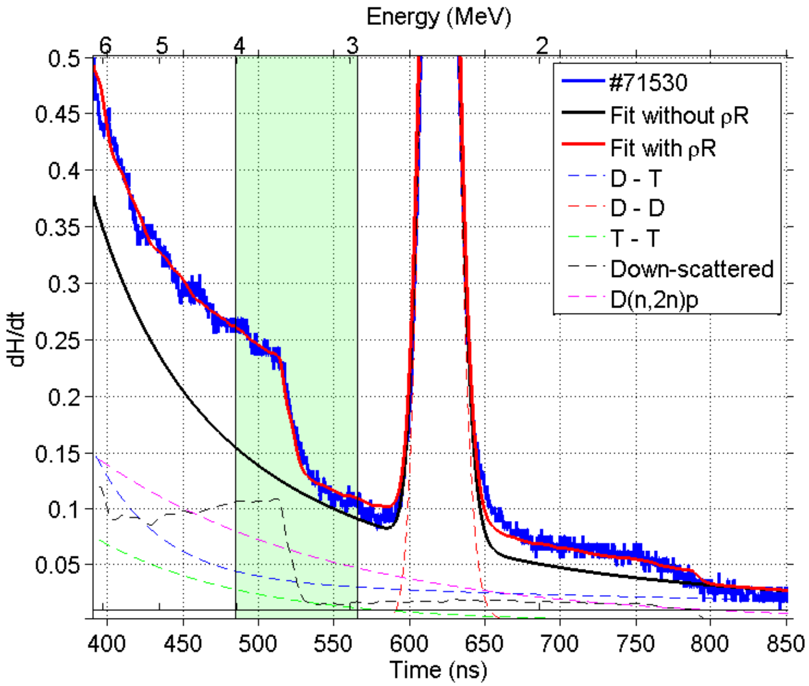

The primary D-T neutrons elastically and in-elastically scatter off the fuel distribution generating two additional neutron components:

<u>Elastic Scattering</u>
n-D and n-T

<u>Neutron-induced breakup</u>
D(n,2n)p

The elastically scattered component at the kinematic edge from 3.5 to 4.0 MeV is adjusted to achieve a best fit by minimizing the error sum from the experimental data

The n-T scattered yield is calculated from the signal in the region from 3.5 to 4.0 MeV

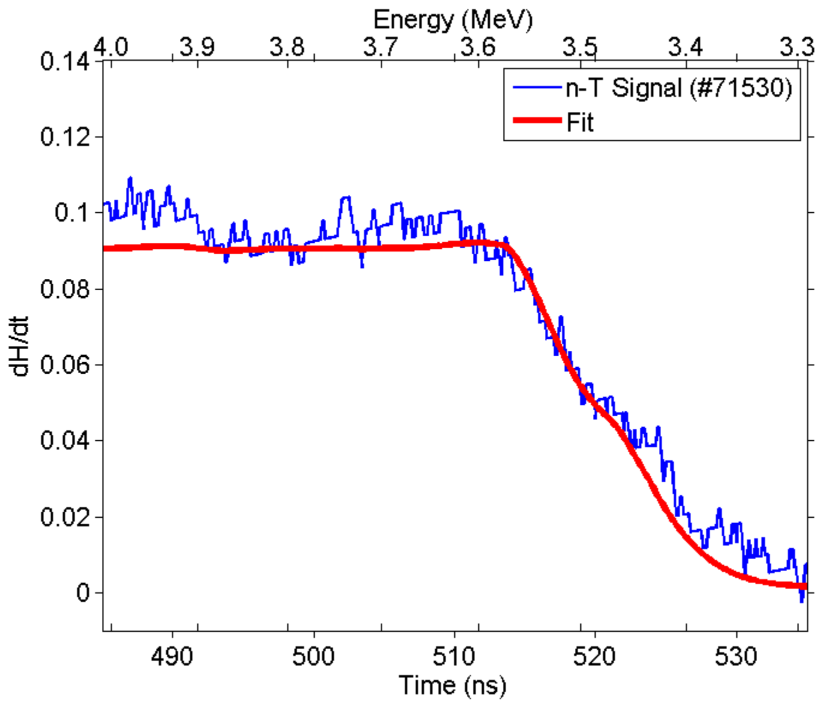

Extracting the n-T scattering component is used to calculate the scattered yield

The n-T yield is directly related to the areal density

$$\frac{Y_{nT}}{Y_{DT}} = \frac{N_A}{M_A}\frac{3}{5}\rho R \int_{3.5}^{4.0} \frac{d\sigma}{dE}\,dE$$

The primary D-T yield is very sensitive to the inferred areal density.

-- The primary yield is used to normalize the 13.4 meter data

-- An areal density is then inferred from the (Y_{nT}/Y_{DT}) ratio

The response of liquid Xylene (oxygenated) has been measured using x-rays from a 10 ns pulse on a gold foil

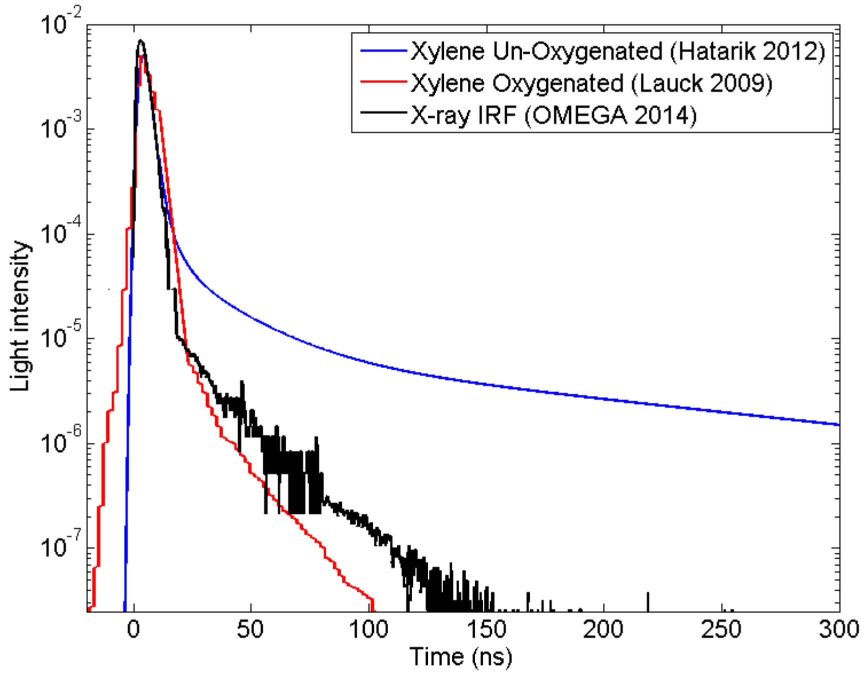

The light output from un-oxygenated Xylene (blue) has decay characteristics typical of most organic (plastic) scintillators

* R. Lauck, "IEEE Trans. Nucl. Sci." 56, 989-993 (2009)

** R. Hatarik, "Rev. Sci. Instrum" 83, 10D911 (2012)

Re-evaluating the nTOF areal density with the adjusted background gives better agreement with the MRS

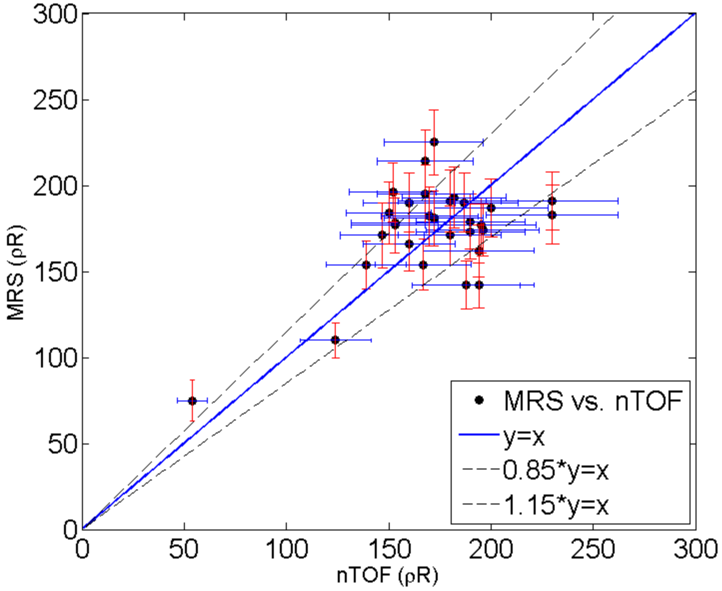

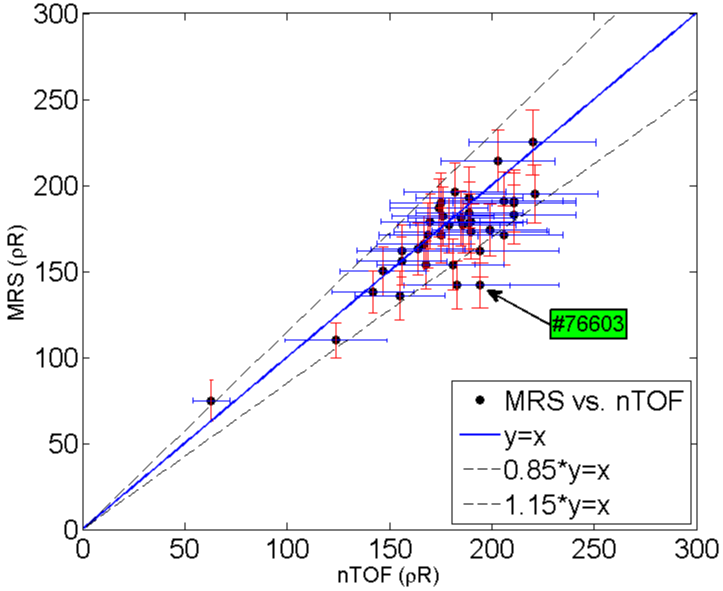

The last background measurement was on April 2014 with TIM-4 Empty.

Inferred the areal density with TIM-4 occupied and un-occupied using the same background.

The primary yield from the 12 meter nTOF was compromised on several campaigns.

A background measurement was on August 2015.

The analysis was re-evaluated using the corrected yields and the updated background with and without TIM-4 occupied.

The FULL neutron source distribution illustrates the regions where the scattered neutrons probe pR.

Detector

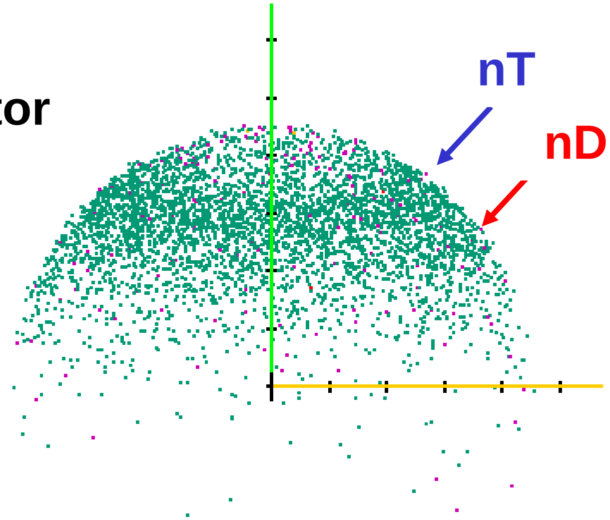

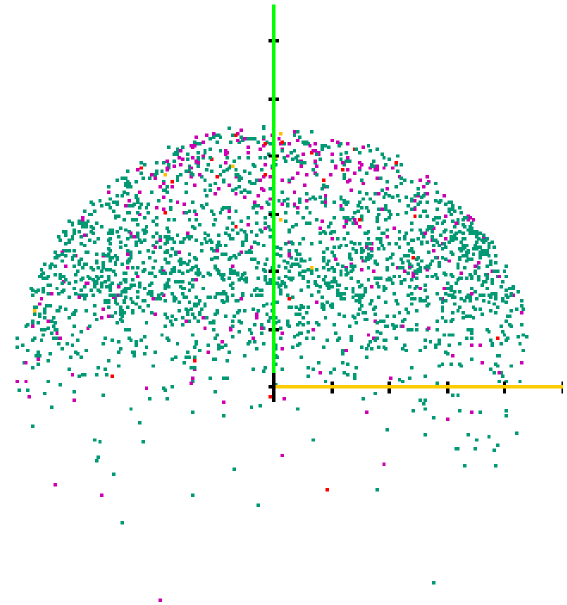

nD and nT scattering is less clear

10-12 MeV

8-10 MeV

The FULL neutron source distribution illustrates the regions where the scattered neutrons probe pR.

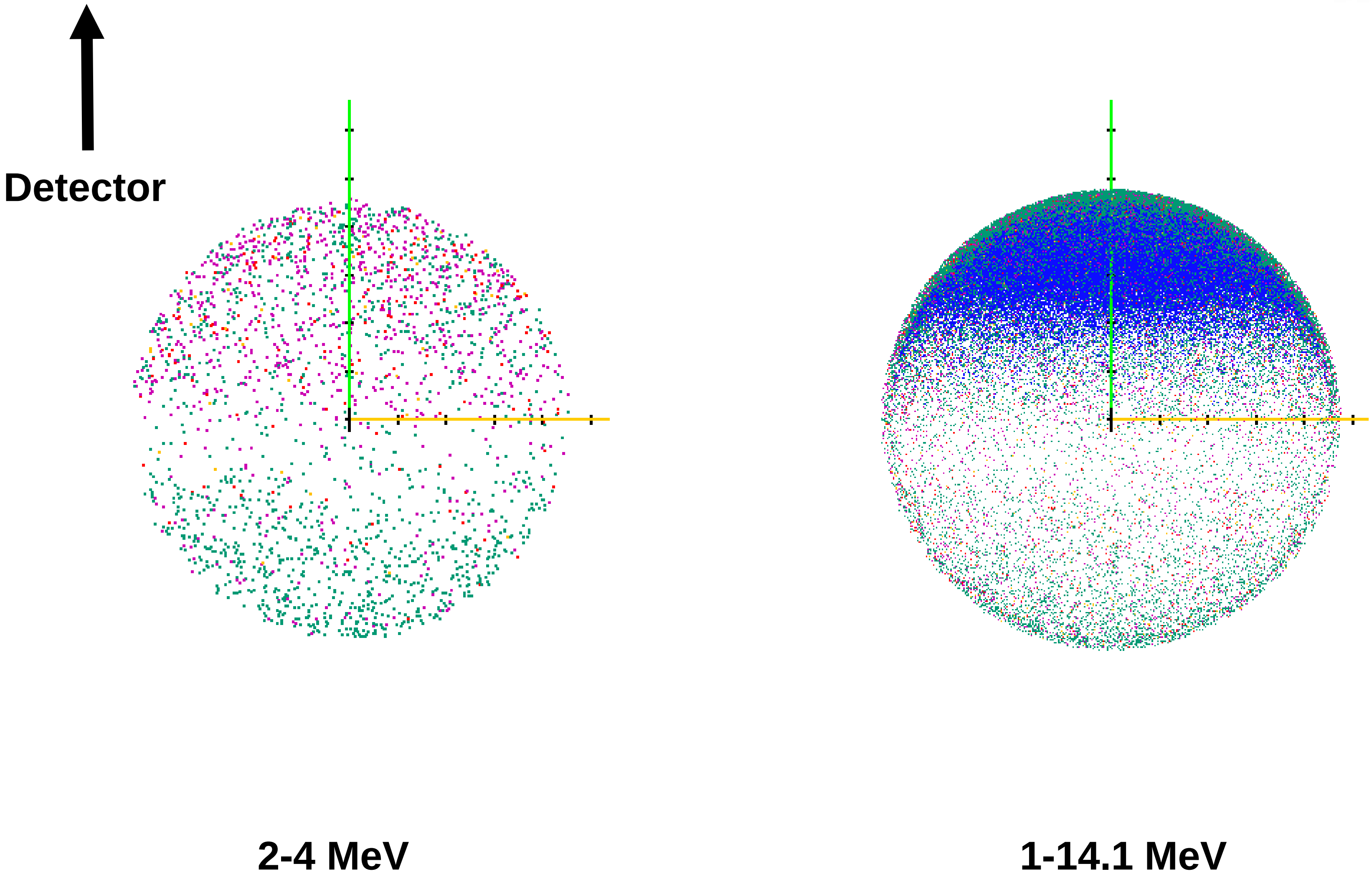

Current OMEGA yield may make precision NTOF on OMEGA problematic

OMEGA cryogenic targets – 1 detector at 13.4 m

- **DT Yield 5 10^{13} neutrons**
- **Relative solid angle ($\Omega/4\pi$) 10^{-5} = 5 10^{8} incident neutrons**
- **Spec detection efficiency ~ 10% = 5 10^{7} detected neutrons**
- **Signal dynamic range ~ 7 10^{3} (4X larger at NIF)**

Current OMEGA NTOF development will focus on DT and DD peak location and width (1st and 2nd moments) along the same line-of-sight

- **1st moment – bulk velocity of fusion plasma**
- **2nd moment – residual kinetic energy[1] of fusion plasma**

[1]T. J. Murphy, Phys. of Plasmas 21, 072701 (2014)

OMEGA NTOF detectors measure T_{ion} (Brysk/Ballabio) and the cold fuel areal density

- Measurement of the ion temperature with nTOF detectors is evolving
  - Data are now fit with an exponential convolved with a Gaussian
  - A forward fit analysis using a measure IRF is in development (Used for 13.4 m data)
- Ion temperature for non-cryogenic targets have an error of 3%
- Ion temperatures of cryogenic implosions show an angular variation
- The areal density is directly proportional to the down-scattered neutron yield from the neutron-tritium (n-T) elastic scattering
- A background measurement and a transport code to model the individual neutron contributions is required to fit the nTOF data
- OMEGA NTOF systems will focus on measurement of 1st and 2nd moments of DT and DD neutron spectra peaks

The OMEGA MRS measures the neutron spectrum from ~4-18 MeV

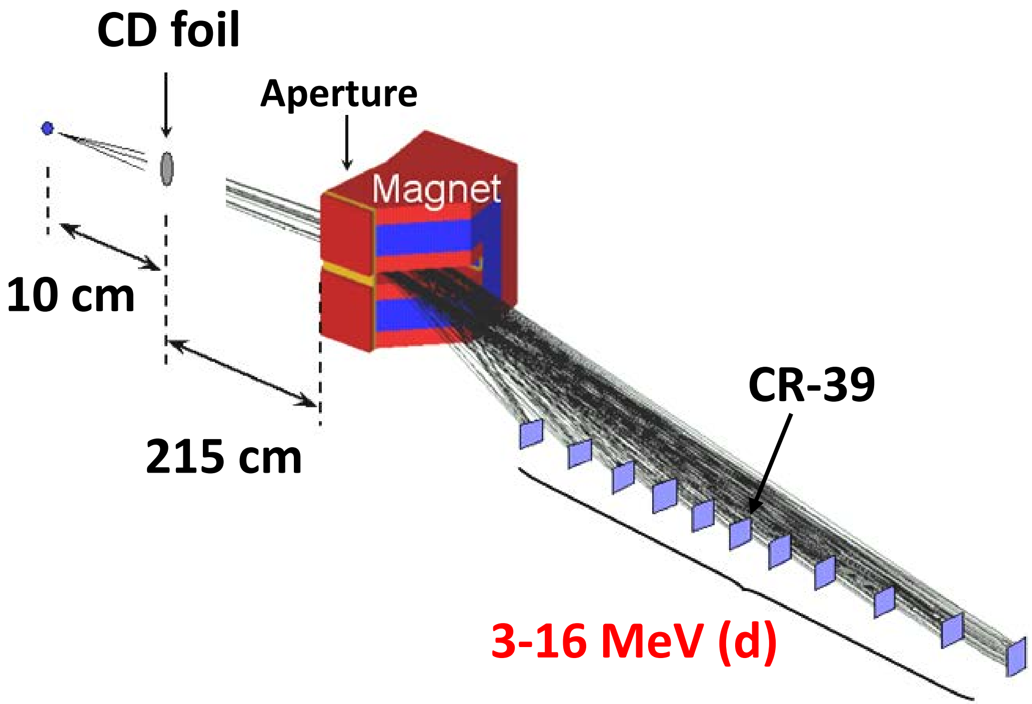

J.A. Frenje et al, Rev. Sci. Instrum. 79, 10E502 (2008)
J.A. Frenje et al, Phys. Plasmas 17, 056311 (2010)
D.T. Casey et al., Rev. Sci. Instrum. 83, 10D308 (2012)
D.T. Casey et al., Rev. Sci. Instrum. 84, 043506 (2013)

Yield and ρR are inferred from the data using a forward fit approach

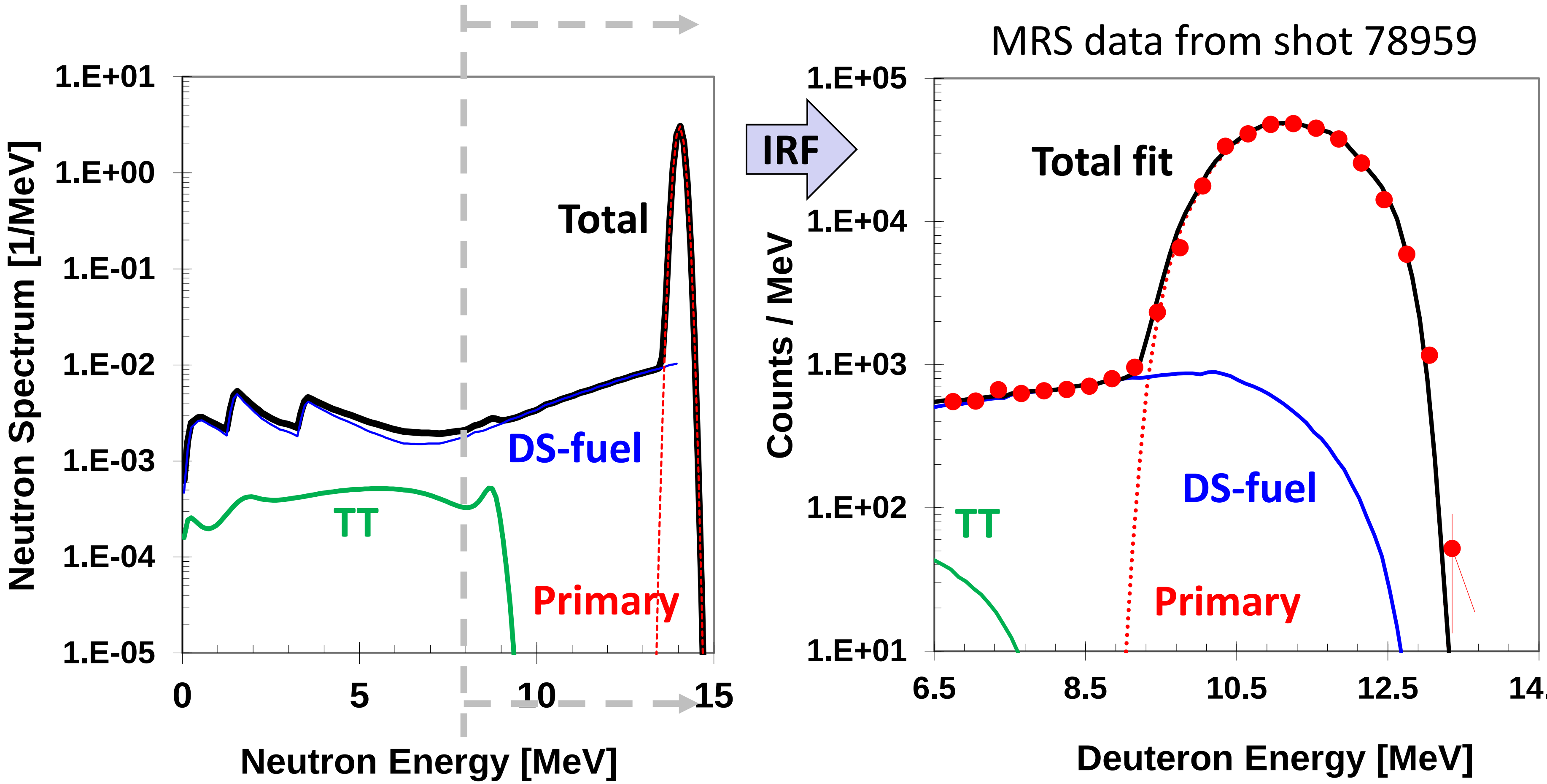

Y_{DT} = (4.1±0.3) x 10^{13}

ρR=203±18 mg/cm^2

Fit components for the ρR analysis are calculated from the cross sections for n,D, n,T & n,H elastic scattering and D(n,2n) & T(n,2n)

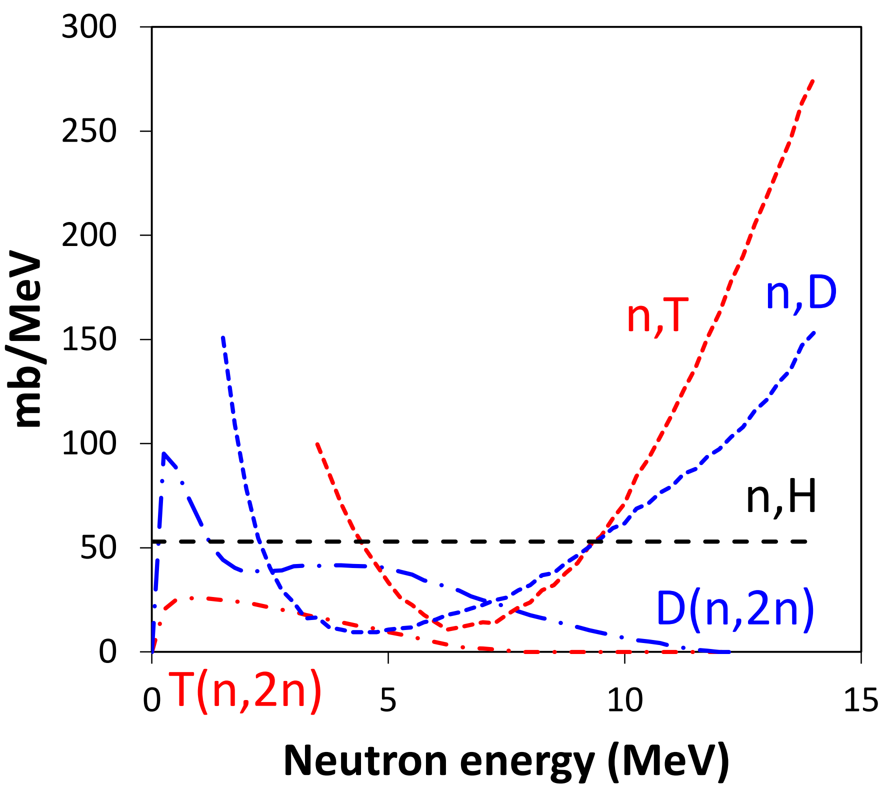

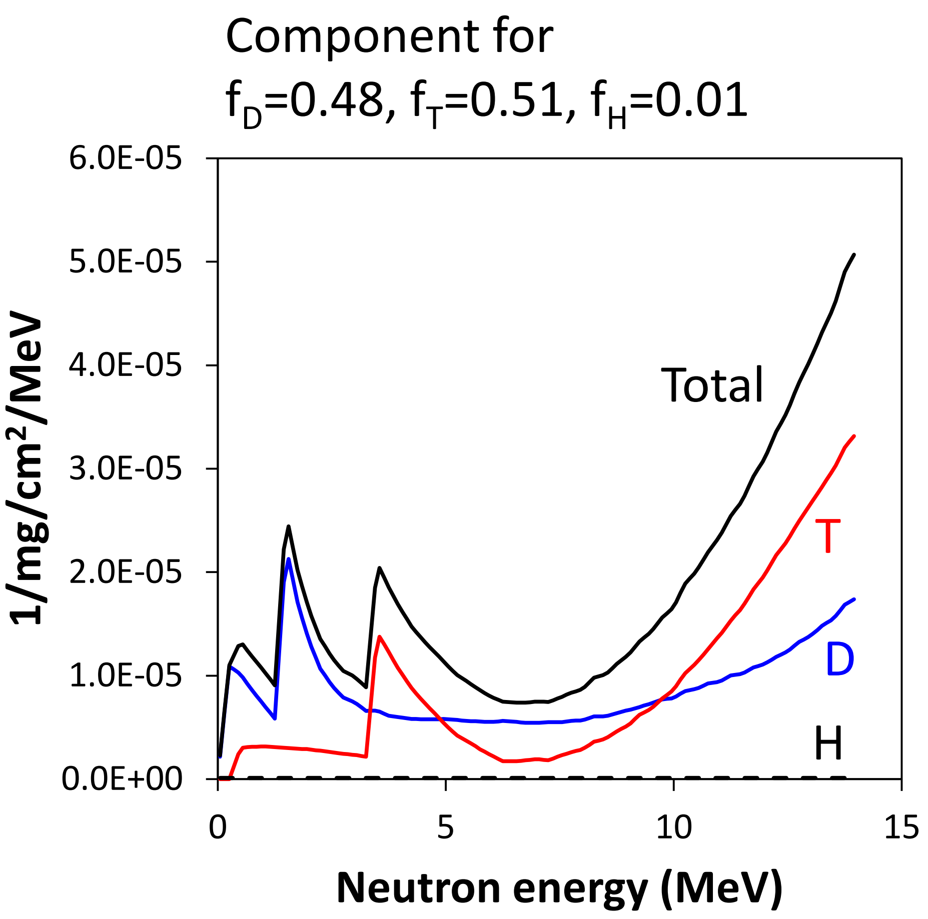

This assumes a hot-spot model

A TT component, locked in intensity relative to primary DT, is included in the fit for improved accuracy

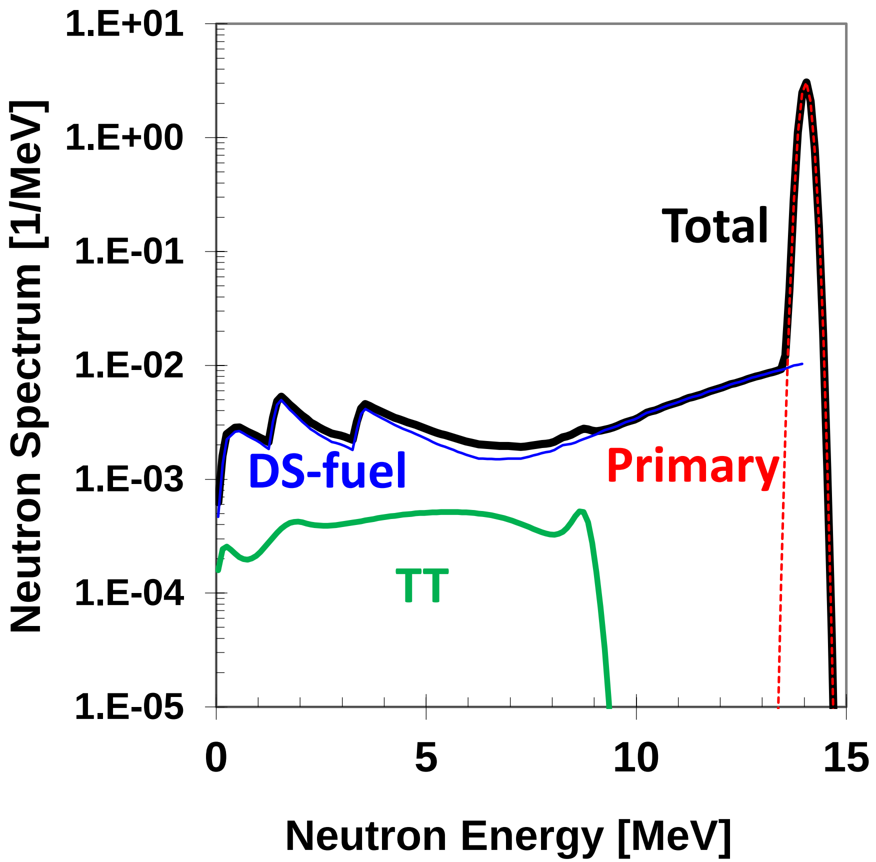

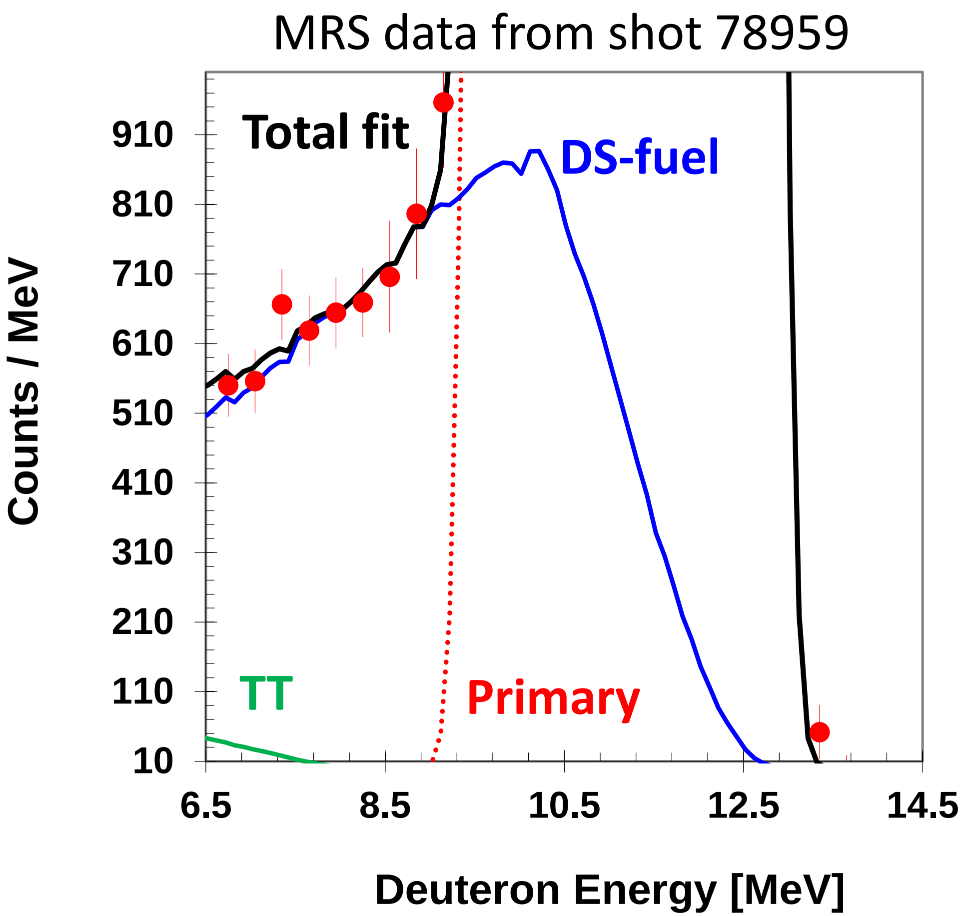

- The TT component shape is as given by Sayre et al. (PRL 2013)
- The intensity is locked relative to DT, considering the known D:T fuel ratio

A systematic error of 7.8% for the DT neutron yield has been determined for the MRS configuration (CD-Low-Res)

MRS setting	CD-Low-Res	Abs. unc	% unc
Foil distance to TCC (R_f) [cm]	10.1	± 0.2	± 2.0
Foil area (A_f) [cm^2]	13.0	± 0.4	± 3.1
CD-foil thickness (t_f) [μm]	265.2	± 2.0	± 0.8
Magnet aperture area (A_a) [cm^2]	22×cos(14.2°)	± 0.2	± 0.9
Magnet distance to TCC (R_a) [cm]	225	± 0.2	± 0.09
d-number density (n_i) [cm^{-3}]	7.6×10^{22}	± 1×10^{21}	± 1.3
nd scattering cross section (at 0°) [mb/sr]	501	± 12	± 2.4
Interception correction*	0.86	±0.03	±3.5
Transmission at 14 MeV**	0.79	±0.03	±3.8
Total systematic uncertainty for Y_{1n}			± 7.8

$$\frac{\sigma_{Y_{1n}}}{Y_{1n}} \approx \sqrt{4\left(\frac{\sigma_{R_f}}{R_f}\right)^2 + \left(\frac{\sigma_{A_f}}{A_f}\right)^2 + \left(\frac{\sigma_{t_f}}{t_f}\right)^2 + \left(\frac{\sigma_{A_a}}{A_a}\right)^2 + 4\left(\frac{\sigma_{R_a}}{R_a}\right)^2 + \left(\frac{\sigma_{n_i}}{n_i}\right)^2 + \left(\frac{\sigma_{\frac{d\sigma(1n,0^\circ)}{d\Omega_{lab}}}}{\frac{d\sigma(1n,0^\circ)}{d\Omega_{lab}}}\right)^2}$$

*D.T. Casey et al., Rev. Sci. Instrum. 83, 10D308 (2012)

**D.T. Casey et al., Rev. Sci. Instrum. 84, 043506 (2013)

A systematic error of 6.4% for the *dsr* has been determined for the MRS configuration (CD-Low-Res)

Primary nd cross section (at 0°) [mb/sr]	**501**	**± 12**	**± 2.4**
Down-scatt nd cross section (at 0°) [mb/sr]	**891**	**± 39**	**± 4.4**
Transmission function uncertainty*			**± 4.0**
Total systematic uncertainty for *dsr*			**± 6.4**

*D.T. Casey et al., Rev. Sci. Instrum. 84, 043506 (2013)

EXTRAS

MRS and nTOF ρR measurements complement each other

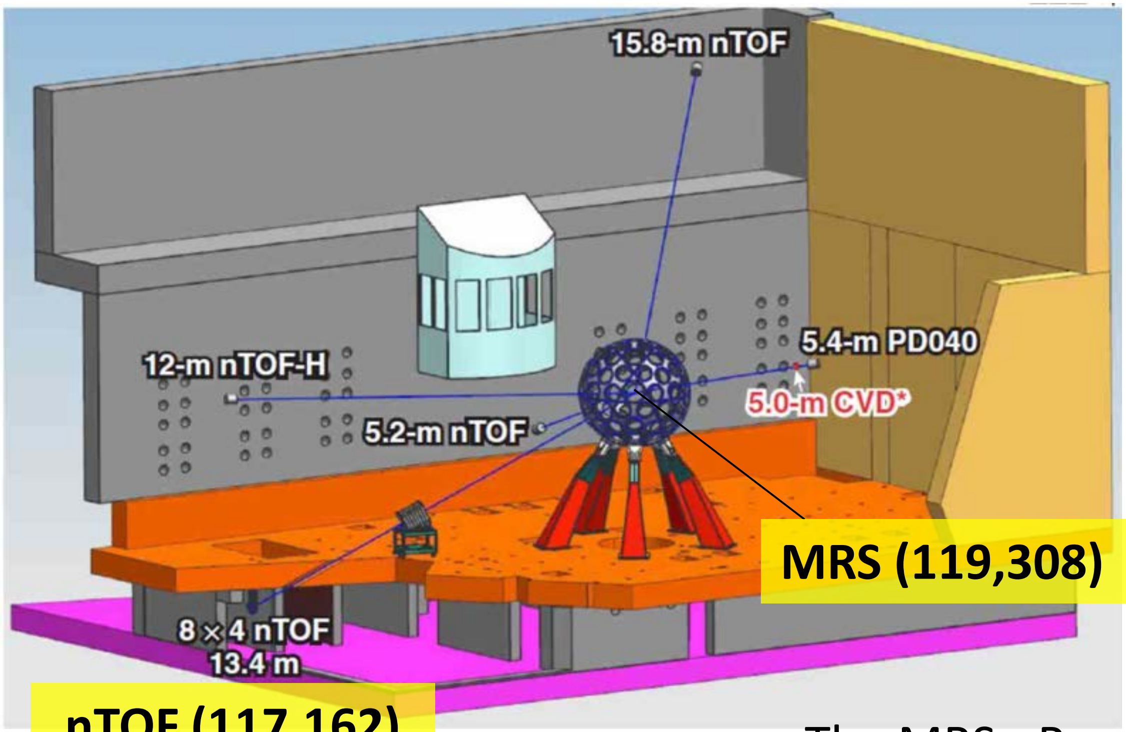

MRS (119,308)

nTOF (117,162)

nTOF measures the backscatter edge (~180°)

The MRS ρR result is based on the E_n~ 8-11 MeV range → ~ 40-80° cone

In a hot-spot model and considering elastic scattering only, there is a direct kinematic relationship between neutron energy and sampled region of the shell

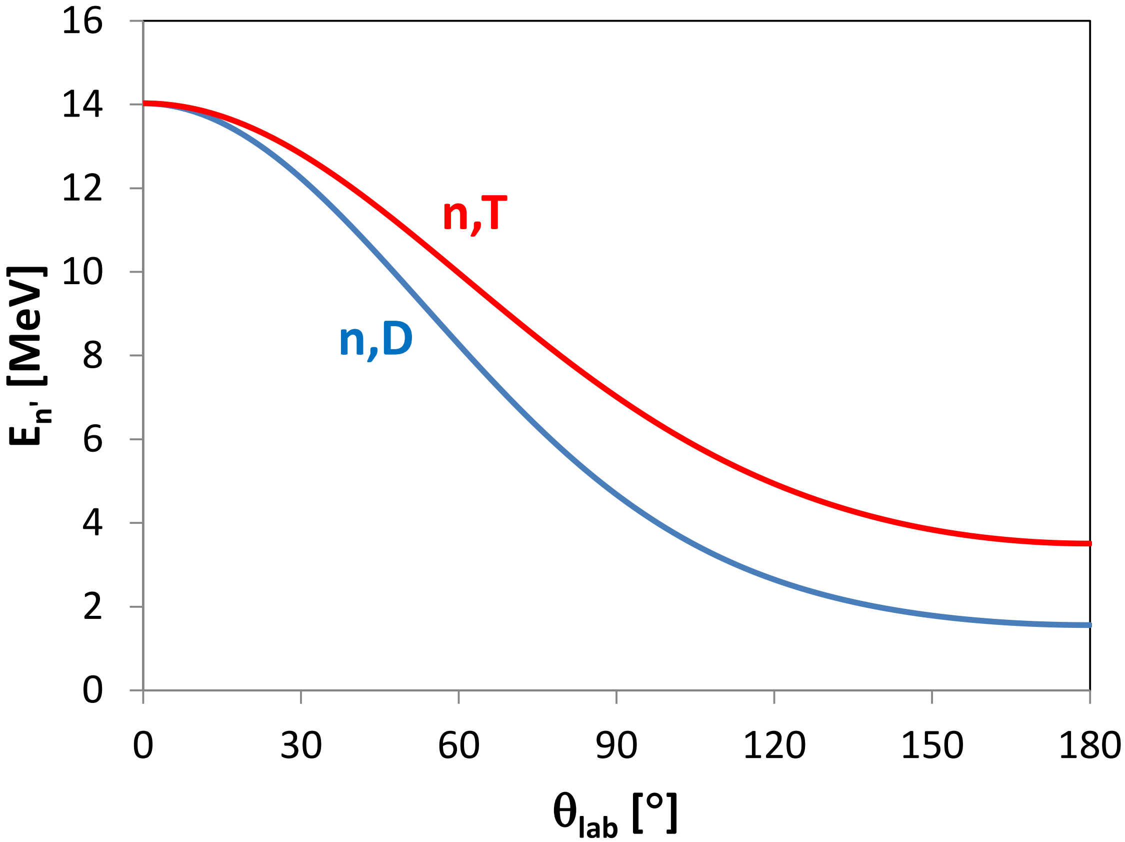

The transmission function T(Er) accounts for particles that slip-off the detector array for the OMEGA MRS

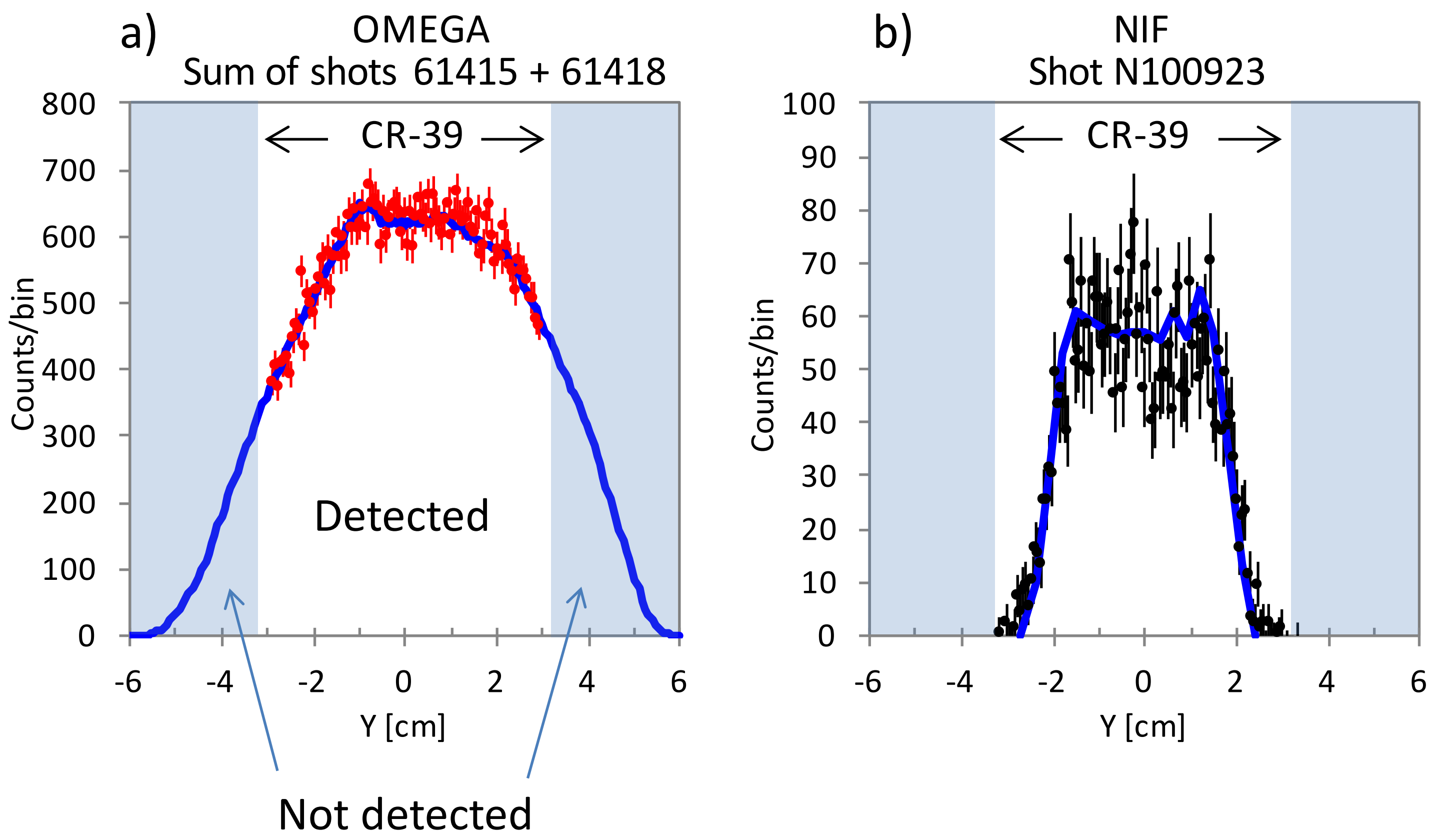

T (for primary neutrons) = 0.79

T (all energies) = 1.0

DC 9/20/2012

Different models of the magnetic field produce different transmission functions on the ~3% level, indicating a possible source of systematic error

OMEGA Med resolution foil used in TT meas

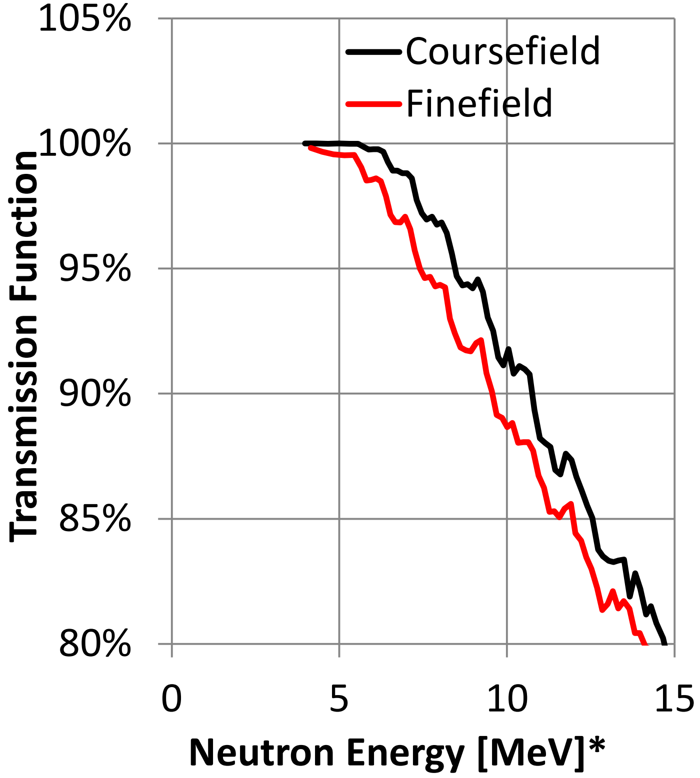

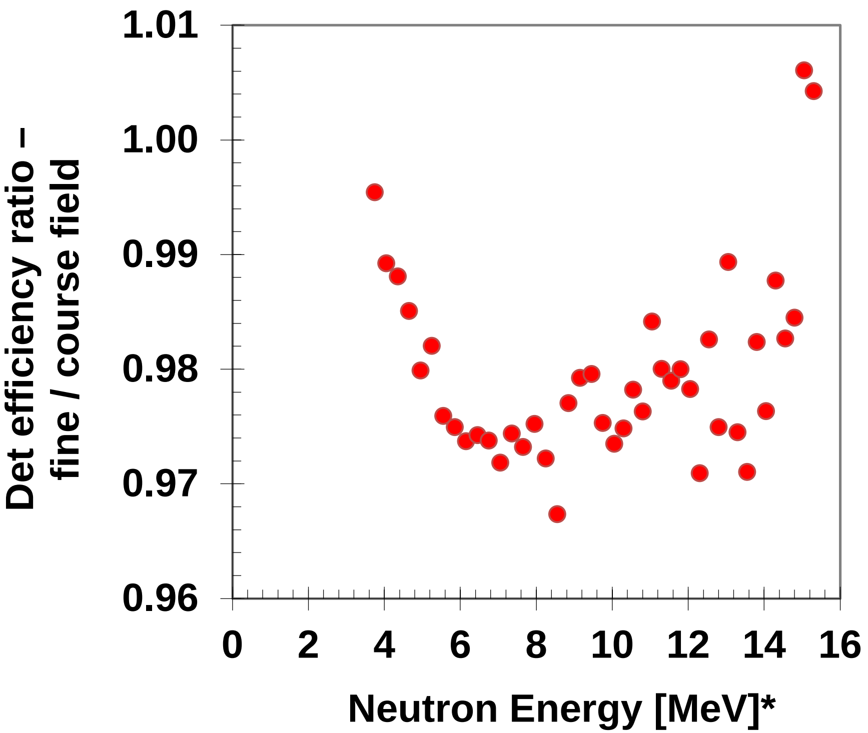

*Here recoil energy has been converted to neutron energy

DC 9/20/2012